The Dissertation Committee for Mitchell Tyler Butler Certifies that this is the approved version of the following dissertation:

Mechansims of planar cell polarity patterning by Prickle and Vangl and the control of collective cellular behaviors during tissue morphogenesis

Committee:

John B. Wallingford, Supervisor

Johann K. Eberhart

Lauren I. R. Ehrlich

Theresa J. O'Halloran

Jeanne C. Stachowiak

Mechansims of planar cell polarity patterning by Prickle and Vangl and the control of collective cellular behaviors during tissue morphogenesis

by

Mitchell Tyler Butler

Dissertation

Presented to the Faculty of the Graduate School of

The University of Texas at Austin

in Partial Fulfillment

of the Requirements

for the Degree of

Doctor of Philosophy

The University of Texas at Austin

August 2017

Acknowledgements

Earning my doctoral degree has been an invaluable experience, highly challenging and rewarding. In order to succeed, I needed the help and support of many people, and this is what I will remember most fondly when I think back on the years of my graduate studies. I would like to thank my undergraduate mentors Elena Silva and Doreen Cunnigham for introducing me to my love for developmental biology and working in a lab filled with fun, intelligent, and passionant individuals. I am thankful that Rasika Harshey, Quinfeng Wang, and the Harshey lab helped train me further to become an independent researcher, and I will be forever grateful for Rasika challenging me and encouraging me to start on the path towards a graduate degree. I consider myself very fortunate for having done my graduate work in the Wallingford lab, and I will always value my friendship with the Wallingford lab members I overlapped with, both past and present. I need to thank Asako Shindo, Mei-I Chung, Airon Wills, Fan Tu, and Michinori Toriyama for assisting me in various ways and offering countless valuable advice. I would like to thank Jacqui Tabler, Eric Brooks, Jakub Sedzinski, and Rebecca Fitch for being wonderful coworkers and friends that were always there for me both inside and outside the lab, each leaving their own lasting mark on me that I will cherish. A special thanks is owed to Linda Nguyen, who has become my best friend and seemingly biggest fan, as she has provided an overwhelming amount of selfless support. I would also like to thank my committee, Johann, Lauren, Terry, and Jeanne, for all of their time, attention, critical thought and feedback that have helped fine-tune my research. Lastly, I cannot thank John enough for the opportunity to work in his lab and for being such an excellent and thoughtful mentor. It has been an honor and a privilege studying with you and an incredibly fun and enlightening chapter in my life.

Mechansims of planar cell polarity patterning by Prickle and Vangl and the control of collective cellular behaviors during tissue morphogenesis

Mitchell T. Butler, Ph.D.

The University of Texas at Austin, 2017

Supervisor: John B. Wallingford

Planar Cell Polarity (PCP) signaling establishes asymmetric molecular patterns that control polarized cellular behaviors within the plane of a tissue or organ. This feature is conserved among metazoans and essential for proper development and tissue homeostasis. Owing to its important role in establishing tissue function, PCP signaling defects have been associated with diverse human pathologies, most notably birth defects. Tissue development is a dynamic process that requires the coordinated, temporal control of polarized cell behaviors, and here, I present the first vertebrate platform for the study of asymmetric PCP tissue patterning dynamics *in vivo*. Using *Xenopus laevis* as a model allows for relatively rapid and highly tractable studies of PCP patterning function in developing tissues, affording both subcellular analysis of PCP protein dynamics and multiple readouts for various planar- polarized cellular and tissue behaviors. I identified specific members of core PCP gene families that serve as faithful reporters for molecular planar polarity in the multiciliated epidermis and neural plate epithelia and uncover an essential role for Pk2 in the asymmetric PCP patterning of both of these tissues. I demonstrate that Pk2 function influences the progressive anterior localization of Dvl1 and posterior localization of Vangl1 in the epidermis, which when disrupted, results in severe ciliary orientation defects. Structure-function analysis reveals the conserved domains essential for Pk2 and Vangl1 asymmetry here. After characterizing the dynamic behaviors of apical cell-cell junctions that mediate convergent extension movements in

the *Xenopus* neural plate, I also show that Pk2 and Vangl2 are dynamic and increasingly asymmetrically enriched at shrinking cell-cell junctions during cellular rearrangements. I present evidence that suggests the polarized enrichment of Pk2 promotes the polarized accumulation of the actomyosin contractional machinery that facilitates mediolateral cell intercalations. Lastly, I detail how PCP point mutant alleles identified in human neural tube defect patient studies impact polarized protein localization behavior. Together, these findings establish a robust *in vivo* platform for the quantitative study of vertebrate PCP signaling and demonstrate the potential of this platform for furthering our understanding of dynamic tissue patterning processes and the molecular etiology of human birth defects.

Table of Contents

List of Figures

CHAPTER 1: PLANAR CELL POLARITY SIGNALING

Portions of this chapter are modified from: Butler, M.T. and Wallingford, J.B. Planar Cell Polarity in development and disease. Nat. Rev. Mol. Cell Biol. (2017). 18 (6) 375-388

1.1: CELL POLARITY AND POLARITY SIGNALING PATHWAYS

Cell polarization refers to the organized establishment of asymmetries within cells. Just as intracellular functions are compartmentalized in organelles, many cellular functions are made more effective by partitioning them along an axis of polarization. Cell polarization typically involves the localization of specific molecular determinants to specific cellular domains, and the coordination of polarity across tissues is essential for the development of specialized form and function in multicellular organisms. Cell polarity is best understood in the context of epithelia, and epithelial cells are generally considered to display two key forms of polarity: apical—basal polarity, which refers to polarized distribution of cellular components and specialized functions between the opposing surfaces of an epithelial sheet, and planar polarity, which refers to organization along the perpendicular axis, in the plane of the epithelial sheet (Figure 1).

Epithelial cells must be polarized in order to execute specialized functions. Some examples include mature cells of the intestinal epithelium, with protrusive microvilli to help increase the absorptive apical surface area, mucus-secreting goblet cells that deliver surfactants to the surface of lung and gastrointestinal tissues, and multiciliated cells, which provide the forces for fluid flow in the ependymal, respiratory, and reproductive tissues through the beating
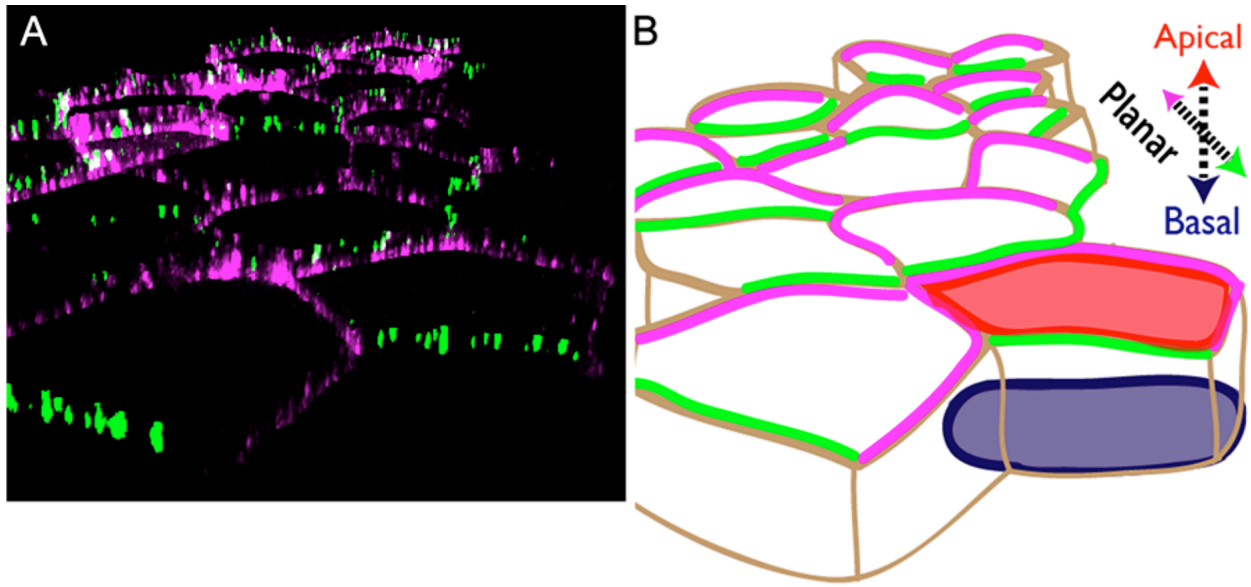
Figure 1: Epithelial cells exhibit apico-basal and planar cell polarity. **(A)** Pseudo-3D render of a confocal image of *Xenopus laevis* muliticiliated epithelium mosaically labeled with Dvl1-GFP and RFP-Pk2. (B) Schematic of the cells in **(A)** with tissue polarity axes denoted

of apical motile cilia (Davis & Dickey, 2008; Brooks & Wallingford, 2014). While these examples have unique properties and structures that facilitate their different physiological functions, the signaling pathways that establish cell polarity necessary for their development remains conserved between them and across metazoans (Bryant & Mostov, 2008).

The establishment of asymmetric localization of different cell polarity determinants in all three axes can be differently regulated during developmental processes. Protein localization and function along the Z-axis of epithelia, thus establishing apico-basal polarity, is relatively well understood and requires well-conserved proteins and lipids to organize into apical and basolateral domains through signaling feedback loops (Rodriguez-Boulan, E. & Macara, 2014). These proteins tend to specify the "inside" and "outside" of an epithelial sheet or tube and are often required for proper lumen formation in the latter. By contrast, PCP signaling establishes domains orthogonally to apico-basal polarity along the X and Y axes and allow for the coordination of cell behaviors across the plane of the tissue. In general, PCP signaling is not as well characterized as the pathways responsible for apico-basal polarity establishment, yet it can similarly be thought of a network of protein-protein interactions and feedback loops that are not typically associated with the control of gene expression as being the major downstream event. Thus, these cell polarity signaling pathways are fundamentally different from many other common developmental signal transduction networks that are typically associated with gene regulation, such as Canonical Wnt signaling, Hedgehog signaling, Notch signaling, and others.

Planar tissue patterning is governed by two major signaling pathways: the "core" planar cell polarity (PCP) and "Fat, Dachsous, and Four-Jointed" (Ft-Ds-Fj) modules. These signaling pathways were initially identified in *Drosophila melanogaster* screens for regulators of the coordinated orientation of external bristles and hairs (Adler 2012, Goodrich & Strutt 2011, Lawrence & Casal 2013, Peng & Axelrod 2012, Yang & Mlodzik 2015) (Figure 2A). A key

3

feature of planar polarization through these pathways is the complementary and mutually exclusive distribution of transmembrane signaling complexes, resulting in their asymmetric enrichment in distinct cell compartments within each cell of a patterned tissue (Figure 2B). This in turn directs the orientation of subcellular structures and cell behaviors through the regulation of cytoskeletal elements and cellular adhesions. Proper establishment and maintenance of planar polarity is essential during development and involved in tissue homeostasis and repair, and defects in PCP signaling are associated with diverse human pathologies.

1.2: ESTABLISHMENT OF CORE PCP PATTERNS

The establishment of planar polarity involves several fundamental processes, including sensing cues that govern the global orientation of polarity, establishing molecular asymmetries according to these cues, refining polarity patterns throughout neighboring cells, and executing respective polarized cell shape changes and behaviors.

1.2.1: Core PCP signaling components

When considering the roster of molecular players at work in PCP, it is useful to understand that distinct molecules participate in these diverse processes. The transmembrane components of this system allow for exchange of polarity information between cells. In *D, melanogaster* these include Flamingo, ((Fmi, also known as Starry Night (Stan); CELSR in vertebrates), Frizzled (Fz; FZD in vertebrates), and Van Gogh, (Vang also known as Strabismus or Stbm; VANGL in vertebrates). By contrast, the cytoplasmic components encoded by Dishevelled (Dsh; DVL in vertebrates), Prickle (Pk), and Diego (Dgo; ANKRD6 in vertebrates)

are involved in amplifying intracellular asymmetries and translating polarity cues into cell behavioral changes (Adler 2012, Goodrich & Strutt 2011, Lawrence & Casal 2013, Peng & Axelrod 2012, Yang & Mlodzik 2015). The basis of PCP establishment is the localization of mutually exclusive subsets of the core PCP proteins to opposing domains along the cell cortex, forming a pattern that propagates throughout the tissue. PCP protein patterns develop from an initially symmetric distribution that gradually sorts out into two complementary domains, with Fz, Dsh, and Dgo complexes typically accumulating on one side of each cell, and Vang and Pk enriched on the other; Fmi is present on both sides (Adler 2012, Goodrich & Strutt 2011, Lawrence & Casal 2013, Peng & Axelrod 2012, Yang & Mlodzik 2015) (Figure 2C). Asymmetric sorting and symmetry breaking is driven by dynamic trafficking, binding, and signaling interactions that differentially control stable localization of PCP components at discrete regions of the cell, and as detailed in following sections, the resulting stable accumulations ultimately coordinate planar-polarized cell behaviors.

1.2.2: Cell-cell communication and propagation of PCP asymmetry

The asymmetric localization of a molecular cue can be sufficient to polarize a single cell's behavior, but for groups of cells in an epithelium to *collectively* polarize, polarity information must be transmitted between neighboring cells. Such cell-cell communication of planar polarity is primarily facilitated through the physical interactions of PCP signaling complexes at cellular junctions, of which the seven-pass atypical cadherin Fmi is an essential component (Chen et al. 2008, Lawrence et al. 2004, Strutt & Strutt 2008, Usui et al. 1999). Extracellular interactions of cadherin repeat domains promotes the formation of Fmi homodimers across apical cell–cell junctions, which in result become increasingly stable (Chen et al. 2008, Strutt & Strutt 2008, Strutt et al. 2011, Wu & Mlodzik 2008). These stable
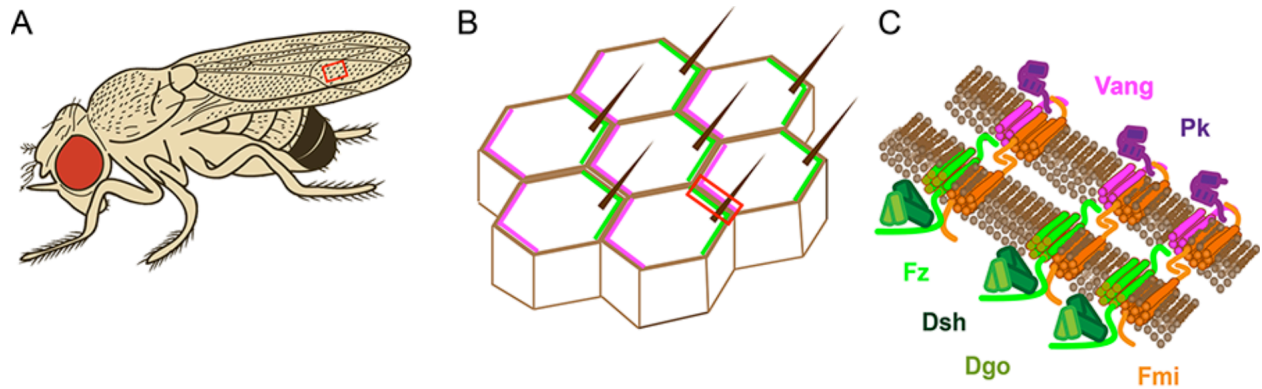
Figure 2: Asymmetric signaling complexes pattern planar polarity. **(A)** *Drosophila melanogaster* has many planar-polarized external features, including actin-based, distally or posteriorly oriented hairs and bristles that cover the legs, wings, and notum, which serve as a robust readout of planar cell polarity signalling. The box drawn on the wing blade demarcates the region illustrated in (**B**). **(B)** Cells of the *D. melanogaster* wing blade are asymmetrically patterned by proximal accumulations of Van Gogh (Vang) and Prickle (Pk) (both shown in purple) that are complementary to distal accumulations of Frizzled (Fz), Dishevelled (Dsh), and Diego (Dgo) (shown in in green). These patterns govern the distal positioning and orientation of a single actin-based trichome in each cell of the wing epithelium. The box drawn on the tissue demarcates the region illustrated in (**C**). **(C)** Asymmetric PCP signalling components form junctional signaling complexes that are physically linked from cell to cell. Both Fz and Vang are transmembrane proteins that associate with physically linked Flamingo (Fmi) homodimers established between the opposing membranes at cell–cell junctions. Distal accumulations of Fmi and Fz are asymmetrically clustered through the activity of Dsh and Dgo, while proximal Fmi and Vang complexes are enriched by the activity of Pk. Note that the proteins as they are portrayed are not necessarily to scale and merely approximations as there is no high-resolution protein structural data available to support them.

transmembrane accumulations then link PCP signaling complexes in neighboring cells (Figure 2C), propagating a uniform, cooperative pattern of polarity information (Figure 2B). In addition to serving as the molecular bridges that link *intercellular* polarity, Fmi also promotes the assembly of *intracellular* asymmetric directional signaling complexes. Junctional Fmi helps recruit PCP components Fz (a seven-pass transmembrane Wnt receptor) or Vang (four-pass transmembrane protein) to lateral regions of the apical cell surface (Bastock et al. 2003, Strutt 2001, Usui et al. 1999). These interactions help stabilize PCP components at cellular junctions but also mutually influence Fmi localization; Fmi is diffusively apically localized rather than apicolaterally enriched in a *Vang*, *fz* double mutant background, similar to Vang and Fz localizations in *fmi* mutant cells (Bastock et al. 2003, Strutt 2001, Strutt & Strutt 2008, Usui et al. 1999). Once recruited to apicolateral junctions, directional Fmi–Fz and Fmi–Vang signaling complexes can be progressively assembled in a coordinated, collective fashion across the tissue. Fmi molecules seem to preferentially bind Fz over Vang, and a Fmi–Fz complex is more likely to stably associate with a junctional Fmi molecule of an adjacent neighboring cell that is not bound to Fz – that is, it is either bound to Vang or bound to neither Fz nor Vang (Chen et al. 2008, Lawrence et al. 2004, Struhl et al. 2012, Strutt & Strutt 2008). This cell-cell interaction appears to help maintain the junctional localization of these signaling components in both cells, and the association of Vang with such a complex, specifically by binding a Fmi molecule linked to a Fmi-Fz complex in an adjacent cell, appears to further increase the combined apicolateral stability of all signaling components involved (Strutt & Strutt 2008, Strutt et al. 2011). This occurs by bolstering resistance to the endocytic flux that these molecules are subject to in the absence of such an assemblage (Figure 3).

Binding of Fmi to Fz or Vang induces differential Fmi signaling behaviors across cellular junctions that promote the propagation of a uniform PCP pattern (Chen et al. 2008, Lawrence et
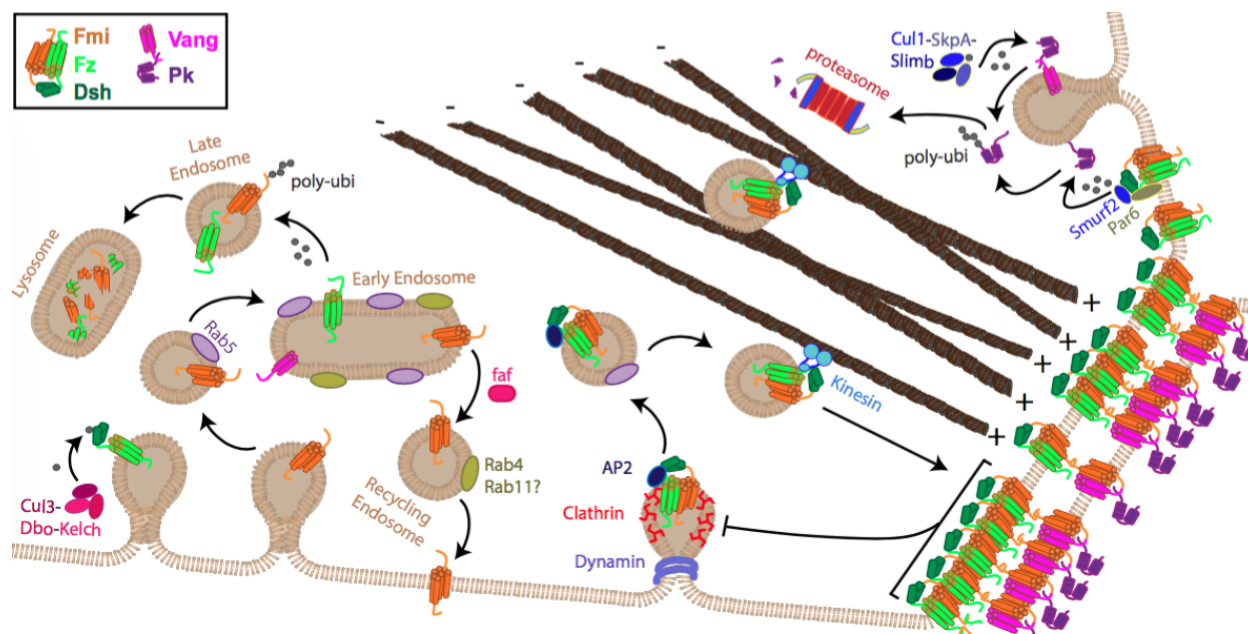
Figure 3: Graphical summary of endocytosis, trafficking, and degradation events that facilitate the dynamic patterning of planar cell polarity. PCP signaling components are resistant to endocytic flux when stably linked across junctions (Strutt & Strutt 2008, Strutt et al. 2011). The internalization of PCP components is partially dependent upon dynamin- and Clathrin-mediated endocytosis (Classen et al. 2005), and the interaction of membrane-associated Dsh (Simons et al. 2009) with Clathrin-associated protein AP-2 is essential for PCP signaling (Yu et al. 2007). The activity of a Cul3-Dbo-Kelch complex promotes the internalization but not degradation of Dsh, while faf deubiquitinase prevents the accumulation of Fmi in Rab5-positive endosomes (Strutt et al. 2013a). Although faf loss of function does not lead to a reduction in the overall levels of Fmi, inhibition of lysosomal maturation leads to the overaccumulation of endosomal Fmi, and Fz, and PCP component recycling to the membrane appears to be mediated by Rab4 and potentially Rab11 (Strutt & Strutt 2008). Microtubule-dependent trafficking of Fmi, Fz and Dsh towards plus ends appears to direct these complexes to sites of junctional enrichment (Shimada et al. 2006). Pk appears to have a dual role in both clustering stable Fmi-Vang complexes as well as mediating the internalization of unstable Vang (Cho et al. 2015). Vang mediates the proteasomal degradation of farnesylated Pk (Strutt et al. 2013b), likely through a Cul1-SkpA-Slimb complex (Cho et al. 2015), while phosphorylated Dvl2 can associate with Par6 and Smurf2 to poly-ubiquitinate Pk1, also leading to proteasomal degradation to control Pk localization and protein levels (Narimatsu et al. 2009).

al. 2004, Struhl et al. 2012, Strutt & Strutt 2008). Because signaling through Fmi occurs also when the extracellular domains of Fz and Vang are not intact, this indicates that Fmi signaling can be modulated by the binding to its cytoplasmic partners – with Fz, Vang or neither Fz nor Vang being bound to the C-terminal region of Fmi. Thus, it seems that even though Fmi is localized to both sides of a PCP-patterned epithelial cell, it can exhibit asymmetry in behavior that will influence the potential interactions between PCP signaling complexes of adjacent cells. Demonstrating this, *fz* mutant cells (over a distance of several cells) can be polarized quite remarkably by a neighbouring clone of cells, as long as both cell populations retain Fmi function and the neighbouring clone expresses *fz* (Struhl et al. 2012). Vang function does not appear to be required for a cell to be polarized by signals from a nearby *fz* expressing clone expressing *fz*, though the effects of this polarizing activity are less strong than when Vang is present in the signal receiving cells (the distance over which the polarization induced by the *fz* expressing clone is maintained is less for *fz* and *Vang* double mutants as compared to *fz* single mutants) (Struhl et al. 2012). Lastly, *fz* mutant cells can be polarized by Fz positive cells that do not express *Vang* (Struhl et al. 2012). Cumulatively, this analysis shows that to ensure directional non-autonomous cell polarization, Fmi must be present in both signal sending and receiving cells, and Fz must be present in at least one of the two cell populations. Vang activity does not seem to be absolutely essential to initiate polarization, but it appears to facilitate the polarization of the receiving cells. Thus, Fmi is essential for the intercellular communication of axial planar polarity and appears to assume one of two signaling states. The first state requires Fz binding to establish a stable, vectorial planar polarity signal. In the second state Fmi is either unbound or bound to Vang and associates with Fmi–Fz in the neighbouring cell across the cell–cell junction (Lawrence et al. 2004, Struhl et al. 2012, Strutt & Strutt 2008).

1.2.3: Feedback amplification of PCP asymmetry

The recruitment of junctional PCP complexes by Fmi is necessary for intercellular communication of polarity, but not sufficient for the establishment of robust PCP patterns within planar-polarized cells. The differential signaling states of Fmi with either Fz or Vang, which promote stability of the oppositely associated complexes across junctions, can set the stage for such patterns (Chen et al. 2008, Strutt & Strutt 2008). However, the concomitant sorting and enrichment of PCP signaling complexes is mediated by positive and negative interactions between the asymmetric PCP components. While some of these interactions may be driven by the membrane components, such as the extracellular domain of Fz potentially acting as a ligand for Vang (Strutt & Strutt 2008, Wu & Mlodzik 2008), much of the feedback amplification process occurs through activity of the cytoplasmic components Dsh, Dgo, and Pk. These cytoplasmic components act by clustering transmembrane signaling complexes into stable PCP enrichments (Axelrod 2001, Axelrod et al. 1998, Jenny et al. 2003, 2005; Strutt & Strutt 2007, Strutt et al. 2011), which are not necessarily required for intercellular PCP signaling, but rather for locally accumulating these signaling complexes to amplify the asymmetric pattern of PCP signaling complexes (Strutt & Strutt 2007) (Figure 2C). Thus, these interactions that promote PCP patterning are often collectively referred to as the feedback amplification of asymmetry (Peng & Axelrod 2012, Tree et al. 2002). Notably, for robust amplification to occur, the activities of all the core PCP components seem to be essential. Significant perturbation of any single core PCP protein is often sufficient to disrupt the asymmetric patterning of them all, adversely affecting tissue structure and collective cell behavior (Strutt & Strutt 2007).

In a polarized epithelial cell, one half of the hallmark PCP pattern consists of Fmi, Fz, Dsh and Dgo assembled into asymmetric junctional enrichments (Fig 2C). As Fmi homodimers recruit Fz to apicolateral regions of the cell, Dsh can be recruited as well in a Fz-dependent manner through the binding of the DEP domain of Dsh to the Fz cytoplasmic tail (Axelrod 2001,

Axelrod et al. 1998, Strutt 2001). In addition, the ankyrin repeat domain of Dgo can bind the PDZ domain of Dsh, serving as an additional interaction that promotes the unilateral clustering of the Fmi–Fz–Dsh–Dgo complex (Jenny et al. 2005). The asymmetric enrichment of Fz and overall junctional levels of Fmi appear greatly diminished in *dsh* mutant cells (Bastock et al. 2003, Strutt 2001, Strutt & Strutt 2008, Usui et al. 1999), likely due to a reduction in junctional stability (Strutt et al. 2011).

Complementary to the Fz, Dsh and Dgo accumulations that decorate one side of a planar-polarized cell, Fmi, Vang and Pk assemble along the opposite half of the apical membrane, generating the characteristic PCP pattern (Bastock et al. 2003, Tree et al. 2002) (Figure 2C). Vang and Pk accumulate through interactions of their respective C-terminal regions, mediating the heterotypic binding of Vang with Pk, as well as homotypic Pk and Vang binding (Jenny et al. 2003). These binding interactions, similarly to with Fz–Dsh (Strutt et al. 2011), facilitate the clustering of Vang and Pk and increase the stability of their junctional localization (Butler & Wallingford 2015).

The positive interactions that promote the clustering of PCP signaling components appear to be sufficient to drive the enrichment of these complexes in any given junctional region of the cell, yet there must be additional negative interactions in order to develop and maintain the mutually exclusive enrichment of Fmi–Fz–Dsh–Dgo and Fmi–Vang–Pk complexes to the opposing cell membranes. One simple mechanism would be for PCP signaling components to "exclude" the complementary set from localizing in the same region. Indeed, interactions between members of oppositely localizing complexes, namely between Vang, Pk and Dsh and Dgo, were observed (Das et al. 2004, Jenny et al. 2003, 2005; Park & Moon 2002, Tree et al. 2002). Interestingly, it is the C-terminal regions of Pk and Vang (through which they cluster with each other to accumulate on the one side of the cell) that have been demonstrated to

associate with both the PDZ domain of Dsh and ankyrin repeats of Dgo (Das et al. 2004, Jenny et al. 2005). Utilizing the same binding region to interact with members of both asymmetric domains could establish a framework for negative feedback mechanisms, and it has been proposed that Pk inhibits the association of Dsh with Fmi–Vang by competing for the same binding region of Vang, while Dgo competes with Pk for binding to Dsh (Das et al. 2004, Jenny et al. 2003, 2005). Along with the positive interactions that promote clustering PCP complexes, these negative interactions appear to allow for the self-sorting of PCP asymmetry and short-range propagation of polarity patterns, likely in the absence of any additional molecular inputs or guidance cues (Aw et al. 2016, Strutt & Strutt 2007, Vladar et al. 2012).

1.2.4: Endocytosis and endosomal trafficking facilitate the asymmetric sorting of PCP signaling components

It stands to reason that in order to generate and maintain PCP patterns, mislocalized or unstable components need to be removed from the membrane, and endocytosis, endosomal trafficking and degradation can indeed influence core PCP localization and signaling (Figure 3). Both Rab GTPase Rab5 and Dynamin have been shown to play a role in the internalization of unstable PCP signaling components (Classen et al. 2005, Strutt & Strutt 2008, Mottola et al. 2010). Inhibition of endocytosis leads to the overaccumulation of Fmi at the plasma membrane, and owing to the apparent role of Fz and Vang in stabilizing junctional Fmi, there appears to be an increased rate at which Fmi is internalized in *fz* and *Vang* mutant wing blade cells (Strutt & Strutt 2008, Strutt et al. 2011). Along with Fmi, both Fz and Vang also appear to be subject to membrane turnover, and Fz may facilitate the feedback amplification of asymmetry by promoting removal of Fmi–Vang–Pk complexes where Fz is accumulated (Cho et al. 2015, Strutt & Strutt 2008, Strutt et al. 2011). Ubiquitylation of Pk by an E3 ubiquitin ligase complex

consisting of Cullin-1, SkpA and Supernumerary limbs can promote the internalization of Fmi–Vang–Pk complexes, and the Pk-dependent internalization of Fmi in this manner is significantly reduced in *fz* mutants (Cho et al. 2015) (Figure 3).

Both Dsh-dependent and -independent mechanisms contribute to control of Fmi internalization (Strutt & Strutt 2008), and the former is likely to require Fz bound to Fmi due to known Fz-Dsh binding interactions (Wong et al. 2003). Interfering with the ability of DVL2 (one of the vertebrate Dsh homologues) to interact with the Clathrin adaptor AP-2 leads to a reduction in internalized FZD4, which in turn results in PCP-defective gastrulation movements in *Xenopus laevis* (Yu et al. 2007). As described before, Pk has similarly been shown to mediate the internalization of Fmi and Vang, which may be related to its function in clustering Fmi–Vang–Pk accumulations (Cho et al. 2015). Together, the cytoplasmic PCP signaling components appear to have a dual regulatory role on PCP, clustering their associated transmembrane components in some regions and mediating their internalization in others (Figure 3).

Although the internalization of PCP proteins is important for patterning of the PCP axis, this is only the first step in the intracellular sorting of these signaling components. Following endocytosis, PCP proteins are subject to one of several downstream processes, including recycling back to the membrane, trafficking to another region of the cell, or degradation. Inhibition of lysosomal maturation leads to the intracellular accumulation of internalized Fmi, suggesting some fraction of Fmi is normally turned over via lysosomal degradation (Strutt & Strutt 2008, Chen et al. 2008). Internalized Fmi colocalizes with endosomal makers such as Rab4, Rab5, Rab7 and Rab11, and both Rab4 and Rab11 appear to be capable of mediating the recycling of Fmi back to the membrane (Classen et al. 2005, Strutt & Strutt 2008, Strutt et al. 2011). As unstable components are likely continually degraded, it would seem that newly synthesized proteins must be continually added to the plasma membrane to help

maintain generate stable PCP patterns. Indeed, factors such as Clathrin adaptor protein AP-1 and trafficking GTPase ARF1, which are thought to facilitate trafficking from the Golgi and endosomes to the plasma membrane, have been identified as important factors in PCP establishment, as and their perturbation results in strong PCP phenotypes (Yang & Mlodzik 2015). These findings further underline the importance of membrane trafficking in the regulation of PCP complex distribution.

Endocytosis is essential not only for establishing PCP patterns, but also for adjusting patterns during cell rearrangements and in the face of frequent mitotic events in proliferative tissues. In the developing mammalian epidermis, PCP components are internalized and redistributed during mitoses, which appears to be essential for the proper patterning of the skin and planar polarization of hair follicles (Devenport et al. 2011). The events of internalization and redistribution are synced with cell division through the control of CELSR phosphorylation by Polo-like kinase-1 (PLK1), and phosphorylation promotes the internalization of CELSR1 and associated FZD proteins (Shrestha et al. 2015). Thus, the endocytic control of PCP components is an important part of maintaining uniform polarity, particularly during dynamic cellular behaviors.

1.2.5: Polarized microtubule trafficking facilitates PCP protein anisotropy

Feedback amplification and endosomal trafficking mechanisms facilitate the asymmetric sorting of PCP proteins, but these rely upon an initial anisotropic bias in order to become enriched and stable. This initial bias can be subtle, or random even, and with amplification can result in locally aligned asymmetry (Strutt & Strutt 2007, 2008; Vladar et al. 2012, Aw et al. 2016). However, in order to uniformly align PCP asymmetry across a given tissue, there must be an additional, reliable input that influences PCP patterning. Microtubules and microtubule-based

trafficking are used throughout development to introduce biases that break symmetry and specify axes, and arrays of planar-polarized microtubules have been visualized in various PCP-patterned tissues (Eaton et al. 1996, Hannus et al. 2002, Vladar et al. 2012). As it turns out, these polarized microtubule arrays can bias the transport of core PCP particles consisting of Dsh, Fz and Fmi towards one side of the cell, aiding the PCP patterning process (Shimada et al. 2006, Matis et al. 2014, Olofsson et al. 2014). These Fmi–Fz–Dsh accumulations are preferentially trafficked towards the plus ends of microtubules, showing a bias in directionality similar to plus-end tip tracking proteins such as EB1 (Olofsson et al. 2014) (Figure 3). However, while this process has been visualized in cells of the wing blade and likely is working similarly in the abdomen of *D. melanogaster*, the distal bias of microtubule plus ends is diminished in the most distal regions of the wing, demonstrating that this is just one potential mechanism for globally aligning PCP asymmetry.

Interestingly, while polarized microtubules are essential for establishing some PCP asymmetries, they may be dispensable for maintaining these patterns once they have been stably generated (Sepich et al. 2011, Shi et al. 2016), and this supports the notion that the key role of microtubules in PCP patterning is to introduce an initial directional bias. It has separately been shown that intact PCP patterns are necessary for the polarization of microtubule arrays (Vladar et al. 2012, Olofsson et al. 2014, Chien et al. 2015), demonstrating that intricate and mutual relationships exist between microtubule polarity and planar polarity patterning.

1.2.6: Post-translational modifications fine-tune PCP protein function

Protein localization and function is often regulated through post-translational modifications. Similar to the PLK1-1 mediated internalization of CELSR1 during murine epidermal divisions mentioned previously (Shrestha et al. 2015), other PCP component

phosphorylations are known to occur, and this has been demonstrated to impact PCP signaling in several contexts. VANGL and DVL proteins have multiple phosphorylation sites, modification of which can regulate protein localization and behavior (Yang and Mlodzik 2015, Cervenka et al. 2016). For example, mouse DVL2 is phosphorylated in response to WNT5a stimulation and can associate with the ubiquitin ligase SMURF2 and apical polarity protein PAR6 as a result of this phosphorylation, and this complex regulates PK1 protein stability by ubiquitylating PK1, and thereby promoting its proteasomal degradation (Narimatsu et al. 2009). WNT5a can also promote VANGL2 phosphorylation through tyrosine-protein kinase receptor ROR2, which is essential for governing planar-polarized cellular behaviors in the mouse limb bud (Gao et al. 2011). In addition, serine/threonine kinase misshapen-like kinase 1 (MINK1) phosphorylates a conserved residue of PK1, which promotes membrane localization with VANGL2 and apical clustering and enrichment of PK1–VANGL2 complexes (Daulat et al. 2011). The localization of FZD3 may also be regulated through its phosphorylation, which is disrupted upon loss of DVL1 in murine axon growth cones (Shafer et al. 2011). On the other hand, VANGL2 promotes the dephosphorylation and internalization of FZD3 in this same context (Shafer et al. 2011).

Transmembrane proteins are often sorted into lysosomes following ubiquitylation, and because both Fmi and Fz accumulate intracellularly upon the prevention of lysosomal maturation, these proteins are likely subject to lysosomal turnover (Strutt & Strutt 2008) (Figure 3). Along these lines, a deubiquitylating enzyme, fat facets (faf), was identified in a *D. melanogaster* genetic screen for enhancers of a hypomorphic *fz* allele (Strutt & Strutt 2003). It was shown that the presence of faf is important for proper junctional localization of Fmi, but faf knockdown does not affect total protein levels, suggesting that the faf-mediated deubiquitylation of Fmi serves to regulate Fmi recycling back to membranes (Strutt et al. 2013a). A related mechanism influences Dsh localization, with a Cullin-3–Diablo–Kelch ubiquitin ligase complex

mediating the removal of Dsh from junctions without impacting overall Dsh levels (Strutt et al. 2013a).

Following ubiquitylation, PCP components can also be subject to proteasomal degradation (Figure 3). For example, ubiquitylation and degradation of PK1 mediated by the before-mentioned DVL2, PAR6, and SMURF complex is essential for normal PCP signaling during mouse development (Narimatsu et al. 2009). In *D. melanogaster*, Vang appears to additionally play role in the ubiquitin-mediated proteosomal degradation of Pk (Strutt et al. 2013b). Here, as well as in *X. laevis*, Pk overexpression results in an increase in junctional Vang, yet Vang overexpression counter intuitively results in diminished levels of junctional Pk (Bastock et al. 2003, Butler & Wallingford 2015, Strutt et al. 2013b). Similarly, loss of Vang function can lead to higher overall Pk protein levels, which is likely the result of decreased Pk degradation (Strutt et al. 2013b). This Vang-dependent degradation of farnesylated (that is, membrane associated) Pk is likely mediated through the ubiquitin ligase Cullin-1 (Cho et al. 2015).

1.3: GLOBAL ALIGNMENT OF PCP PATTERNING

While interactions between core PCP proteins and the regulated dynamics of their localization can coordinate PCP asymmetries between neighboring cells and can propagate them throughout a tissue, global inputs into these patterns must govern their overall directionality with respect to the axis of an entire organ. Recent work has helped identify multiple, potentially overlapping influences on the global orientation of PCP, which apparently include expression gradients of *fj* and *ds* – the components of the "global" Ft–Ds–Fj PCP pathway, Wnt ligand gradients, and anisotropic tissue strain (Figure 4).

17

1.3.1: Ft, Ds and Fj signaling and asymmetry

Ft and Ds are atypical protocadherins that hetereotypically interact across cellular junctions, and Fj is a transmembrane kinase that modulates Ft and Ds interactions (Thomas & Strutt 2011). In addition to having roles in controlling tissue growth through the Hippo pathway, Ft-Ds-Fj signaling components participate in the planar polarization of the ommatidia the eye, trichomes in the wing, and abdominal bristles of *Drosophila*, similarly to the core PCP pathway (Lawrence & Casal 2013, Matis & Axelrod 2013). A vertebrate ortholog of Fj (Fjx1) and multiple homologs of Fat (Fat1-4) and Ds (Dchs1 and Dchs2) exist in vertebrates (Rock et al. 2005), and Fat4 and Dchs1, which have the highest homology to *Drosophila* Ft and Ds, are clearly important for PCP-mediated processes in mice, such as cell elongation orientation and division orientation (Mao et al. 2011, 2016; Saburi et al. 2008, Zakaria et al. 2014). However, the molecular functions of Ft-Ds-Fj signaling components in vertebrates and how well they are conserved with their *Drosophila* counterparts in this respect are currently poorly understood.

In *Drosophila*, planar asymmetries in Ft and Ds localization can be found due the opposing expression gradients of *ds* and *fj* (Ma et al. 2003, Matakatsu & Blair 2004, Strutt & Strutt 2002). Despite the expression of *ft* appearing uniform, the Fj kinase activity promotes Ft binding to Ds (Brittle et al. 2010, Hale et al. 2015, Ishikawa et al. 2008, Simon et al. 2010) and inhibits Ds binding to Ft (Hale et al. 2015), establishing a differential binding state between these two proteins that is influenced in a directional manner. In the *Drosophila* wing, for example, this results in a higher proximal level of ds expression stabilizing Ds protein on the distal side of the cell, down the ds gradient (Brittle et al. 2012, Simon et al. 2010) (Fig.4B). As a result, and similar to the fashion in which core PCP proteins localize, components of the Ft-Ds-Fj signaling pathway are asymmetrically distributed in cells of many planar-polarized tissues (Ambegaonkar

18

et al. 2012, Bosveld et al. 2012, Brittle et al. 2012). Whether expression gradients, localization asymmetries, or similar molecular functions for these proteins are seen in vertebrates has yet to be determined.

1.3.2: Ft-Ds-Fj signaling influences the global alignment of core PCP patterns

Even though Ds and Ft proteins have been shown to influence planar polarity, and while an intersect between these two pathways is becoming increasingly clear (at least in the fly), it has remained contentious whether Ft-Ds-Fj and core PCP signaling are acting in parallel or in consecution (Matakatsu & Blair 2004, Casal et al. 2006). Gene expression gradients are a common mechanism of tissue patterning during development, and opposing gradients of *dachsous* and *four-jointed* expression were observed along the axis of planar polarity in *D. melanogaster,* making these gradients attractive candidates for a global PCP-orienting cue (Yang et al. 2002, Ma et al. 2003). As mentioned before, these expression gradients result in the asymmetric localization of Ft and Ds to opposite sides of the cell, oriented similarly to core PCP asymmetry (Figure 4B). Indeed, while the core PCP pathway appears to retain function in mutant clones of Ft-Ds-Fj signaling components, the locally coordinated cells are not properly aligned along the global tissue axis (Yang et al. 2002, Ma et al. 2003). The differential alignment of core PCP patterns in respect to the *ds-fj* gradient in different tissues challenged this notion. However, this could be explained by the fact that Pk exists in two isoforms, Prickle (Pk) and Spiny Legs (Sple), that only differ in the most N-terminal region of protein (Gubb et al. 1999) and differentially interpret the Ft-Ds-Fj cues (Ayukawa et al. 2014, Matis et al. 2014); cells predominantly expressing *Pk*, such as those in the fly wing, asymmetrically localize Fmi–Vang–Pk on the same side of the cell as Ft, but in cells predominantly expressing *Sple*, Fmi-Vang-Sple localizes in the opposite orientation due to Sple interacting with Ds and Dachs

19

Ayukawa et al. 2014, Ambegaonkar & Irvine 2015) (Figure 4B). Thus, as Fmi–Vang–Sple complexes localize with Ds and Dachs, Fmi–Fz–Dsh complexes then localize on the same side of the cell as Ft.

One of the functional consequences of the differential interpretation of Ft–Ds–Fj through Pk and Sple is the orientation of microtubule polarity along Ft–Ds activity gradients. Microtubule plus ends are often oriented towards Ds in cells predominately expressing Pk and towards Ft in cells predominantly expressing Sple (Olofsson et al. 2014). Using Ft–Ds–Fj polarity cues to orient microtubules results in a bias in the directional transport of core PCP signaling components (Shimada et al. 2006, Olofsson et al. 2014), thereby providing a mechanism means of coupling these two signaling pathways (Matis et al. 2014, Merkel et al. 2014). However, the detailed molecular mechanism through which these microtubules are oriented in response to the Ft–Ds gradient and whether this mode of orienting PCP is conserved in tissues other than the fly wing, as well as in other species, remains unclear.

1.3.3: Wnt ligand gradients can establish the vector of planar polarity

Along with gradients in gene expression, gradients of secreted ligands are also commonly employed in tissue patterning. There are a number of different Wnt proteins which can act as secreted ligands for Frizzled receptors, and the tendency for Wnts to be found in graded distributions along an axis of planar polarity makes them attractive candidates for global PCP orientation cues (Sokol 2015). Indeed, a potentially instructive role for Wnt gradients in PCP pattern orientation is becoming increasingly apparent, with recent breakthroughs having highlighted that various Wnt ligands can influence PCP patterning in different capacities and that some may act redundantly (Wu et al. 2013, Chu & Sokol 2016). For example, both Wg and Wnt4 may be acting in the orientation of PCP complexes in the fly wing, where during early

wing morphogenesis, the distal Fmi–Fz–Dsh complexes are oriented towards the expression gradients of these ligands emanating from the wing margin and the proximal Fmi-Vang-Pk complexes are oriented more towards the central regions of the wing blade (Wu et al. 2013) (Figure 4A, top). Additionally, in the *X. laevis* ectoderm, Wnt5a, Wnt11, and Wnt11b have the capacity to orient Pk and Vang accumulations away from the source of ligand expression (Figure 4C), whereas a closely related ligand, Wnt3a, elicits no such behavior (Chu and Sokol 2016).

With this recently ascribed role for global PCP orientation, the mechanisms through which Wnt gradients could promote global orientation of PCP complexes remain not fully understood. Wnt4 and Wg seemingly inhibit Fz–Vang interactions between cultured fly S2 cells and can attenuate *fz* overexpression defects *in vivo*, which may indicate a role for Wnts in locally competing with Vang for Fz binding (Wu et al. 2013). In mice, Wnt5a can promote the association of PCP-specific component VANGL2 into a signaling complex with ROR2, promoting VANGL2 phosphorylation, which has been shown to be required for planar-polarized rearrangements of osteoblasts that drive elongation of the murine limbs (Gao et al. 2011).

1.3.4: Mechanical Forces provide input to PCP patterning directionality

When tissues change shape during growth and morphogenesis, or when fluid flows across a tissue surface, the anisotropic strains that are introduced can influence the development of PCP asymmetry and the orientation of PCP patterns. Early reports of this phenomenon demonstrated the direct impact of fluid flow on the polarization of ciliary beating patterns in multiciliated epithelia (Mitchell et al. 2007, 2009, Guirao et al. 2010). In addition, the forces exerted by flow throughout the embryonic epidermis of *Xenopus laevis* during gastrulation, which is thought to initially establish the PCP axis (Mitchell et al. 2007), were found to measurably increase the polarized stability of core PCP complexes at cellular junctions along the axis of tissue strain, and

21
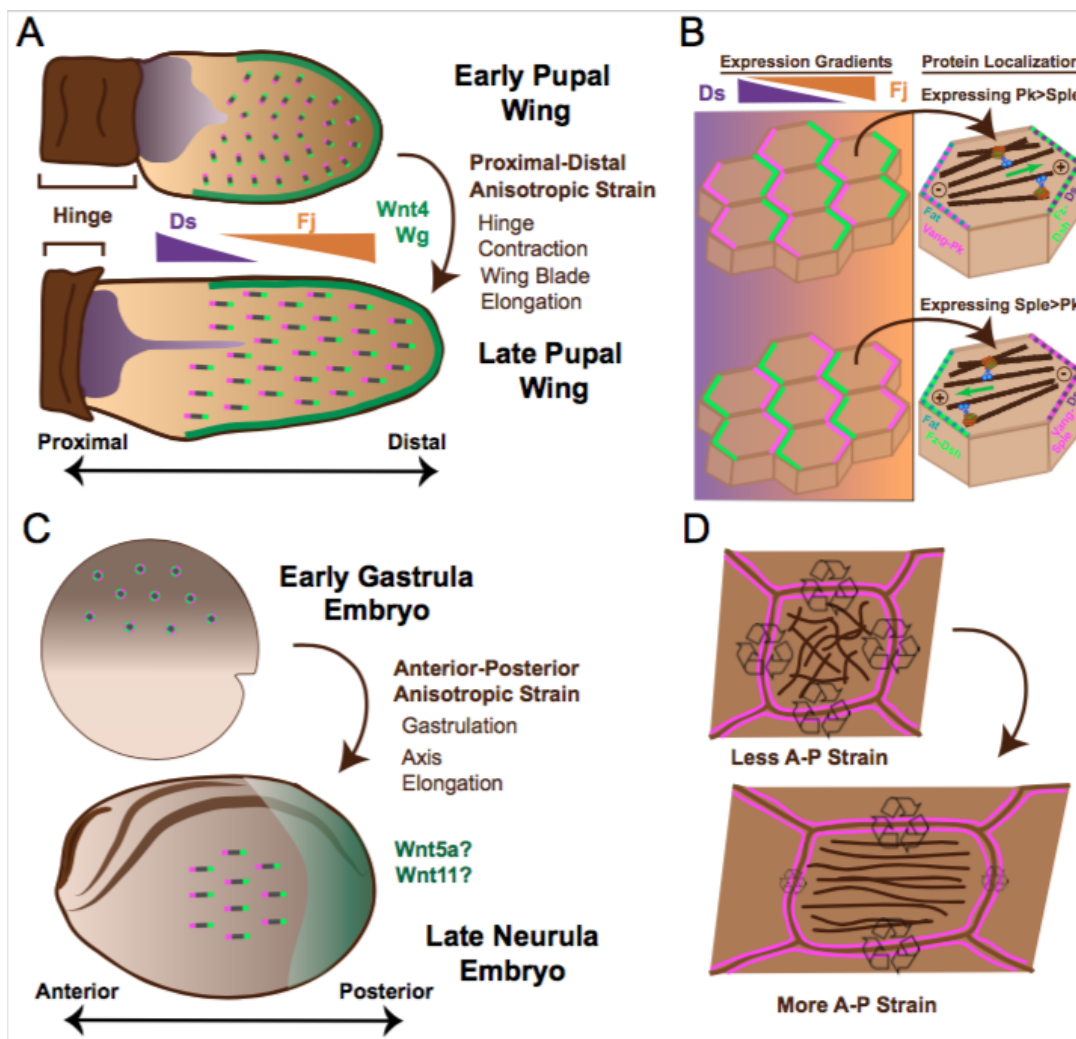
Figure 4: Multiple global inputs can collectively influence PCP orientation and stability across developing tissues. **(A)** The *Drosophila* wing blade exhibits a narrow source of Wnt ligands along the distal margin that may orient PCP (Wu et al. 2013). Expression gradients of *ds* and *fj* oppose one another along the proximal-distal axis and may influence the directionality of early PCP pattern (Ambegaonkar & Irvine 2015, Ayukawa et al. 2014, Matis et al. 2014) so that PCP is oriented in a radial fashion towards the edge of the wing around 5-15 hours after puparium formation (hAPF). Following hinge contraction and rapid wing blade elongation (16-32 hAPF), cell flows reorient microtubule polarity and increasingly asymmetric PCP patterns to be coordinately aligned along the proximal-distal axis (Aigouy et al. 2010). **(B)** Microtubules arrays are polarized according to Ft-Ds in a Pk-Sple-dependent manner (Olofsson et al. 2014). **(C)** PCP axes are established in *Xenopus* embryonic ectoderm during gastrulation (Mitchell et al. 2007), as forces along the axis of elongation increase the cortical stability of GFP-Vangl2 (Chien et al. 2015) (magenta). A posterior source of Wnts is also likely involved by directing the anterior localization of endogenous Vangl2 and exogenous Pk3, Vangl2 coexpressed in the early neurula ventral ectoderm (Chu & Sokol 2016). **(D)** The reduction in dynamic Vangl2 (magenta) along the axis of tissue strain occurs in a microtubule-dependent manner (Chien et al. 2015).

22

these effects were shown to depend on microtubules, which can rearrange in response to high tissue strain (Chien et al. 2015) (Figure 4D). This increase in the stability of Vangl2 at anteroposterior junctions can be measured even prior to the establishment of a clear PCP asymmetry (Chien et al. 2015), and it is interesting that the subsequent emergence of clear PCP asymmetry coincides with both rapid embryonic elongation and increasing strength of fluid flow (Butler & Wallingford 2015) – events associated with directional mechanical strain.

Tissues that already exhibit PCP patterning can also shift their axis of localization orientation in response to morphogenetic forces. For example, in early pupal *D. melanogaster* wings, complexes of PCP proteins are oriented initially towards the wing margin during early stages (towards the source of Wg/Wnt4), as discussed previously; however, as hinge contraction drives rapid wing elongation, promoting large-scale cell shape changes and rearrangements, PCP protein complex orientation also seems to shift and into alignments with proximal-distal axis of the developing wing (Aigouy et al. 2010) (Figure 4A, bottom). This shift in patterning also coincides with an increase in the amount of protein that appears to be asymmetrically enrichment into planar-polarized accumulations seen at later pupal stages, indicative of larger and more stable complexes (Strutt et al. 2011) (Figure 4A bottom, longer vectors compared to Figure 4A top). Similar behaviors are observed in the developing mouse epidermis, where again, PCP is aligned according to tissue strains that are coincident with the remodeling of junctions and tissue shape changes (Aw et al. 2016). Actin regulators such as WDR1 and CFL1 are important for maintaining cortical tension during these rearrangements, which when disrupted, result in the inability to establish robust PCP patterning and in the impediment of coordinated cell movements (Mahaffey et al. 2013, Luxenburg et al. 2015).

Directionally biased strain can clearly promote polarized patterning events, but molecular mechanisms of the force-influenced changes in PCP orientation and magnitude remain poorly

characterized. Rab11-mediated trafficking has been shown to be involved in the delivery and recycling of PCP components to apicolateral junctions and can utilize some of the same actin regulators necessary to maintain cortical tension (Mahaffey et al. 2013, Strutt et al. 2011). Interestingly, Rab11 and Ankrd6 appear to be planar-polarized together towards the central fold of the neural plate during neural tube closure and wound margins during wound healing, thus presumably having asymmetries that are oriented along the axis of tissue strain in these contexts (Ossipova et al. 2014). Perturbing PCP signaling disrupts the localization of Rab11 towards the neural fold, whereas dominant-negative Rab11 disrupts actomyosin-driven cell shape changes and rearrangements, which are required for proper wound healing (Ossipova et al. 2014).

1.4: BRIDGING THE GAP FROM MOLECULAR TO FUNCTIONAL ASYMMETRY

The robust readout of polarized bristles and hairs on insects provided the foundation for genetic screens identifying PCP proteins that direct assembly of these structures through control of the actin cytoskeleton (Adler 2012) (Figure 2A). These studies also facilitated the use of mutant clones to explore signaling mechanisms, for example in the discovery of directional non-autonomy, which refers to directional non-autonomous effects of specific PCP mutations (Adler et al. 1997, Adler et al. 2000, Taylor et al. 1998, Vinson & Adler 1987). PCP proteins also control both polarized organization and asymmetric cell fate choices in *D. melanogaster* photoreceptors (Jenny 2010).

Following the work in flies, evolutionary conservation of PCP signaling in vertebrates was first revealed in the context of coordinated cell movements during gastrulation in *X. laevis* and zebrafish Heisenberg et al. 2000, Tada & Smith 2000, Wallingford et al. 2000). Referred to as convergent extension cell movements, these cellular rearrangements are most conspicuous for

driving elongation of the embryonic body axis (Tada & Heisenberg 2012), but they also drive tissue elongation during organogenesis, for example in the kidney tubules (Lienkamp et al. 2012) and inner ear structures (Chacon-Heszele et al. 2010). While the asymmetric localization of PCP components is well established in the *D. melanogaster* wing, the control of core PCP localization during convergent extension remains poorly defined. However, predominant features of the system appear to be conserved, as PK and VANGL were described to localize anteriorly in cells undergoing convergent extension, while DVL was shown to localize posteriorly (Ciruna et al. 2006, Jiang et al. 2005, Ossipova et al. 2015, Roszko et al. 2015, Yin et al. 2008).

Another setting in which vertebrate PCP is essential is the oriented positioning of cilia within cells. First reported in the mouse inner ear, planar polarization of hair cells is organized by the asymmetric kinocilium positioning, which is preceded by asymmetric PCP patterning (Rida & Chen 2009). More recently, PCP signaling was also revealed to control planar polarization of motile ciliary beating in diverse ciliated cell types, and has been implicated in a wide array of developmental events, including the orientation of cell division, the migration of facial motor neurons, and the planar orientation of hair follicles in the mammalian epidermis (Devenport 2016, Wallingford 2012).

1.4.1: PCP signaling governs cell behavior through the control of actin cytoskeleton

Defects in actin dynamics and actin-based structures often result from disrupting PCP signaling. As is the case for our understanding of PCP patterning, the links between PCP signaling and actin regulation are perhaps best understood in the context of the assembly of a single, actin-based wing hair in each cell of the Drosophila wing blade (Devenport 2016). Some notable examples in vertebrates include the loss of polarized, stable llamelipodial protrusions in converging and extending mesenchyme (Wallingford et al. 2000) and similar filopodial proteins

in neural ectoderm (Williams et al 2014). In addition, defects in contact inhibition of locomotion, which is essential for the proper collective migration of the neural crest and involves highly dynamic regulation of the actin cytoskeleton, can result from defects in PCP signaling (Stramer and Mayor 2016). Conversely, inhibiting actin dynamics can lead to loss of planar polarity. This can be visualized in the context of basal body spacing in Xenopus MCCs, for example (Werner et al. 2007).

From the very beginning of molecular studies into PCP in Drosophila, it was clear that the actin cytoskeleton was a likely target to be under the governance of PCP signaling (Wong & Adler 1993, Eaton et al. 1996, Turner and Adler 1998). Genetic studies revealed direct links between PCP, Rho family small GTPases (Strutt et al. 1997), the myosin-activating Rho Kinase (ROCK), and the actomyosin machinery (Eaton et al. 1996, Winter et al. 2001). A similar mechanism was then identified in vertebrate convergent extension, in Xenopus (Habas et al. 2003, Shindo & Wallingford 2014), zebrafish (Marlow et al. 2014), mice (Ybot-Gonzalez et al. 2007), and chicks (Nishimura et al. 2012). Actomyosin contraction is clearly an important downstream effector of PCP function, and it appears that actin assembly is also an important factor. In vertebrate convergent extension, PCP proteins were found to act via Daam1 (Habas et al. 2001), a member of the formin family of the linear actin nucleators (Chesarone et al. 2009). This link may be conserved, as PCP proteins interact genetically with Drosophila DAAM to control axon growth and guidance (Dollar et al. 2016). Moreover, in the Drosophila Wing, the PCP effector Multiple Wing Hairs (Mwh) encodes a divergent Formin-related protein that negatively regulates actin assembly (Lu et al. 2010).

Additional links between PCP and actin regulation have been uncovered when examining the role of actin disassembly, particularly when mediated through cofilin proteins. Various mutant alleles of the Drosophila cofilin/ADF homolog, twinstar, results in defective PCP in the

wing and eye, among other tissues (Blair et al. 2006). It was later shown that Cofilin and Vangl2 work together to control planar-polarized process in mouse development, such as convergent extension of the midline and coordinated asymmetric positioning of nodal cilia (Mahaffey et al. 2013). In the context of mouse epidermal polarity, depletion of f-actin binding protein Wdr1 results in the misalignment of hair follicles, a PCP defect, and loss of junctional Celsr1 localization (Luxenburg et al. 2015). Wdr1 depletion genetically interacts with Cofilin and destrin in eliciting cell polarity defects, though this extends to apico-basal polarity perturbation in this case. In summary, there are many essential links between actin regulators and PCP signaling components in the establishment of planar polarity, which include the control of not only actin assembly, but also disassembly.

1.4.2: Directional beating in multiciliated cells is controlled by PCP signaling

Multiciliated cells (MCCs) bear dozens of directionally beating cilia that act in concert to drive fluid flow across the tissue (Figure 5A). Such cells are critical for development and homeostasis of the airway, the central nervous system (CNS), and reproductive tracts (Wallingford 2012) (Figure 5B). Directional beating of MCCs has been studied on the amphibian epidermis for nearly 200 years (Sharpey 1836), and not surprisingly, the first description of a role for PCP genes in these cells was in this context (Mitchell et al. 2009, Park et al. 2008). PCP signaling is now known to control polarized beating in all MCCs examined to date, including in the mammalian brain (Boutin et al. 2014, Guirao et al. 2010, Ohata et al. 2014, Tissir et al. 2010), airway (Vladar et al. 2012), and oviduct (Shi et al. 2014, 2016). Core PCP localization examined in these tissues reflects that seen in the fly wing; PK and VANGL occupy a domain complementary to that of DVL and FZ (Figure 5A, C); however several additional cilia-associated proteins not found in *D. melanogaster* are required for normal core
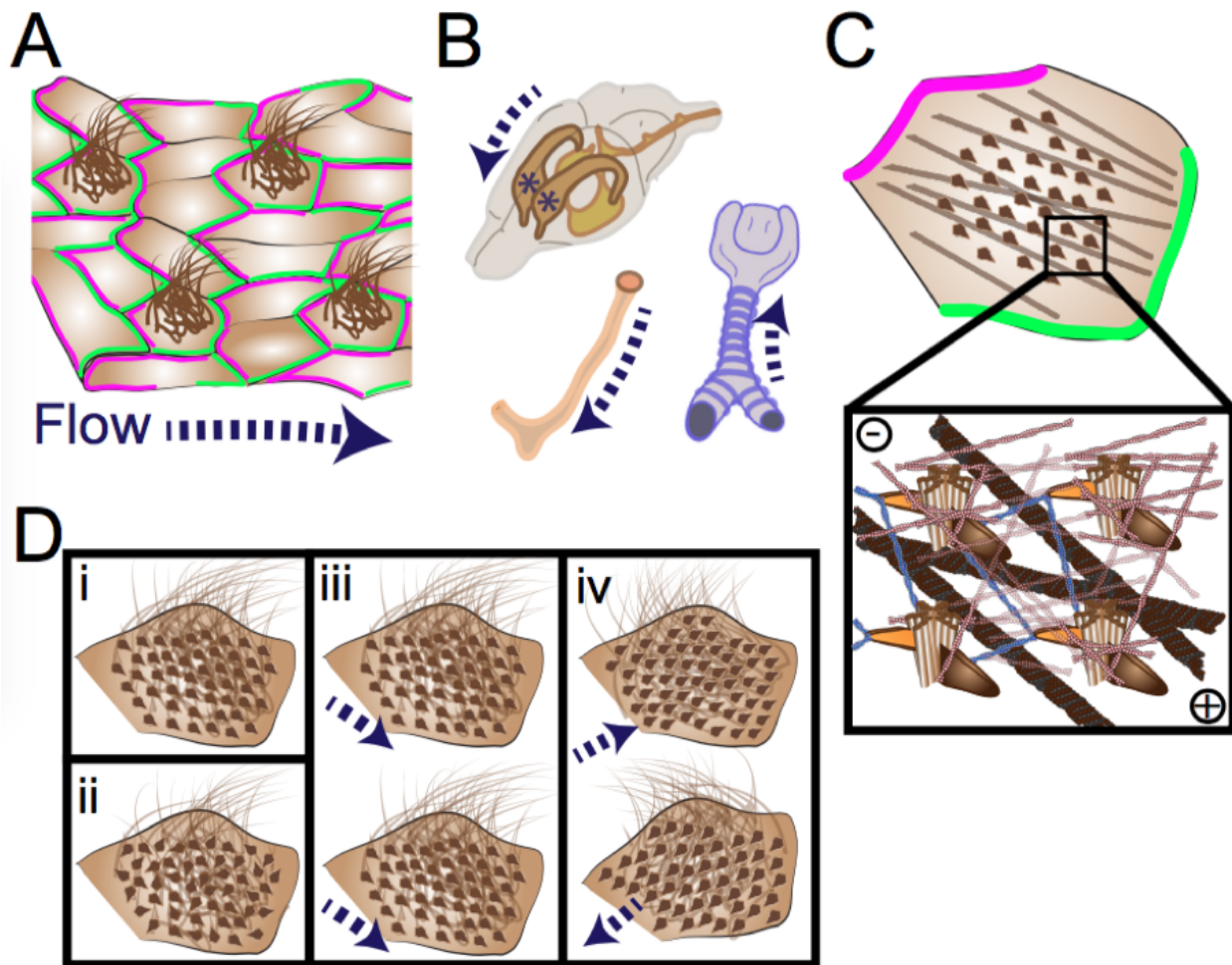
Figure 5: PCP patterns direct the cytoskeletal organization and ciliary polarity of multicilated cells. (**A**) Multicilated epithelia are patterned by asymmetric PCP complexes, which direct polarized fluid flow across the surface of the tissue along the axis of PCP asymmetry. (**B**) PCP patterning directs the rostal flow of cerebrospinal fluid in the lateral ventricles (Guirao et al. 2010) (asterisks), rostral mucociliary flow in the trachea (Vladar et al. 2012), and medial flow in the oviduct of mice (Shi et al. 2014). (**C**) PCP signaling is essential for the organization of the apical cytoskeletal elements responsible for ciliary orientation (Boutin et al. 2014, Park et al. 2008). An apical actin network (pink) spaces basal bodies, a subapical actin network (blue) links basal feet (orange) to neighboring basal bodies (light brown) to control rotational polarity, and polarized microtubules (dark brown) orient groups of basal bodies along the axis of planar polarity (Boutin et al. 2014, Vladar et al. 2012), with the microtubule plus-ends oriented towards Fzd-Dvl accumulations (Vladar et al. 2012). (**D**) Rotational polarity, the uniform orientation of cilia within MCCs (i), can be disorganized (ii) by perturbation of Dvl2, Pk2, and Celsr2/3 (Boutin et al. 2014, Butler & Wallingford 2015, Ohata et al. 2014, Park et al. 2008). Tissue-level polarity, the uniform orientation across multiple MCCs (iii), is disrupted upon perturbation of Fzd3, Vangl1/2, and Celsr1 (Boutin et al. 2014, Butler & Wallingford 2015, Mitchell et al. 2009).

PCP protein localization in MCCs, including the myosin motor Myo1d (Hegan et al. 2015) and novel proteins Spag6 (Sperm-associated antigen 6) and c21orf59/Kurly, which physically interacts with the core PCP protein Dishevelled (Teves et al. 2014, Jaffe et al. 2016).

MCCs display multiple levels of planar polarization (Figure 5D), a "rotational polarity" (organization of ciliary basal bodies within each cell) and distinct "tissue-level polarity (coordination of polarity between all cells across a tissue) Devenport 2016, Wallingford 2012). Cell-autonomous defects in rotational polarity result from disruption of DVL or PK (Butler & Wallingford 2015, Ohata et al. 2014, Park et al. 2008), but mild rotational with more striking non-autonomous, tissue-level polarity defects result from disruption of the transmembrane proteins VANGL, FZ, or CELSR (Boutin et al. 2014, Guirao et al. 2010, Mitchell et al. 2009). Interestingly, in mouse ependymal cells, CELSR1 appears to coordinate tissue-level polarity by influencing microtubule patterning, whereas CELSR2 and CELSR3 appear instead to be required for the rotational polarity and organization of individual basal body patches through the control of actin (Boutin et al. 2014).

Exactly how polarity information is communicated between PCP proteins and ciliary basal bodies is not yet known, but the cytoskeleton clearly plays a key role. Actin and microtubules comprise the cortical cytoskeleton and at the same time interact with accessory structures of the basal body, and both cytoskeletal elements are implicated in polarizing beating (Boutin et al. 2014, Devenport 2016, Wallingford 2012) (Figure 5C). Planar-polarized apical microtubules are a conserved feature of MCCs in the mouse airway (Vladar et al. 2012) and *X. laevis* epidermis (Chien et al. 2015), and this is reminiscent of the microtubule arrangement observed in the *D. melanogaster* wing cells discussed previously (Eaton et al. 1996, Hannus et al. 2002, Shimada et al. 2006). It is important, then, that PCP proteins localize both to the cell cortex, where they are known to control cell polarity, and to the basal body, where they could act

to control basal body polarity (Guirao et al. 2010, Ohata et al. 2014, Park et al. 2008, Vladar et al. 2012), and there is a growing roster of additional proteins asymmetrically localized to basal bodies, including ODF2, non-canonical tubulins, and Centrin2, that may additionally be involved (Kunimoto et al. 2012, Turk et al. 2015, Ying et al. 2014). Among these, ODF2 is perhaps the most interesting, as mice lacking ODF2 display overt defects in the apical microtubule lattice (Kunimoto et al. 2012). Thus, these proteins provide excellent entry points for future studies exploring the interplay between PCP proteins, polarization of the cytoskeleton, and polarization of ciliary beating.

1.4.3: PCP signaling coordinates convergent extension cell rearrangements

Convergent extension was the first context in which vertebrate PCP signaling was studied (Heisenberg et al. 2000, Tada & Smith 2000, Wallingford et al. 2000), so that it remains among the most poorly understood processes with respect to the instructive role of PCP might be a bit surprising to some. Convergent extension is driven by the mediolateral intercalation of cells, resulting in the subsequent narrowing and consequent elongation of the tissue in the anteroposterior axis (Figure 6A,B). Two mechanisms have been evoked to explain force generation for cell movement during vertebrate mesenchymal convergent extension, though the two are not mutually exclusive. In one model, cellular protrusions at the mediolateral cell faces exert traction force, pulling on cell neighbors and driving intercalation by a mechanism akin to cell crawling (Shih & Keller 1992). In the second model, junctions between apposed anterior and posterior cell faces are actively contracted, drawing mediolaterally-attached neighbors toward one another (Shindo & Wallingford 2014) (Figure 5C). Interestingly, PCP proteins can be implicated in both paradigms, as their manipulation disrupts both the stability and the polarity of mediolateral protrusions and the shrinkage of cell junctions to be biased towards those
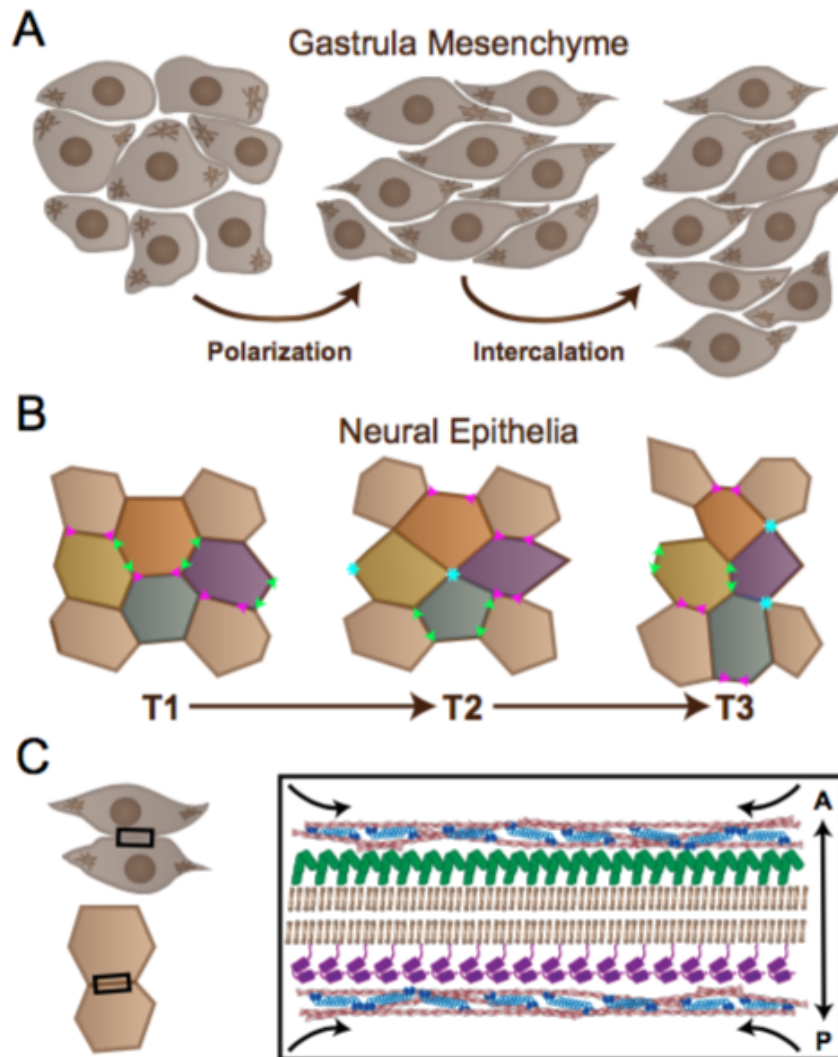
Figure 6: PCP signaling directs polarized cell rearrangements. **(A)** Gastrula mesenchymal cells adopt a polarized cellular shapes by stabilizing mediolateral actin-based protrusions and collectively elongating along the mediolateral axis, and then mediolaterally intercalate to narrow and lengthen the tissue, both of which require intact PCP signaling (Kim et al. 2010, Wallingford et al. 2000. **(B)** Neural ectodermal cells mediolaterally intercalate by preferentially shrinking anteroposterior (AP) junctions (magenta arrows), which resolve (blue asterisks) and elongate form new mediolateral (ML) junctions (neon green arrows). The stages of this intercalation behavior are often referred to "T" transitions, where T1 to T2 involves the shrinking of the AP junction, and T2 to T3 transitions involve the lengthening of a new ML junction between two cells previously separated along the ML axis at T1. **(C)** Core PCP components can be found asymmetrically enriched along AP junctions of cells undergoing convergent extension in vertebrates, with Pk and Vangl typically localizing to the anterior cell faces and Dvl along the posterior cell faces (Ciruna et al. 2006, Ossipova et al. 2015, Roszko et al. 2015, Yin et al. 2008). As it also is typically enriched there in the same context, PCP signaling components are concomitant with the localization of filamentous actin enrichments and phosphorylated non-muscle Myosin II, comprising contractional actomyosin machinery shrinks AP junctions (Nishimura et al. 2012, Ossipova et al. 2015, Shindo & Wallingford 2014, Williams et al. 2014).

31

anteroposterior cell faces (Wallingford et al. 2000, Yen et al. 2009, Shindo and Wallingford 2014). PCP-dependent stable cell protrusions and polarized junctional shrinking are also characteristics of cells undergoing convergent extension in vertebrate neural plate epithelia (Figure 5B) (Nishimura et al. 2012, Williams et al. 2014), with slight differences arising due to differing tissue architecture and context.

Our understanding of the molecular biology of PCP during vertebrate convergent extension emerged from prior work in *D. melanogaster*, where PCP genes were shown to directly control actomyosin machinery via Rho GTPases and Rho Kinase (Strutt et al. 1997, Winter et al. 2001). Indeed, PCP-mediated convergent extension requires RhoA and Rho Kinase, as well as a host of other actin regulators such as the formin Daam1 and Rho GTPase Cdc42 (Wallingford 2012). This conserved role for PCP in regulating actomyosin contraction makes it possible to assemble a preliminary model of how planar-polarized PCP protein localization directs collective cell movements.

Most evidence suggests that the PCP proteins form complementary asymmetric zones of localization on the anterior and posterior cell faces during convergent extension (Ciruna et al. 2006, Jiang et al. 2005, Ossipova et al. 2015, Roszko et al. 2015, Yin et al. 2008) (Figure 6C). There is precedent for PCP asymmetries in the mechanical control of cell intercalation, as the atypical myosin Dachs, asymmetrically localized by Ds, has been shown to drive anisotropic junctional tension in the developing *D. melanogaster* thorax, promoting planar-polarized cell rearrangements (Bosveld et al. 2012). With this in mind, it seems feasible that PCP proteins could directly recruit contractile actomyosin regulators and thereby drive junction shrinkage. Indeed, live imaging has demonstrated pulses of actin, phosphorylation of myosin II, and enrichment of myosin regulators at sites of shrinking junctions in *X. laevis* gastrula mesenchyme and chick neural epithelial cells (Nishimura et al. 2012, Shindo & Wallingford 2014) (Figure 6c).

Additional recent insights have come from studies of PTK7, which is a vertebrate-specific regulator of core PCP function (Lu et al. 2004). PTK7 is required for convergent extension-associated cell behaviors during gastrulation and neurulation (Hayes et al. 2013, Lu et al. 2004, Yen et al. 2009), but more recent work in the inner ear has revealed a mechanism linking PCP and PTK7 to phosphorylation of Myosin II activation through Src kinase phosphorylation of myosin regulatory light chains (Andreeva et al. 2014, Lee et al. 2012). While this preliminary model provides a parsimonious explanation of asymmetric PCP protein function during junction shrinking, it does not explain the effect of PCP proteins on formation of polarized membrane protrusions during convergent extension, which are also PTK7-dependent (Williams et al. 2014). Among the possible mediators of this effect are septins, which have conserved functions in compartmentalizing cortical actomyosin during cytokinesis and are required for proper PCP function during convergent extension (Kim et al. 2010, Shindo & Wallingford 2014).

1.4.4: Evidence that PCP signaling defects contribute to a range of human pathologies

Given the widespread role for planar cell polarity (PCP) in embryonic development, it is not surprising that PCP gene mutations underlie human birth defects, which happen to be the number one cause of infant mortality in the United States and among the leading causes of death for children of all ages (Kochanek et al. 2016). Indeed, PCP genes are now among the most well defined genetic risk factors for neural tube defects, which remain a common birth defect (Wallingford et al. 2013). Neural tube defects (NTDs) arise from a failure of the initially flat neural epithelium to fold and fuse to form the hollow central nervous system. Several studies have emerged implicating PCP genes in human NTDs, and as the first identified mutations Vangl1 (Kibar et al. 2007), variants in essentially all the core PCP genes have now been

identified in human NTD patients; these individual findings have been comprehensively delineated (De Marco et al. 2014, Juriloff & Harris 2012). Several studies also provide mechanistic insights, revealing that NTD-associated mutations disrupt known interactions among PCP proteins or disrupt subcellular localization (Iliescu et al. 2014, Kibar et al. 2007, Lei et al. 2014, Robinson et al. 2012).

Animal models are increasingly providing solid evidence that defective PCP signaling can give rise to NTDs. For example, mutations of *Vangl2* and *Celsr2* were found to elicit neural tube closure defects in mice (Kibar et al. 2001, Murdoch et al. 2001), and several other PCP mutant mice have been demonstrated to exhibit similar phenotypes since, including mutants of Celsr1 (Curtin et al. 2003), Dishevelleds (Wang et al. 2006a, Etheridge et al. 2008), Fzd3 and Fzd 6 (Wang et al. 2002, Wang et al. 2006b), and Prickle1 (Tao et al. 2009). Furthermore, time-lapse imaging in *X. laevis* revealed that PCP-related neural tube closure defects arise from a failure of convergent extension (Wallingford & Harland 2001, Wallingford et al. 2000). Therefore, better understanding of how PCP proteins direct cell behaviors during convergent extension can shed more light on the role of PCP gene mutations in human birth defects.

In addition to NTDs, PCP gene mutations also contribute to the etiology of Robinow Syndrome, a severe skeletal dysplasia characterized by short limbs and craniofacial anomalies. Mutations for this syndrome were first identified in the Ror2 tyrosine kinase (Afzal et al. 2000, van Bokhoven et al. 2000), which now has an established role in the PCP-mediated elongation of the murine limb in response to Wnt5a (Gao et al. 2011). More recently, Robinow Syndrome has been associated with genetic variants in the core PCP genes Dvl1 (Bunn et al. 2015, White et al. 2015) and Dvl3 (White et al. 2016), as well as Wnt5a (Person et al. 2010). It is significant that these gene-association studies are supported by functional assays in model animals, providing mechanistic insights to supplement genotype-phenotype correlations.

Recent work indentifies links from PCP signaling functions to the proper formation of the spine and PCP mutations could lead to the onset of idiopathic scoliosis phenotypes. This link was additionally uncovered in the study of Ptk7 mutant zebrafish, which exhibit late-onset severe spinal curvatures that are likely due to defective multiciliary flow (Grimes et al. 2016, Hayes et al. 2014). In a recent survey of a patient cohort with adolescent idiopathic scoliosis (AIS), which screened for mutations in VANGL1, two missense mutations of interest were identified as potentially contributing to the AIS phenotypes (Andersen et al. 2016).

1.5: CONCLUDING REMARKS

Given the broad roles ascribed to PCP signaling in development in model animals, it is perhaps surprising that so few human disorders have yet been linked directly to mutation in PCP genes. One potential explanation is that more severe birth defects mask the subtler phenotypes that have been characterized in animal models. For example, some patients with neural tube closure defects associated with PCP gene mutations present with hydrocephalus (Bosoi et al. 2011, Kibar et al. 2007, Seo et al. 2011), which could be a secondary consequence of neural tube defects or, alternatively, might be the manifestation of defects in MCC planar polarity in the brain (Tissir et al. 2010). Moreover, examination of patients with spina bifida with underlying PCP gene mutations recently revealed a high prevalence of congenital kidney defects that reflects those seen in PCP mutant mice (Brzoska et al. 2016), so perhaps broadening the focus of phenotypes on human PCP patients will reveal more potential disorders. These data highlight the complex nature of human birth defects and the potential role of PCP genes in their etiology.

Although significant strides have been made in understanding the establishment of PCP patterns and how they influence collective cell behaviors, much work remains to fully understand

the instructive roles of PCP in morphogenesis and tissue organization. Importantly, many PCP effectors appear to be context-specific, especially in vertebrates, and the potential outcomes of establishing a directional PCP signal become increasingly complex in multifaceted tissues comprising multiple layers, cell types, and behaviors. Animal models are excellent platforms for the study disease etiology and often necessary for the study of developmental signaling pathways such as PCP signaling, at least without removing essential inputs or components. It was with these themes in mind that work detailed below was carried out, in an attempt to establish a robust animal model to facilitate the study of vertebrate PCP signaling and provide the potential to study how PCP mutations might contribute to human pathologies.

CHAPTER 2: CONTROL OF PCP PATTERNING DYNAMICS BY PRICKLE2 IN THE XENOPUS MULTICILATED EPIDERMIS

Portions of this chapter are modified from: Butler, M.T. and Wallingford, J.B. Control of vertebrate core PCP protein localization and dynamics by Prickle2. Dev. (2015). 32 (6) 707-718

2.1: SPECIFIC PCP PROTEINS ASYMMETRICALLY PATTERN *XENOPUS* MULTICILIATED CELLS

The surface of tailbud stages *Xenopus* embryos is populated by dozens of multiciliated cells (MCCs) which drive polarized fluid flow across the surface of the tissue (Figure 7), and a role for PCP proteins in oriented multiciliary beating was first described here, in the *Xenopus* epidermis (Mitchell et al., 2009; Park et al., 2008). Surprisingly, there had not yet been reports of asymmetric localization of PCP proteins at the cell cortex in these cells or the tissue at large, though such localization was reported for both mouse airway (Vladar et al., 2012) and ependymal MCCs (Guirao et al., 2010). As *Xenopus* is a powerful tool for rapid localization screens *in vivo* and for studies of PCP signaling, I set out to identify faithful reporters of molecular PCP patterning in this tissue.

Several examples of cell- and tissue-specific differences in protein localization and function have been observed for different vertebrate PCP family members in the context of multiciliated epithelia. For example, Dvl2 is present at the basal bodies of MCCs, but does not display cortical asymmetry, while Dvl1 and Dvl3 are not at basal bodies, but rather are present at planar-polarized cortical crescents (Park et al., 2008; Vladar et al., 2012). The increased complexity seen in vertebrate PCP warranted further study of individual core PCP family members and challenging any assumed redundancy in their activity. To ensure adequate

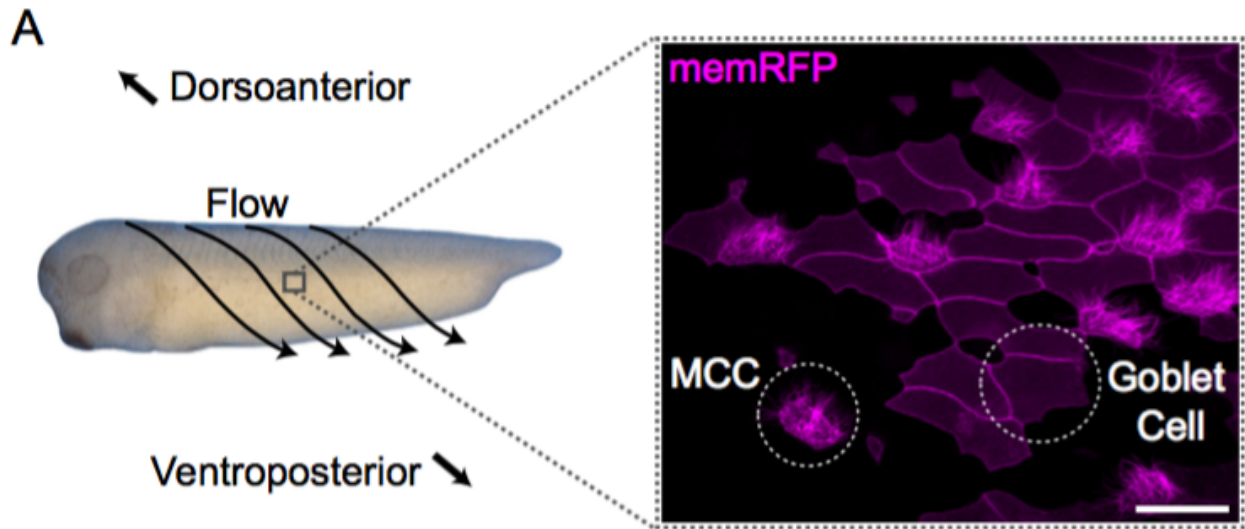**Figure 7**: Multiciliated cells drive polarized flow across the Xenopus epidermis. **(A)** *Xenopus laevis* embryo with flow and anatomical directionality denoted along with a confocal slice showing different cell types visualized via memRFP in a mosaically labeled epidermis. MCC, multiciliated cell. Note all images for Chapter 2 (Figures 7-24) are presented in this orienation. Scale bar: 50 μm

coverage over several members of the PCP multi-gene families, the localization of a wide range of GFP fusions to *Xenopus* PCP proteins were surveyed using mosaic expression for accurate assessment of asymmetric localization. While many previously studied *Xenopus* core PCP proteins localize symmetrically around the cell cortex, including Dvl2, Dvl3, Fzd7, Fzd8, and Vangl2, others, such as Fzd6, Dvl1, Pk2, and Vangl1 displayed striking asymmetric localization (Figures 8 and 9).

In *Xenopus* embryos, fluid flow is directed across the epidermis from the dorsoanterior to ventroposterior direction (Figure 7A); accordingly, punctate accumulations of Dvl1-GFP that were restricted to the dorsoanterior apical cell cortex of MCCs are found here, corresponding to asymmetry in the direction upstream of flow (Figure 9A). Mucociliary epithelia are comprised of two principal cell types, MCCs and mucus-secreting goblet cells, and because the MCCs are separated from one another by intervening goblet cells (Figure 7A), PCP signaling must be transmitted evenly across both cell types. It is notable then, that asymmetric accumulations of Dvl1 also occurred in goblet cells (Fig. 9B). Comparable asymmetry appeared to occur in other intercalating cell types, such as ioncytes (Dubaissi and Papalopulu, 2011; Quigley et al., 2011) and small secretory cells (Dubaissi et al., 2014; Walentek et al., 2014), which were identifiable by their significantly smaller surface area and lack of cilia in regions where only intercalating cells had been labeled.

Typically, asymmetric Dvl co-accumulates with asymmetric Frizzled at the cell cortex (Seifert and Mlodzik, 2007), and indeed, Fzd6-GFP also localized to the dorsoanterior cell cortex (Figure 8A). In most planar polarized tissues, domains enriched for Dvl and Fzd are mirrored by complementary accumulations of Prickle and Vangl (Seifert and Mlodzik, 2007), and I observed asymmetric accumulations of GFP-Pk2 (Figure 9C,D) and GFP-Vangl1 (Figure 9E,F) at the ventroposterior cell cortex in both MCCs and goblet cells as well. Moreover, co-expression of

39
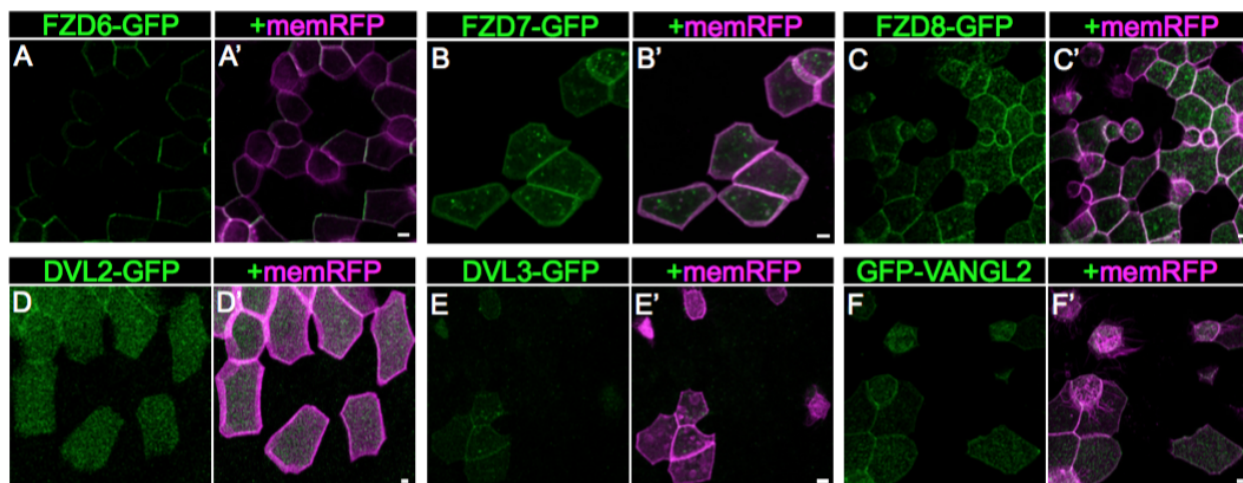
Figure 8: Cell localization can differ betwen particular PCP family members. **(A-F')** Mosaically labeled cells in stage 31 embryos labeled with PCP proteins fused to GFP and membraneRFP and surrounded by unlabeled neighbors. Frizzled-6 **(A)** displays asymmetric localization while Frizzled-7 (B), Frizzled-8 **(C)**, Dishevelled-2 **(D)**, Dishevelled-3 **(E)**, and Vangl2 **(F)** all decorate the cortex in a symmetric fashion. Scale bar = 5 μm

Dvl1-GFP and RFP-Pk2 revealed mutually exclusive domains of enrichment (Figure 10A), and clear colocalization was observed for RFP-Pk2 and GFP-Vangl1 proteins (Figure 10B). These observations of a Fzd family member on the anterior cell face and Vangl at the posterior are consistent with previous functional studies of domineering non-autonomy of PCP signaling in this tissue (Mitchell et al., 2009), though on the other hand, it was surprising that their orientation relative to the direction of ciliary beating is reversed compared to that of MCCs in the mouse trachea (Vladar et al., 2012).

2.2: DYNAMICS OF THE ASYMMETRIC LOCALIZATION OF PK2, VANGL1, AND DVL1

Having identified useful reporters for PCP patterning in the *Xenopus* embryonic epidermis, I next sought to characterize the developmental dynamics of core PCP protein localization here. MCCs are derived from a basal layer of progenitor cells and insert into the mucociliary epithelium at the early tailbud stage (~St. 22), after which cilia are assembled and polarization of ciliary beating is established progressively over the next several hours (until roughly St. 30) (Billett and Gould, 1971; Drysdale and Elinson, 1992; König and Hausen, 1993). Prior to the insertion of MCCs, Dvl1-GFP decorated the apicolateral regions of goblet cells symmetrically and in a punctate fashion (Figure 11A). During tailbud stages, as ciliogenesis is completed and the refinement of ciliary orientation begins, Dvl1-GFP asymmetry is present, though the degree and coordination of asymmetry is variable at this time. Dvl1-GFP asymmetry finally reaches a maximal level in both goblet cells and MCCs across the tissue around stage 30 (Figure 11B), a time at which ciliary basal body orientations are locked in place and flow has strengthened across the epithelium (König and Hausen, 1993; Mitchell et al., 2007; Werner et al., 2007). GFP-Pk2 displayed similar dynamics to Dvl1-GFP, with asymmetric accumulations also
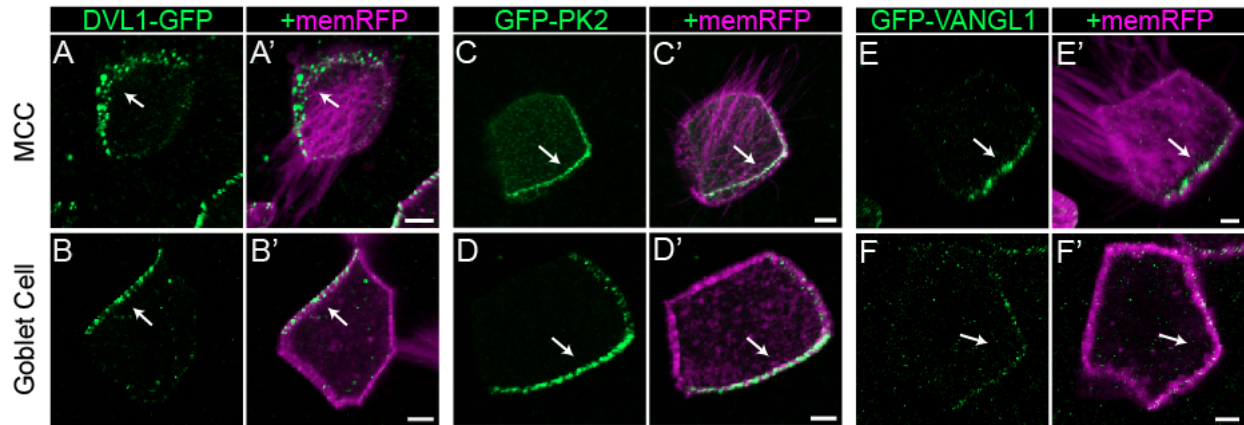
Figure 9: Dvl1, Pk2, and Vangl1 asymmetrically align with Xenopus MCC flow patterns. **(A-F')** MCCs **(A,C,E)** and goblet cells **(B,D,F)** in St.31 embryo surrounded by unlabeled neighbors display asymmetric core PCP protein localization in the direction indicated by the overlying arrows. Scale bar = 5 μm
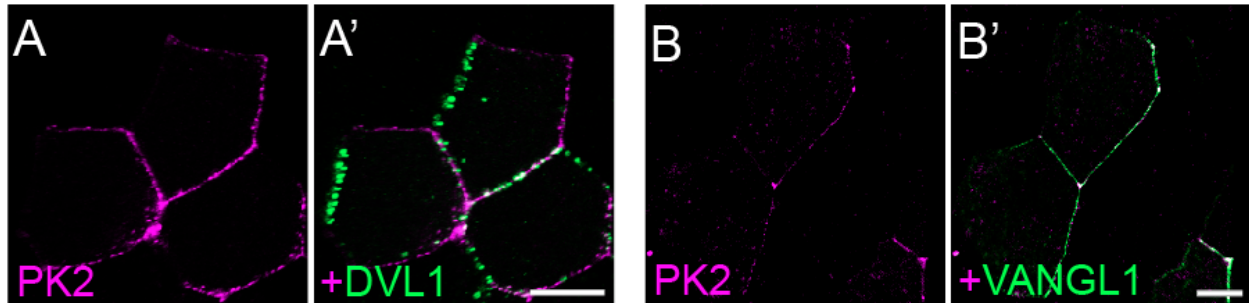
Figure 10: Pk2 forms mutually exclusive domains with Dvl1 and colocalizes with Vangl1. **(A-B)** Groups of *Xenopus* epidermal cells labeled with RFP-Pk2 and either Dvl1-GFP **(A)** or GFP-Vangl1 **(B)**. Scale bar = 10 microns

apparent by stage 24-25 that reach a maximum around stage 30 (Figure 11C,D), though with some notable differences. First, although GFP-Pk2 also localizes symmetrically to apical accumulations just prior to ciliogenesis, the punctate pattern observed for Dvl1-GFP was less prominent for GFP-Pk2 (Figure 11C). Another interesting dissimilarity was the localization of GFP-Pk2 near ciliary basal bodies labeled with Centrin-RFP at later stages (Figure 12). For the transmembrane protein Vangl1, localization of GFP fusions at early stages consisted primarily of cytoplasmic puncta, and labeling at the cell cortex was weak and diffuse at these stages (Figure 11E). This pattern may reflect the vesicular transport proteins known to be important for the processing and trafficking of Vangl proteins (Guo et al., 2013; Merte et al., 2009; Yin et al., 2012). Both the cortical localization and asymmetry of these accumulations increased as development proceeded, with a timeframe similar to that for Dvl1 and Pk2 (Figure 11F).

In efforts to chart the changes in localization asymmetry these markers over time, I quantified these dynamic localization patterns using the relative level of reporter fluorescence intensity at dorsoanterior and ventroposterior cell cortices, and mosaic labeling allowed us score cells abutting unlabeled neighbors (Figure 13). This metric demonstrates the degree to which asymmetry increased over time during PCP patterning for all three reporters examined (Figure 11G-I). Interestingly, PCP enrichment increased along with increased coordination of fluid flow (König and Hausen, 1993), and asymmetries were not easily detectable at times corresponding to stages of initial MCC intercalations. Once MCCs have intercalated and expanded their apical surface, basal bodies are docked and serve as the foundations for cilia formation. Once these cilia are visibly projecting from the apical surface, the surrounding goblet cells can be seen exhibiting asymmetric patterns that are readily detectible by eye; though no such patterns are easily discernible in the MCCs. This result suggests that the initial rotational polarity of basal bodies that is in place at the onset of ciliogenesis, which clearly depends upon intact Dvl2

43
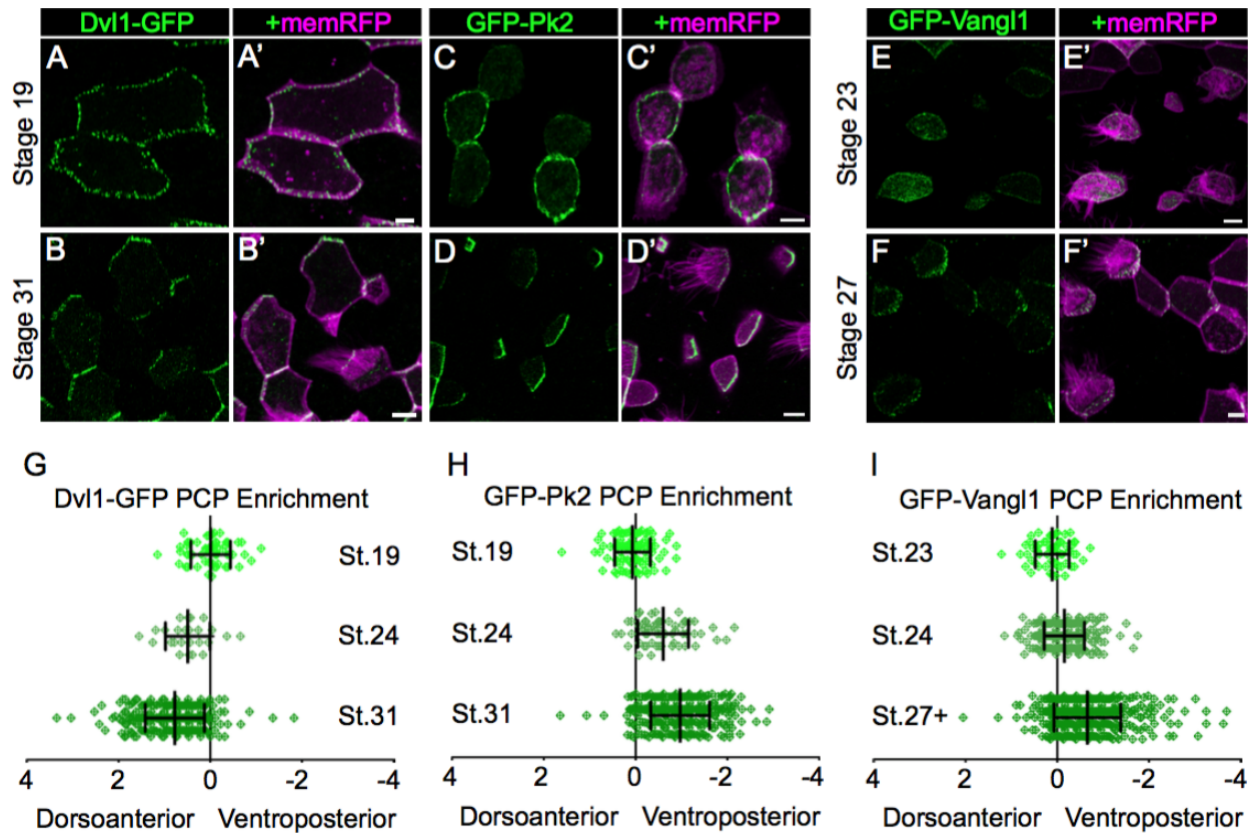
Figure 11: PCP asymmetry is refined over time, coinciding with polarized ciliary orientation. (A-D) Patches of cells mosaically labeled with either Dvl1-GFP (A,B) or GFP-Pk2 (C,D) at stages prior to ciliogenesis (St.19) and after basal body refinements (St.31). (E,F) Patches of cells mosaically labeled with GFP-Vangl1 at stages during ciliogenesis (St.23) and during basal body refinement (St.27). (G-I) Quantifications of PCP Enrichment at different developmental stages show increasing asymmetry develops during basal body refinement. Each mark represents the enrichment value for a single cell. (G) Dvl1-GFP enrichment was measured at St.19 (n = 58), St.24 (n = 25), and St.31 (n = 321). (H) GFP-Pk2 enrichment was also measured at St.19 (n = 58), St.24 (n = 25), and St.31 (n = 321). (I) GFP-Vangl1 enrichment was measured in a narrower window at St. 23 (n = 61), St.24 (n = 268), and St.27+ (n = 465). All comparisons within graphs are highly significant ($P<0.0001$) except for a modest increase between Dvl1 St.24 to St.31 ($P=0.0366$). Error bars indicate Standard Deviation of the mean; Mann-Whitney Statistical tests. Scale bars: 10 μm.
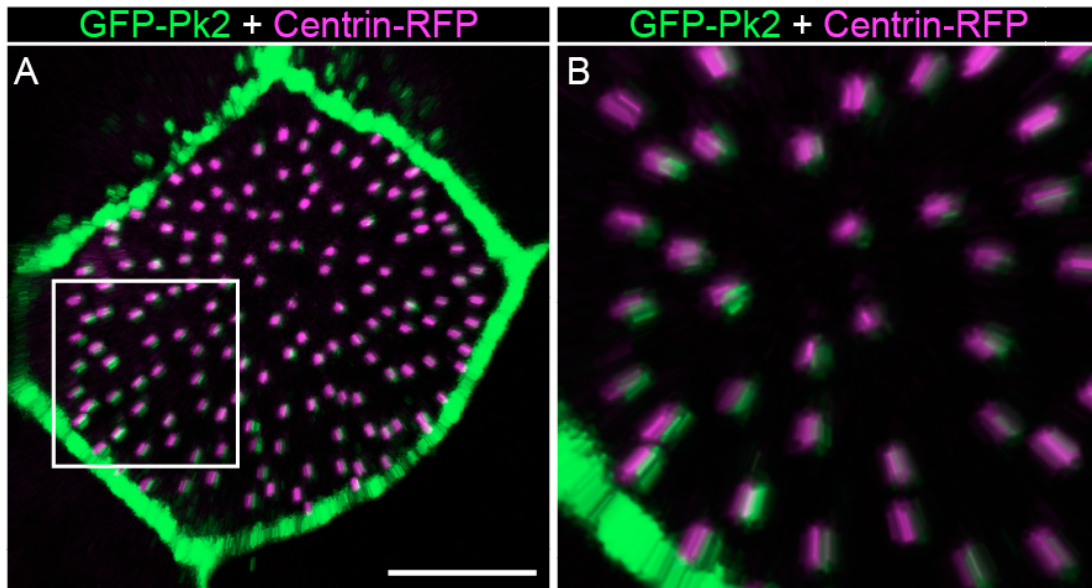
Figure 12: Pk2 localizes to ciliary basal bodies of *Xenopus* MCCs. GFP-Pk2 assumes a polarized localization near basal bodies labeled with Centrin-RFP after the finalization of basal orientation refinement (St.35 shown). Note that this cell is surrounded by similarly labeled cells, making the Pk2 cortical asymmetry less apparent. Box in **(A)** demarcates the area magnified in **(B)**. Scale bar: 10μm.
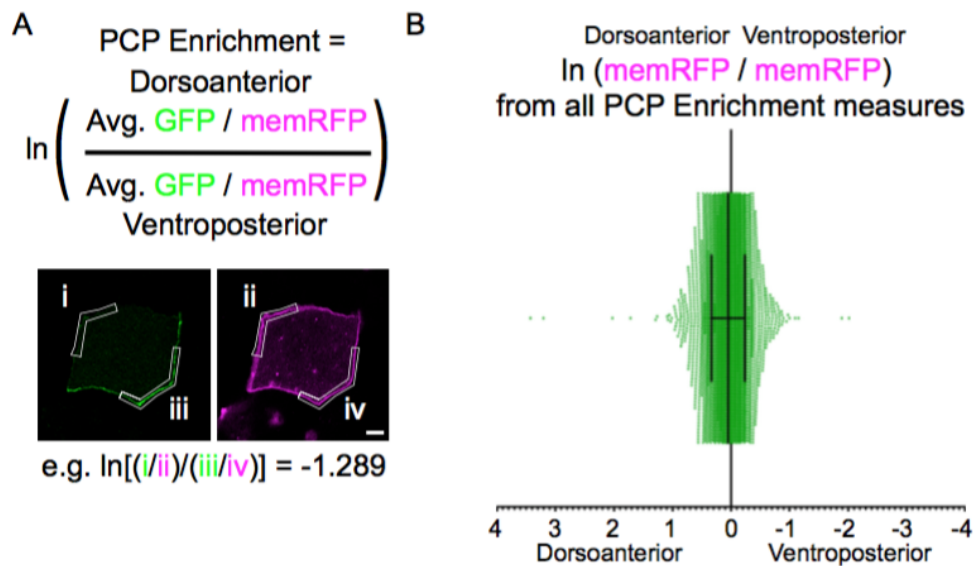
Figure 13: PCP enrichment is a measure of asymmetric localization. (A) Equation used and an example for calculating PCP Enrichment (GFP-Pk2 and memRFP shown). (B) Plot of enrichment values for dorsoanterior and the complementary ventroposterior memRFP measurements in consideration without the associated GFP PCP fusion measurements for all PCP Enrichment measurements in presented in Figures 11, 14, 15, 16, 17, 19 & 21 (n = 5,394). A value of 0 represents no difference in intensity.

45

function (Mitchell et al., 2007), may not be reliant upon intracellular PCP asymmetry, but rather the surrounding tissue imparts that directional information instead. However, it has also been reported that polarity information can be relayed in the absence of detectible asymmetry in the fly wing (Strutt and Strutt, 2007, Chien et al. 2015), so perhaps asymmetric stability or activity in the absence of clear asymmetric localization may be present in this context as well.

2.3: INTERPLAY BETWEEN THE CORTICAL ASYMMETRIC LOCALIZATIONS OF PK2 AND DVL1

The interplay among Pk2 and Dvl1 during asymmetric localization was the next focus of study, as antagonistic interactions between proteins homologous to them are fundamental to amplifying visual intracellular asymmetry in other contexts (Strutt and Strutt, 2007), yet have never been examined for these particular family members or in this tissue. I first determined the effect of the well-characterized and PCP-specific dominant negative, Dvl2-DPDZpartial (Xdd1) (Sokol, 1996), shown to negatively affect PCP signaling in a variety of contexts, including in MCCs (Park et al., 2008; Wallingford et al., 2000). Expression of Dvl2-DPDZpartial significantly disrupted the normal ventroposterior restriction of Pk2-GFP (Figure 14A-C), demonstrating asymmetric Pk2 localization is dependent upon the ability of the cell to adopt a planar-polarized state. I then performed the complementary experiment by reducing Pk2 levels using an antisense morpholino (Pk2-MO1) that disrupts splicing of Pk2 (Figure 15A). While discrete crescents of Dvl1-GFP accumulation were normally oriented in the dorsoanterior direction in controls (Figure 14D), Pk2 knockdown significantly reduced this asymmetric enrichment (Figure 14E-F), and a second morpholino targeting an alternate splicing sequence provided similar results (Figure 15B). Together with the observed progressive asymmetric localization (Figure 11), these data demonstrate the efficacy and veracity of our GFP reporters
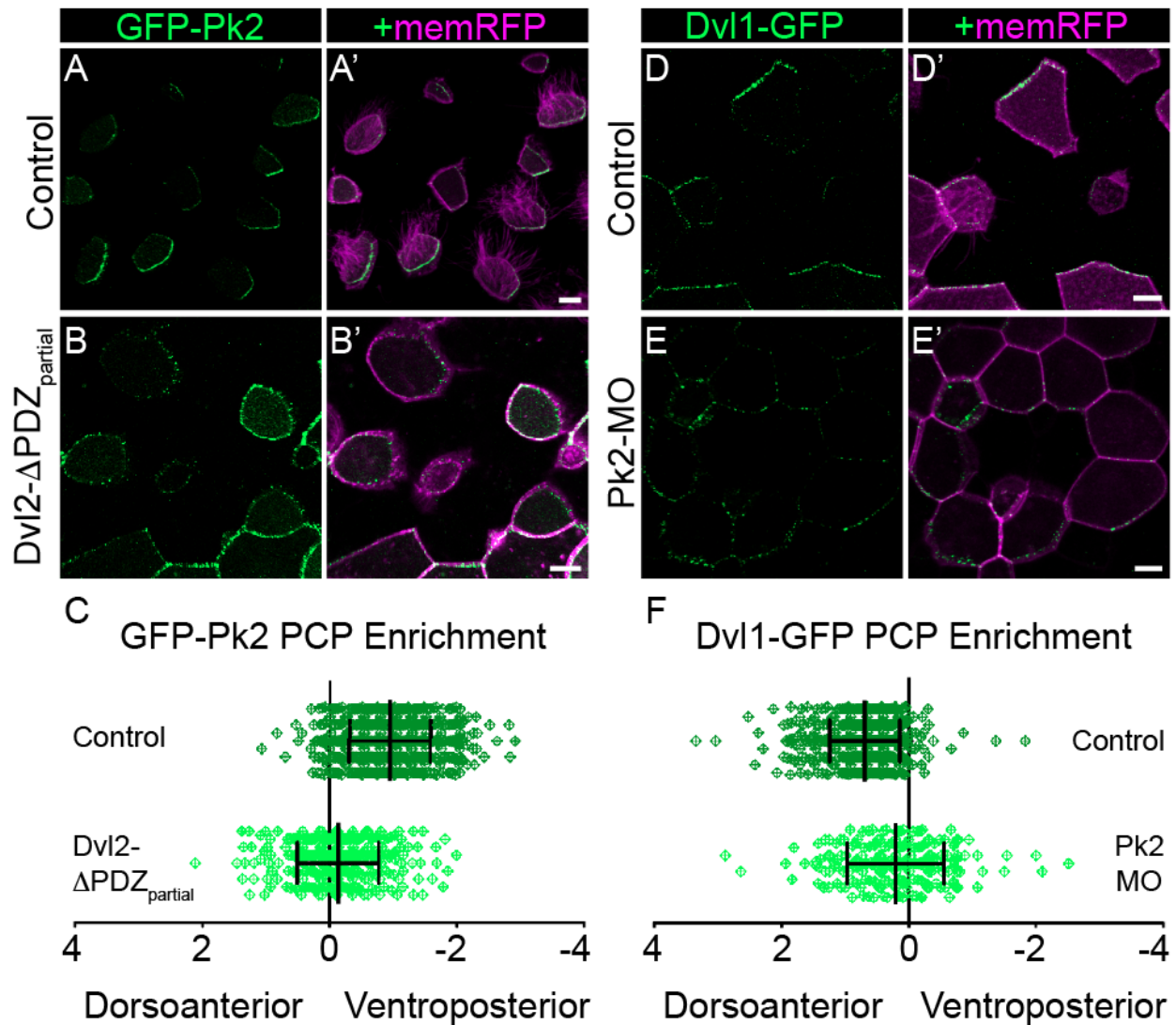
Figure 14: Intact PCP signaling is required for the formation of asymmetric core PCP complexes. **(A,B')** Mosaically-labeled epidermal cells in St.31 *X.laevis* embryos have GFP-Pk2 localized asymmetrically in the control situation **(A)** and symmetrically upon overexpression of Dvl2-ΔPDZ$_{partial}$ **(B)**. **(C)** Quantification of PCP Enrichment shows in that comparison to controls (n = 584), there is a significant shift upon Dvl2-ΔPDZ$_{partial}$ expression (n = 326, P<0.0001). **(D-E')** Mosaically-labeled epidermal cells in St.31 *X.laevis* embryos have GFP-Pk2 localized asymmetrically in the control situation **(D)** and symmetrically upon Pk2-MO knockdown **(E)**. **(F)** Quantification of PCP Enrichment shows that in comparison to controls (n = 508), there is a significant shift upon Pk2-MO knockdown (n = 210, P<0.0001). Error bars indicate Standard Deviation of the mean; Mann-Whitney Statistical tests. Scale bars: 10 μm.
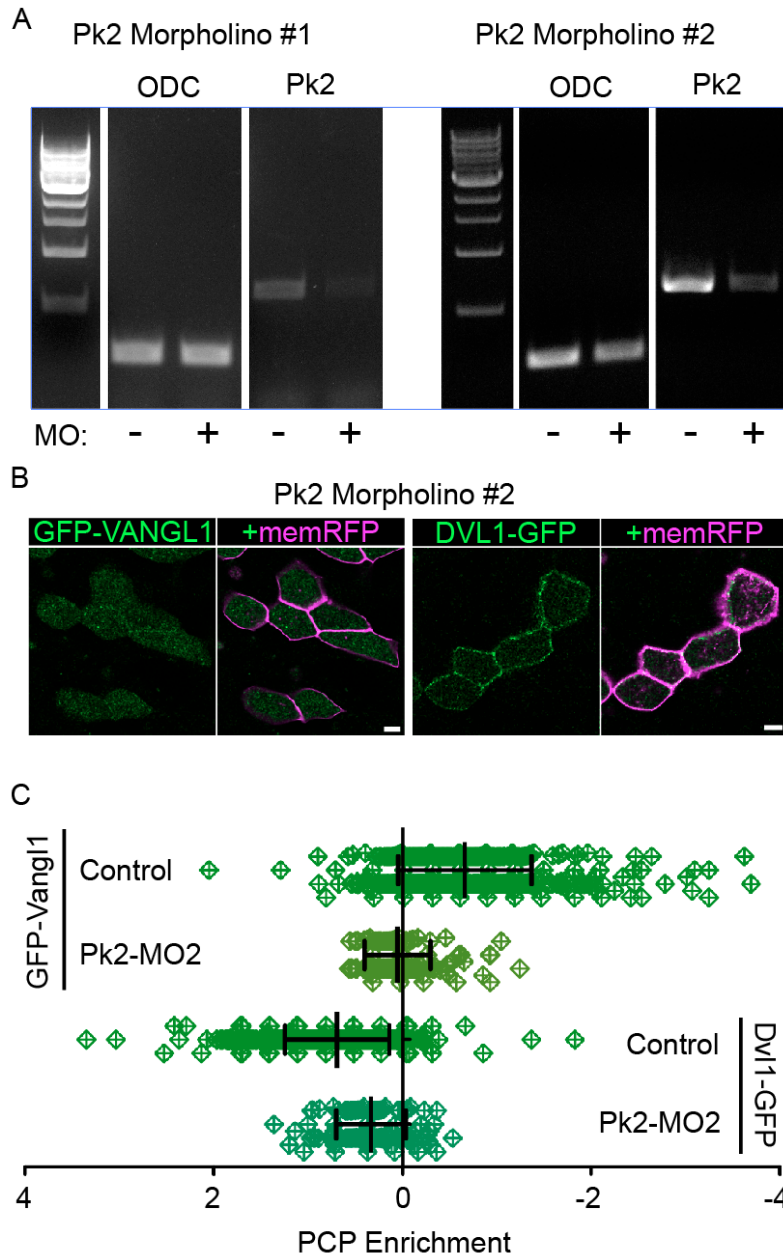
Figure 15: Pk2 morpholinos reduce Pk2 mRNA levels **(A)** RT-PCR results for the amplification of a control, ornithine decarboxylase (ODC), and morpholino-targeted Pk2 sequence from cDNA of embryos that were either uninjected or injected with Pk2 morpholino #1 or #2 into 4 of 4 cells, demonstrating a significant reduction of only the Pk2 PCR product in morpholino-injected embryos. **(B)** Cells in St.31 embryos labeled with PCP proteins fused to GFP and memRFP with an included dose of Pk2 morpholino #2, showing similar effects to Pk2 morpholino #1 shown in Figures 12 and 16. (C) Graph depicting changes in normal localization of Vangl1 (n = 519) and Dvl1 (n = 508) caused by Pk2 knockdown with a second Pk2 morpholino (Pk2-MO#2) targeting an alternative splicing site from the first. PCP enrichment is significantly reduced for both GFP-Vangl1 (n = 137, *P*<0.0001) and Dvl1-GFP (n = 131, *P*<0.0001) in morphant cells.   Error bars indicate Standard Deviation of the mean, Mann-Whitney statistical tests. Scale bars: 10μm.

for core PCP protein localization in this tissue and tools for manipulating PCP signaling in this system.

2.4: ROLE OF PCP EFFECTORS INTURNED AND WDPCP IN PK2 PROTEIN LOCALIZATION

With useful PCP reporters in hand, I sought to uncover novel reporters to address outstanding questions in vertebrate PCP signaling. First, I assessed the role of the "PCP Effector" proteins in the patterning of polarity complexes, as the role for these proteins in PCP signaling remain contentious. First identified as planar polarity proteins by genetic screens in *Drosophila* (Collier et al., 2005; Gubb and Garcia-Bellido, 1982), Inturned and Fritz were placed genetically downstream of core PCP protein function (Collier et al., 2005; Lee and Adler, 2002; Wong and Adler, 1993), though a more recent study suggests that Fritz overexpression can influence core PCP protein localization in *Drosophila* (Wang et al., 2014). Curiously, the vertebrate orthologues, (called Intu and Wdpcp/Fritz) were found to control ciliogenesis, first in the *Xenopus* epidermis (Kim et al., 2010; Park et al., 2006) and later in mice (Cui et al., 2013; Zeng et al., 2010). Intu apparently plays only a modest role in PCP mediated processes such as convergent extension (Park et al., 2006), while Wdpcp is essential for both convergent extension in *Xenopus* (Kim et al., 2010) and planar polarization of cochlear hair cells in the mouse (Cui et al., 2013). I performed knockdown of Wdpcp and Intu using morpholinos whose action has been validated by genetic studies in mice (Cui et al., 2013; Kim et al., 2010; Park et al., 2006; Zeng et al., 2010). Wdpcp knockdown strongly disrupted the planar polarized localization of Pk2, while Intu knockdown had a far more modest, though still significant effect (Figure 16A-C). These data reveal an important role for Wdpcp in control of core PCP protein asymmetry in vertebrates, the mechanism of which will be important to determine.
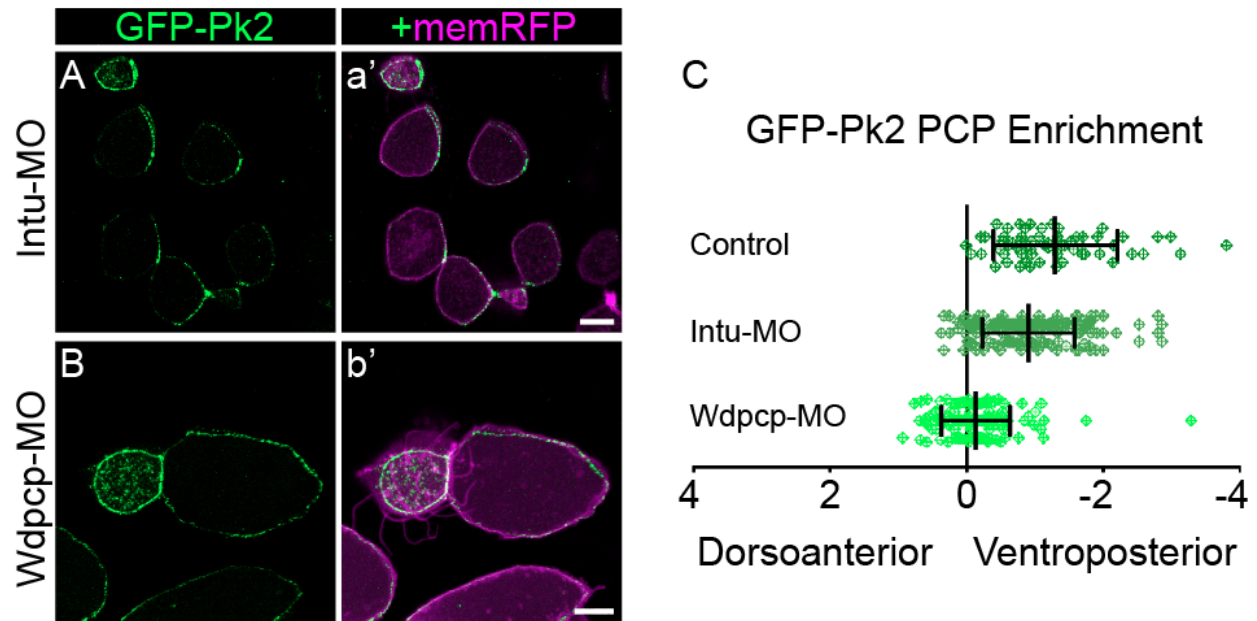
Figure 16: Wdpcp knockdown disrupts core PCP patterning. **(A-B')** Mosaically-labeled epidermal cells in St.31 *X.laevis* embryos have GFP-Pk2 localized asymmetrically upon Intu-MO knockdown **(A)** and symmetrically upon Wdpcp-MO knockdown **(B)**. **(C)** Quantification of PCP Enrichment shows that in comparison to controls (n = 64), there is a significant shift upon Intu-MO knockdown (n =187, *P*=0.0031) and more significant shift upon Wdpcp-MO knockdown (n =137, *P*<0.0001). Error bars indicate Standard Deviation of the mean; Mann-Whitney statistical tests. Scale bars: 10 μm.

2.5: ROLE OF PK2 IN THE CONTROL OF ASYMMETRIC CORTICAL VANGL1 DYNAMICS

The next question I chose to address concerns the interplay between Pk2 and Vangl1. In *Drosophila*, Pk physically interacts with and clusters Vang at the apicolateral membrane, and this behavior promotes Vang accumulation on the proximal side of cells in the wing epithelium (Bastock et al., 2003; Jenny et al., 2003). Though Vangl2 and Pk1 are implicated in vertebrate PCP (Liu et al., 2014; Song et al., 2010; Takeuchi et al., 2003; Torban et al., 2008; Vladar et al., 2012), Vangl1 and Pk2 remain relatively seldom studied, and it is unknown in vertebrates if either Pk protein is required for normal localization of either Vangl protein. I found that Pk2 knockdown eliminated the asymmetric accumulation of GFP-Vangl1 at the ventroposterior cell cortex (Figure 17A,B), while conversely, Pk2 overexpression increased Vangl1 apicolateral enrichment to such a degree that accumulations were no longer as restricted to just ventroposterior regions, but rather enriched in other areas around the cell periphery (Figure 17C). Additional analysis confirms that Pk2 knockdown disrupts asymmetry by suppressing the enrichment of Vangl1 at the cortical regions of the cell (Figure 18A,B), and together, these observations are consistent with a previously defined role for Pk in the clustering of Vang (Bastock et al., 2003; Cho et al., 2015; Strutt and Strutt, 2007). I conclude that Pk2 promotes cortical Vangl1 concentration, while an excess of Pk2 promotes further GFP-Vangl1 enrichment that becomes increasingly unrestricted from the ventroposterior cell face.

In the reciprocal experiment, overexpression of Vangl1 showed a clear reduction in the planar-polarized, cortical accumulation of GFP-Pk2 (Figure 19A,C), while enrichments of Dvl1-GFP were still present yet not asymmetrically polarized (Figure 19B,C). In light of previous evidence that Vang participates in the control of Pk protein levels (Strutt et al., 2013b), our

51
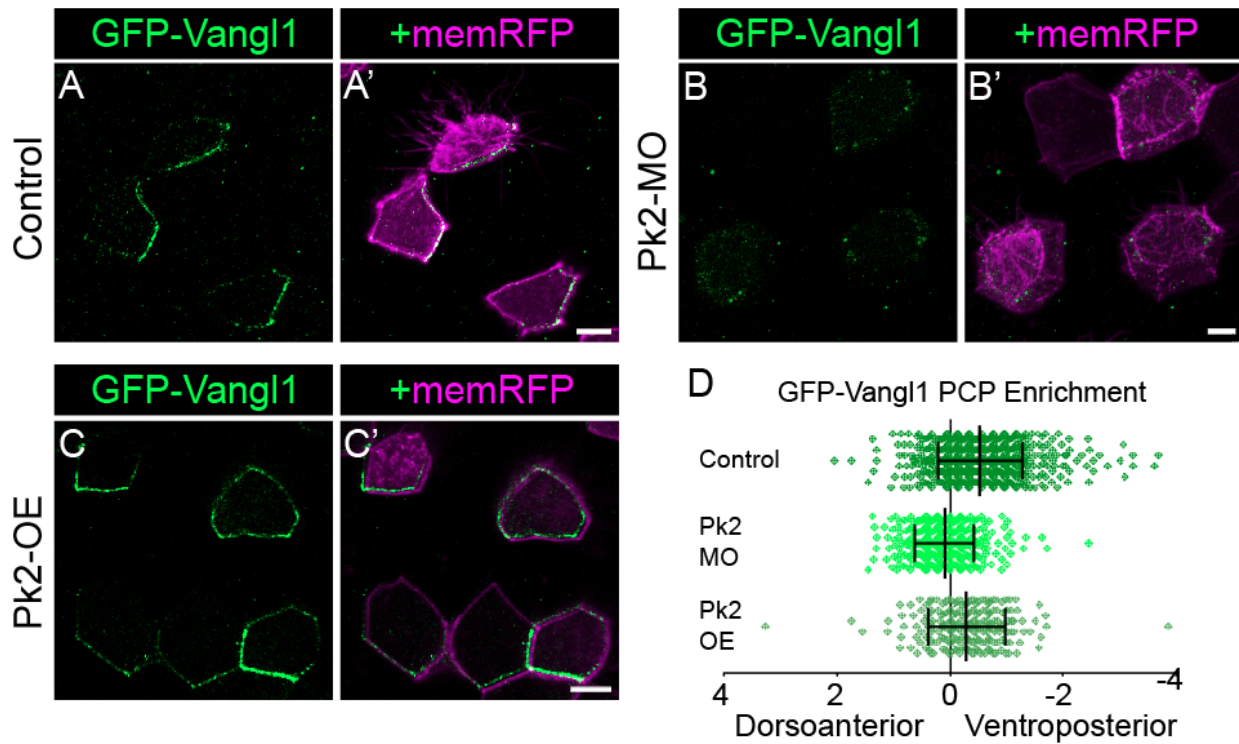
Figure 17: Pk2 expression levels influence the asymmetric localization of Vangl1. **(A-C')** Mosaically labeled epidermal cells in St.31 *X. laevis* embryos have GFP-Vangl1 localized asymmetrically in the control situation **(A)**, whereas it is absent from apicolateral enrichments upon Pk2-MO knockdown **(B)** and localized more symmetrically with Pk2 overexpression **(C)**. **(D)** Quantification of PCP Enrichment shows that in comparison to controls (n = 519), there is a significant shift upon Pk2-MO knockdown (n = 355, *P*<0.0001) and Pk2 overexpression (n = 217, *P*=0.0002). Error bars in D indicate Standard Deviation of the mean; Mann-Whitney Statistical tests. Scale bars: 10 μm.
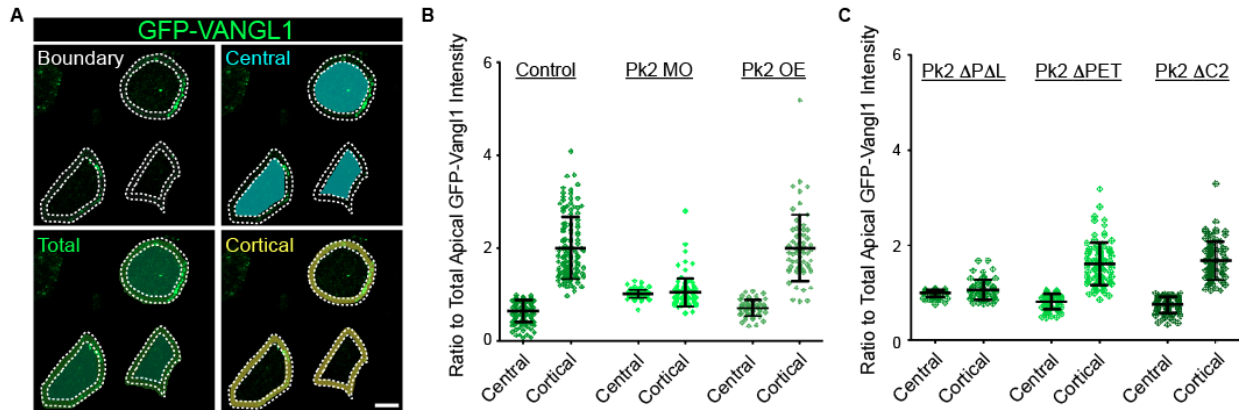
Figure 18: Pk2 influences the apicolateral enrichment of Vangl1. **(A)** Schematic of quantification method of data presented in **(B,C)**. Either the average cortical fluorescence intensity or the average intensity of the remaining central area within each cell was divided by the average fluorescence intensity of the total apical surface area (both regions combined). **(B)** Quantification data showing a significant loss of cortical enrichment of GFP-Vangl1 upon Pk2-MO knockdown. Each dot represents one cell, and each cell has both a Central and a Cortical quotient presented with the total apical fluorescence measure as the divisor. Combined, these two measurements are highly significant from another in the control (n = 123) and Pk2-OE (n = 63) conditions ($P<0.0001$) but not significant for Pk2-MO#1 knockdown (n = 94, $P=0.2854$). Error bars indicate Standard Deviation of the mean; Mann-Whitney statistical tests. **(C)** Quantification data showing a significant loss of cortical enrichment of GFP-Vangl1 upon overexpression of Pk2-ΔPETΔLIM using the same quantification scheme as **(B)**. Combined, these two measurements are highly significant from another in the Pk2-ΔPET (n = 85, $P<0.0001$)) and Pk2-ΔC2 (n = 84, $P<0.0001$)) conditions but not significant for Pk2-ΔPETΔLIM (n =58, $P=0.1519$). Error bars indicate Standard Deviation of the mean; Mann-Whitney statistical tests. Scale bar: 10 μm.
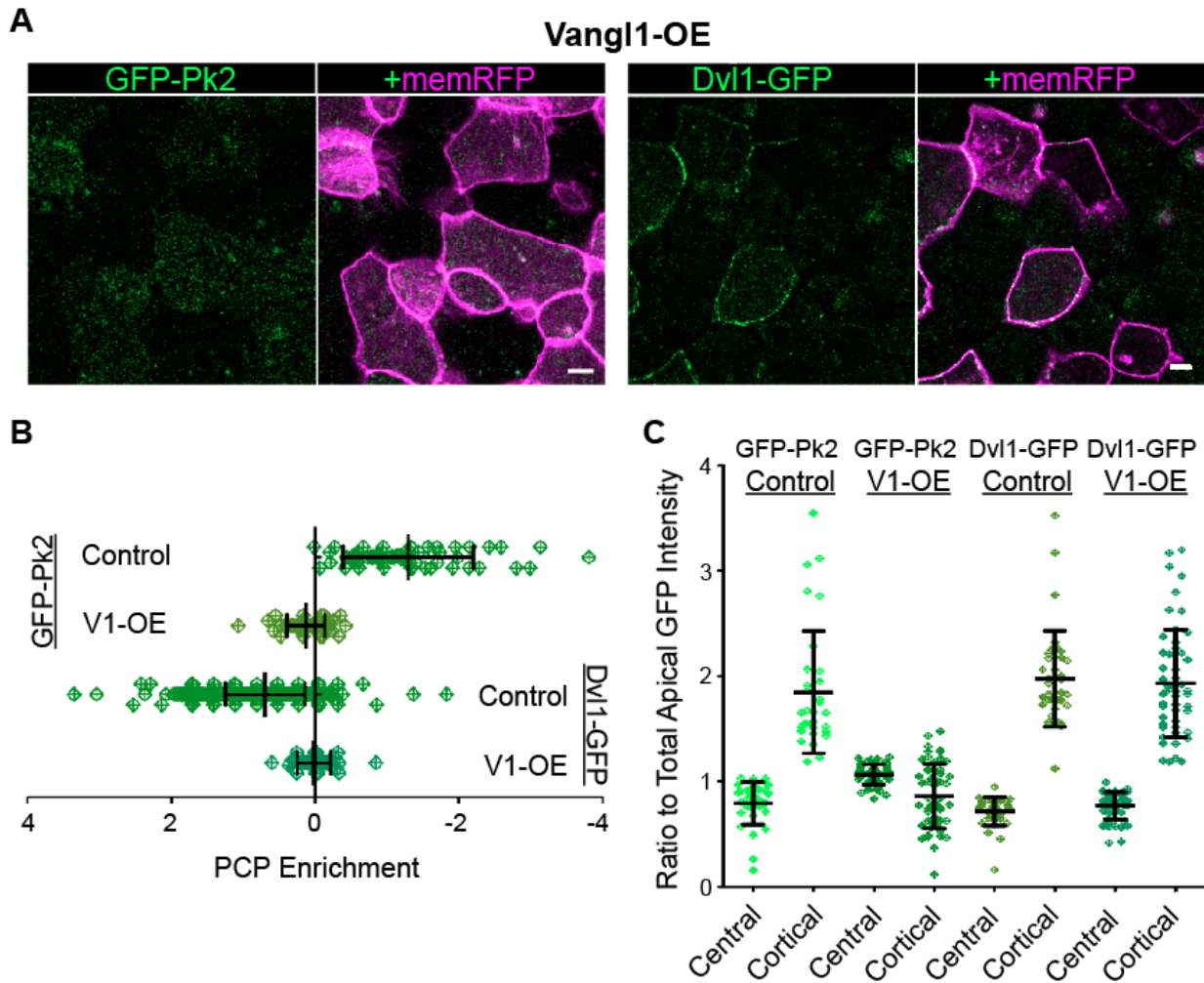
Figure 19: Vangl1 Overexpression leads to PCP patterning defects. (A) Cells in stage 31 embryos labeled with PCP proteins fused to GFP and membraneRFP as well as overexpressing Vangl1 display loss of Dvl1-GFP asymmetry and reduction in GFP-Pk2 cortical enrichment. (B) Graph depicting changes in PCP Enrichment of Pk2 and Dvl1 caused by Vangl1 overexpression (V1-OE). PCP enrichment is significantly reduced in cells overexpressing Vangl1 (n = 60 for Pk2, n = 55 for Dvl1) in comparison to controls for both GFP-Pk2 (n = 64) (p<0.0001***) and Dvl1-GFP (n =243) (p<0.0001***). (C) Quantification data showing a significant loss of cortical enrichment of GFP-Pk2 but not Dvl1-GFP upon Vangl1 overexpression (V1-OE). Each dot represents one cell, and each cell has both a Central and a Cortical measurement presented as divided by the total apical fluorescence (See Fig. 18A for quantification schematic). These Central and Cortical measurements are highly significant from one another in both control Pk (n = 33, *P*<0.0001) and Dvl1 (n = 36, *P*<0.0001), Dvl1 with V1-OE (n = 53, *P*<0.0001), and Pk2 with V1-OE (n = 53, *P*=0.0002) conditions, but only in the case of GFP-Pk2 in V1-OE embryos is the mean Cortical enrichment less than the Central measure. Error bars indicate Standard Deviation of the mean; Mann-Whitney statistical tests. Scale = 10 μm.

results suggest that Vangl1 overexpression may be leading to increased levels of Pk2 degradation, which in turn leads to a reduction in Pk2 and associated Dvl1 patterning defects.

Given the demonstrated effects of Pk2 on the asymmetric enrichment of Vangl1, I next asked if Pk2 influences the dynamics of Vangl1 turnover at the cell cortex. Indeed, asymmetric enrichment of Fzd is driven in part by differences in Fzd turnover at distinct locations along the cell cortex (Strutt et al., 2011), and I wanted to test if a similar mechanism may act on Vangl. I therefore measured fluorescence recovery after photobleaching (FRAP) of GFP-Vangl1. In control embryos, enriched regions at the ventroposterior cortex contained a significantly larger stable fraction of GFP-Vangl1 when compared to the less-enriched dorsoanterior cortex (Figure 20A,B). This result was evident as the ~30% increase in normalized fluorescence recovery at the latter (Figure 20B). This difference was potently extinguished by Pk2 knock down, in which case both dorsoanterior and ventroposterior cortical regions contain similarly unstable fractions of GFP-Vangl1 (Figure 20B). In the complementary experiment, overexpression of Pk2 had the opposite effect, eliciting increased stability of GFP-Vangl1 on both sides of the cell (Figure 20B). These data complement the previous work with Dvl-dependent Fzd stabilization in *Drosophila* (Strutt et al., 2011), not only by extending the work to a vertebrate epithelium, but also by demonstrating that asymmetric protein turnover is an attribute of core PCP protein localization on the Vangl/Pk side of the cell.

2.6: STRUCTURE/FUNCTION ANALYSIS OF PK2 DOMAINS CONTROLLING PCP LOCALIZATION

As the role for Pk2 in the control of core PCP dynamics became quite clear, I sought to determine the structural components of the protein necessary for eliciting the observed polarized behaviors. Pk2 contains three protein domains that are conserved in vertebrate Prickle protein
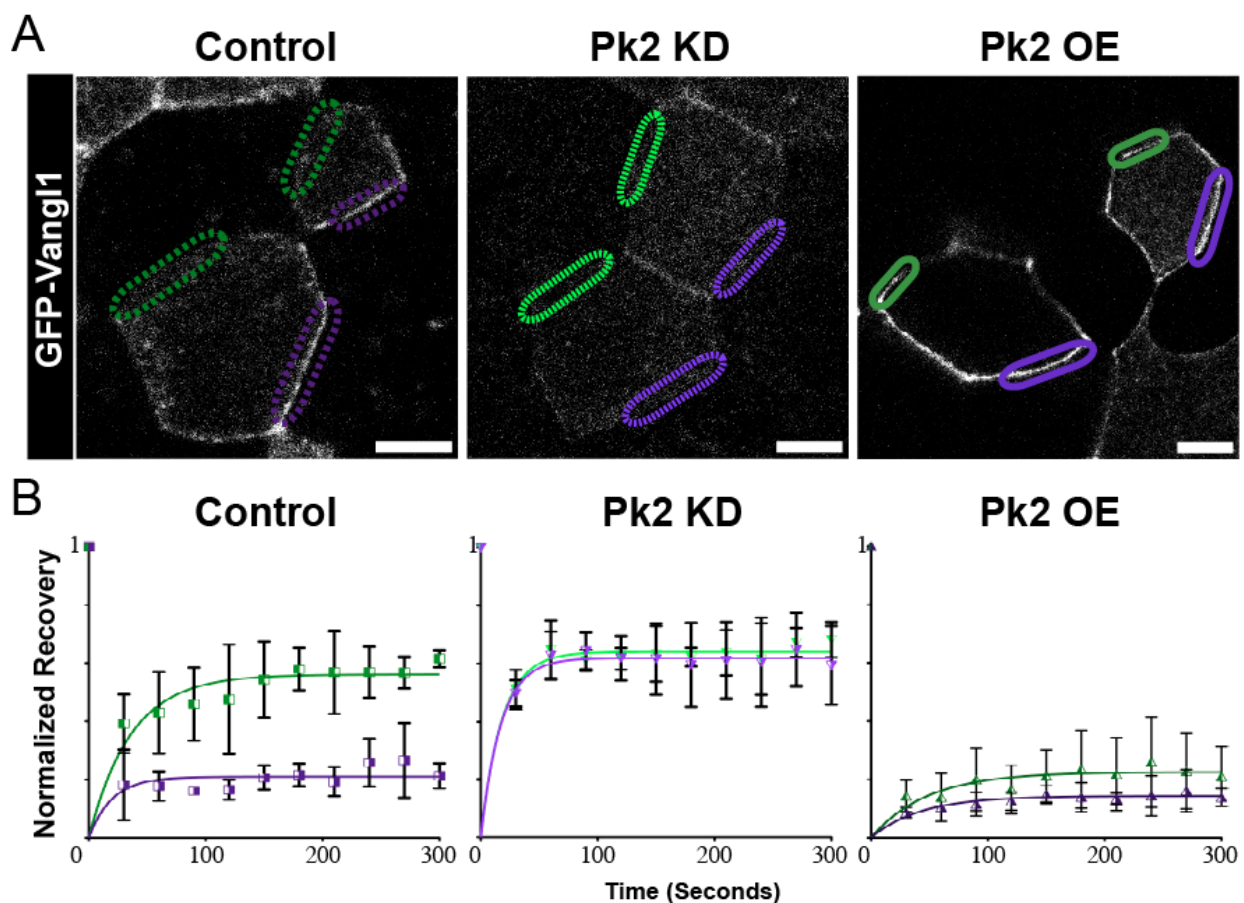
Figure 20: Prickle2 influences the junctional localization dynamics of Vangl1 **(A)** Demonstrations of typical shape and orientation of regions bleached and measured for intensity recovery quantifications shown in **(B)** FRAP recovery curves for GFP-Vangl1 fluorescence intensity following simultaneous bleaching at discrete dorsoanterior (green lines) and ventroposterior (purple lines) cortical regions in St.25 embryos. Error bars represent the standard error of the mean (SEM) from 3 separately bleached cells in 2-3 different embryos. Scale bar: 10 μm in A.

family members and in Prickle proteins across species (Figure 21A). These include the PET and LIM domains, as well as the C2 domain, which populated by many serines and basic amino acids near the C-terminus of the protein (Jenny et al., 2003; Tree et al., 2002). The roles for various domains of vertebrate Prickle proteins in PCP-dependent processes have been assessed (Daulat et al., 2011; Jenny et al., 2003; Lin and Gubb, 2009; Takeuchi et al., 2003), but how these roles relate to PCP protein localization remains unknown in vertebrates. I therefore constructed three Pk2 deletion constructs corresponding to previously described versions of *Xenopus* Pk1 (Takeuchi et al., 2003) and *Drosophila* Pk (Jenny et al., 2003); I then assessed both their localizations and their effects of the localization of Vangl1 and Dvll.

I first examined GFP fusions to a deletion of the PET domain and a combined deletion lacking both the PET and LIM domains. Strikingly, both Pk2-ΔPETΔLIM and GFP-Pk2-ΔPET were enriched ventroposteriorly (Figure 21B,C). While this polarization for GFP-Pk2-ΔPET was not as robust as full-length GFP-Pk2 (Figures 9C-D, 11D, 14A), it was remarkably similar and suggests that neither the PET nor LIM domain is strictly required for proper Pk2 asymmetric localization. Despite their similar localizations, however, these two constructs had divergent effects on Vangl1 when expressed at high levels. Pk2-ΔPETΔLIM severely perturbed not only the asymmetry of Vangl1, but also its association with the cell cortex (Figure 21F), comparable to the effects of Pk2 knockdown (Figure 18C). In contrast, both cortical recruitment and asymmetry of Vangl1 were intact after overexpression of Pk2-ΔPET (Figure 21G) despite a significant reduction in the overall enrichment measure. Together, these findings are consistent with the opposing effects of ΔPETΔLIM and ΔPET deletions of Pk1 on PCP-dependent convergent extension (Takeuchi et al., 2003).

I next assessed a deletion of the C2 domain, which in *Drosophila* allows for binding to Vang, to other Pk molecules, and to Dgo (Jenny et al., 2003). Unlike the other deletions, GFP-
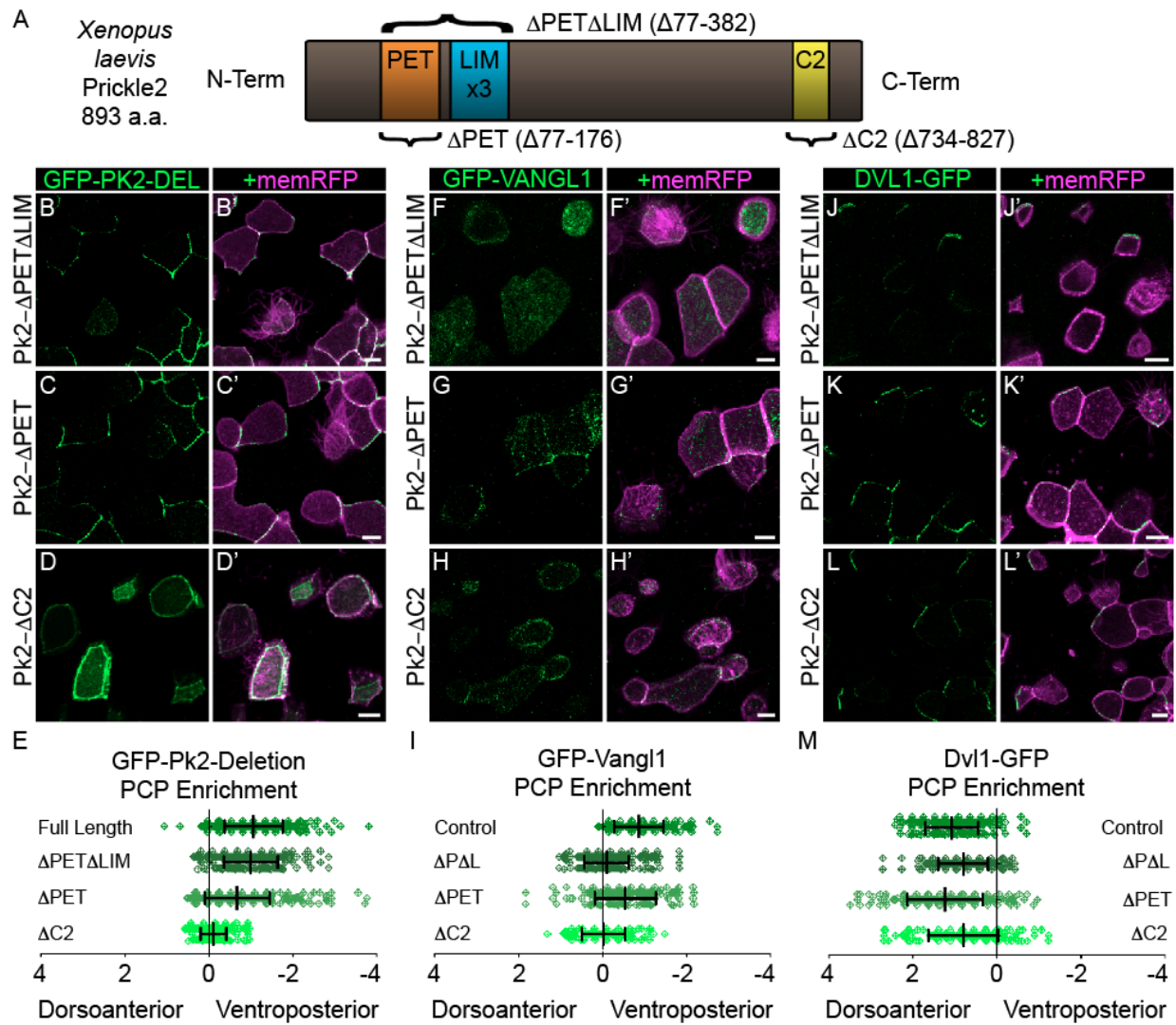
Figure 21: The Pk2 conserved domains differentially influence core PCP patterning. **(A)** Schematic of *X. laevis* Prickle2 and location of conserved domains removed from Pk2 deletion constructs. **(B-D')** Cellular localizations of GFP-Pk2 with sequence deletions that correspond to the PET and LIM domains (B), PET domain alone (C), and C-terminal region C2 **(D)**. **(E)** Graph depicting changes in localization of full length Pk2 (n = 374) caused by conserved domain deletions, with the normal localization of GFP-Pk2-ΔPETΔLIM (n = 312, *P*=0.4037), still asymmetric yet significantly misaligned GFP-Pk2-ΔPET (n = 379, *P* <0.0001), and symmetric GFP-Pk2-ΔC2 (n = 302, *P*<0.0001). **(F-H')** Cellular localizations of GFP-Vangl1 upon the overexpression of Pk2-ΔPETΔLIM (F), Pk2-ΔPET **(G)**, and Pk2-ΔC2 **(H)**. **(I)** Graph depicting changes in the normal localization of Vangl1 (n = 215) caused by overexpression of Pk2 deletions, with a loss of asymmetry upon overexpression of Pk2-ΔPETΔLIM (n = 310, *P*<0.0001) and Pk2-ΔC2 (n = 203, *P*<0.0001) and significant reduction upon Pk2-ΔPET overexpression (n =125, *P*=0.0001). **(J-L')** Cellular localizations of Dvl1-GFP upon the overexpression of Pk2-ΔPETΔLIM (J), Pk2-ΔPET (K), and Pk2-ΔC2 **(L)**. **(M)** Graph depicting changes in the normal localization of Dvl1 (n = 243) caused by overexpression of Pk2 deletions, with a significant shift in but not loss of asymmetric enrichment upon Pk2-ΔPETΔLIM (n = 206, *P*<0.0001), Pk2-ΔPET (n = 212, *P*=0.0181), and Pk2-ΔC2 overexpression (n = 163, *P*=0.0002). Error bars indicate Standard Deviation of the mean; Mann-Whitney statistical tests. Scale bars: 10 μm.

58

Pk2-ΔC2 failed to adopt a polarized localization and instead remained symmetrical around the cell cortex (Figure 21D,E). As such, this domain appears to be the most essential for normal asymmetric localization of Pk2, and perhaps was important for maintaining the appropriate levels of apicolateral enrichment. Increased expression of Pk2-ΔC2 also severely disrupted the asymmetry of cortical Vangl1, though Vangl1 was present around the cell cortex (Figure 21H). These data suggest that the C2 domain is required for the regulation of Pk2 localization and that the mislocalization that results from the C2 domain deletion promotes the co-mislocalization of associated Vangl1 (Figure 21I), though I cannot rule out possibility of an indirect or alternate mechanism of Vangl1 mislocalization around the cortex.

Lastly, I used the Pk2 deletion constructs to assess their potential effects on Dvl1 localization. In *Drosophila*, overexpression of solely the PET and LIM domains together has been suggested to inhibit the membrane association of Dsh (Tree et al., 2002), and the C2 domain that binds Dgo is likely important in the competition between Dgo and Pk for Dsh binding (Jenny et al., 2005). Strikingly, I found that Dvl1 remained polarized in the presence of any of the three Pk2 deletion constructs (Figure 21J-L), though the degree of was modestly reduced in some cases (Figure 21M).

2.7: EFFECTS OF PCP MANIPULATION OF CILIARY POLARITY

To determine how the various PCP patterning defects I observed affect structural and thus functional polarity in this epithelium, I assessed ciliary orientation using a CLAMP-GFP ciliary rootlet marker and Centrin4-RFP basal body marker (Park et al., 2008). Under control conditions, CLAMP-GFP localized to the dorsoanterior side of basal bodies with little variance, as expected due to striated rootlets being oriented opposite the direction of the effective stroke

(Figure 22A). As previously used to provide ciliary orientation data (Mitchell et al., 2009), I present the state of basal body polarity by using a single arrow for each individual cell in a circular diagram; the points in the mean direction of the effective ciliary strokes, and the length of the arrow represents the mean resultant vector, a measure of variation from the mean orientation within that cell. The majority of cells under control conditions were oriented in the ventroposterior direction, with little variation in the individual orientations observed (Figure 22B). With an obvious exception for Pk2-ΔPET overexpression, all manipulations that were used to assess the molecular interactions affecting PCP protein enrichment resulted in clear defects in ciliary orientation (Figure 22C-J). The exception for Pk2-ΔPET overexpression is significant because this reagent also did not disrupt the asymmetry of other core PCP proteins (Figure 20), though this result is dissimilar from a previous report of Pk2-ΔPET overexpression disrupts fly wing hair polarity (Lin and Gubb, 2009). In addition, because Dvl1 and Dvl2 displayed divergent localizations at the cell cortex and basal bodies, respectively, I tested the effects of overexpressing Dvl1-ΔPDZ$_{partial}$, a Dvl1 construct analogous to the Xdd1 deletion of Dvl2 (Mitchell et al., 2009; Park et al., 2008; Sokol, 1996); Similarly to Dvl2-ΔPDZ$_{partial}$, this resulted in a strong perturbation of ciliary polarity (Figure 21K,L).

Comparing the mean vector length of individual cells between Pk2 misexpression conditions with that of Vangl1 overexpression reveals a difference in type of polarity defects observed, with seemingly more defective rotational polarity for the former and tissue-wide polarity for the latter. This interpretation is further supported not only by previous characterization of Vangl2 in this respect (Mitchell et al., 2009), but also by a closer examination of Vangl1 overexpression edge of clones, where basal bodies tend to orient their striated rootlets towards higher Vangl1 levels irrespective of their orientation relative to the body axis (Figure 22). As would be expected from the observed defects in ciliary orientation upon disrupting core

60
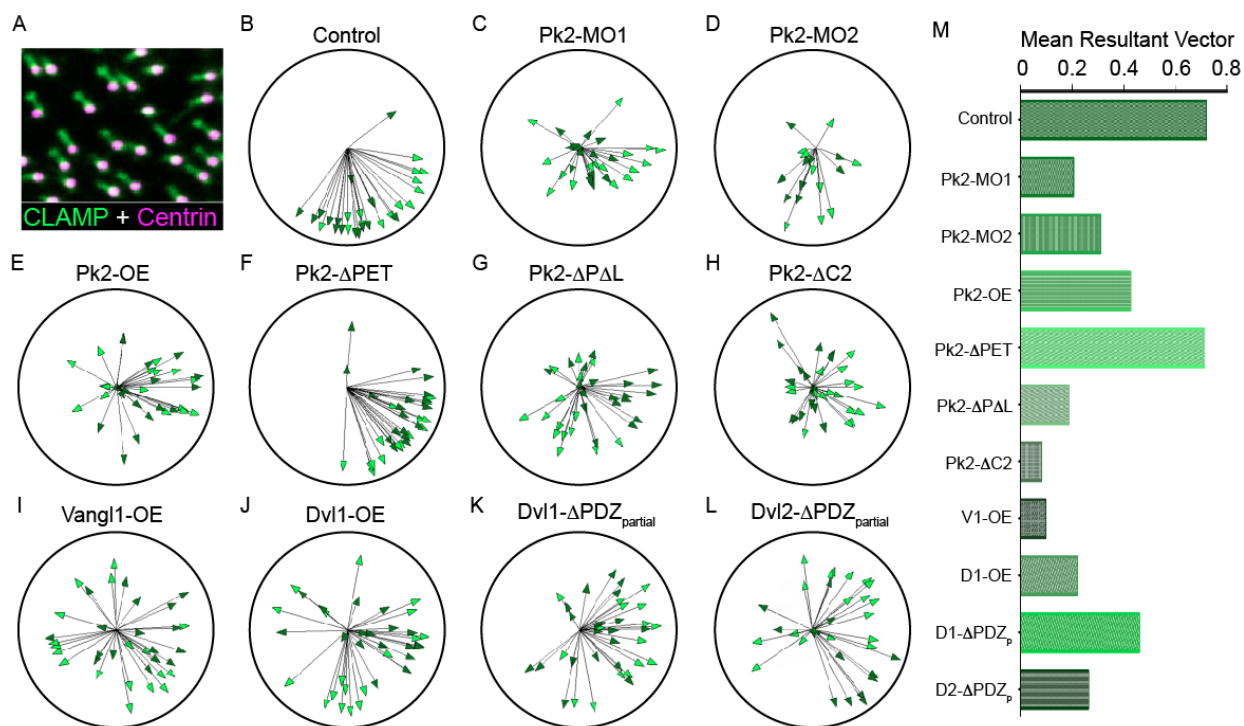
Figure 22: Disrupting PCP patterning leads to structural defects in basal body polarity. **(A)** Apical intercellular region of a single MCC labeled with CLAMP-GFP and Centrin-RFP, which when combined display the orientation of cilia in respect to the direction of ciliary beating (CLAMP points the opposite direction). **(B-L)** Plots displaying the mean basal body orientation and associated mean vector length of MCCs under various experimental conditions. Each arrow represents a measure of the orientations of a single MCC, with increased length correlated with less variation between basal bodies within each MCC. Dark and light arrowheads represent data from separate experimental repeats, with each experiment involving measures from at least 5 cells from at least 3 embryos each. The combined orientations/cells are displayed for **(B)** control (n = 2113/31), **(C)** Pk2-MO#1 knockdown (n = 1556/32), **(D)** Pk2-MO#2 knockdown (n = 1057/18), **(E)** Pk2 overexpression (n = 2426/34), **(F)** Pk2-ΔPET overexpression (n = 3122/35), **(G)** Pk2-ΔPETΔLIM overexpression (n = 1941/34), (H) Pk2-ΔC2 overexpression (n = 2275/33), **(I)** Vangl1 overexpression (n = 2843/35), (J) Dvl1 overexpression (n = 2086/37), (K) Dvl1-ΔPDZ$_{partial}$ overexpression (n = 2797/36), and **(L)** Dvl2-ΔPDZ$_{partial}$ (Xdd1) overexpression (n = 2177/32) conditions. **(M)** Graph illustrating the mean resultant vector length from the combined measurements for all MCCs across all embryos from both experimental treatments, serving as an overall metric for PCP disruption.
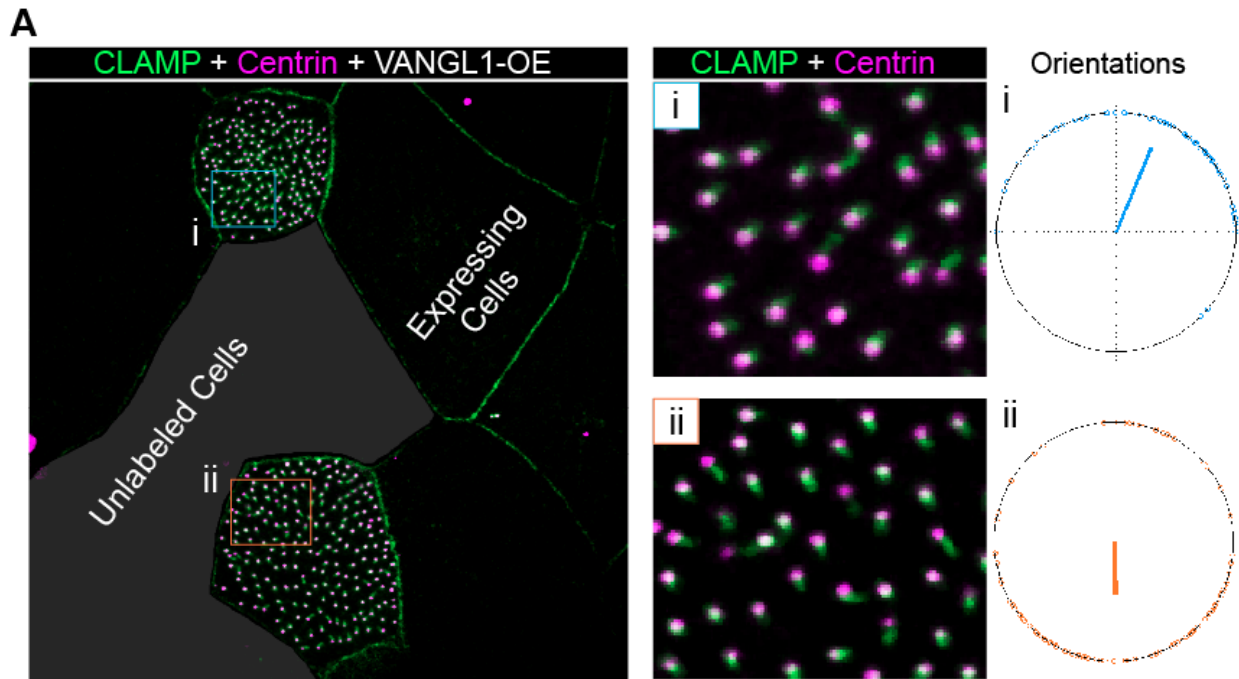
Figure 23: Vangl1 affects the orientation of ciliary basal bodies cell non-autonomously. (A) Two multicilated cells situated at the edge of a clone labeled with Centrin-RFP and CLAMP-GFP and overexpressing Vangl1, with cell (i) outlined in blue situated above unlabeled cells and cell (ii) outlined in orange situated below. Magnification of boxed areas and quantification of ciliary orientations and mean polarity vector for i (n = 95 orientations) and ii (n = 124 orientations) demonstrate the tendency for striated rootlets (opposite the effective stroke) to be oriented towards higher Vangl1 levels (towards labeled cells and away from unlabeled cells).
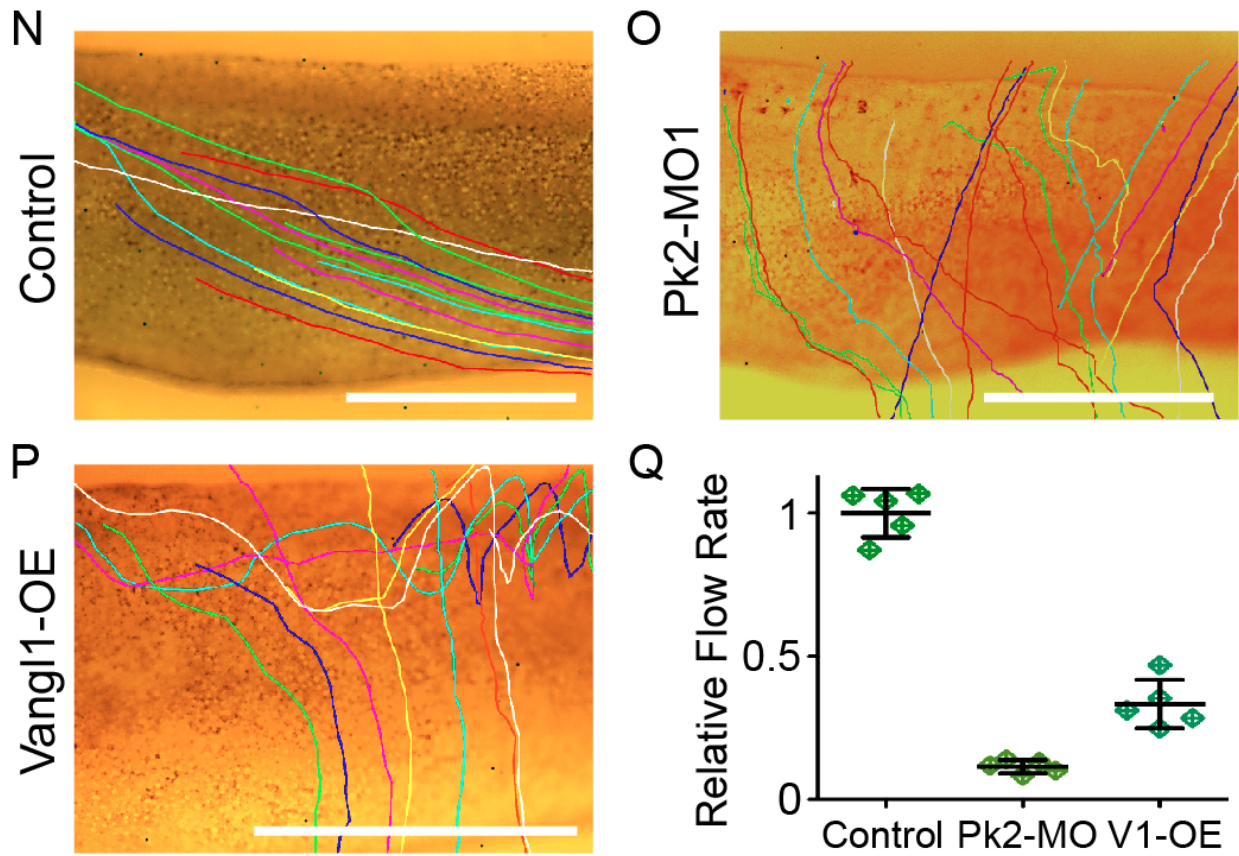
Figure 24: Disrupting PCP patterning leads to defective ciliary flow **(A-C)** Stills from the end of movies showing the traces of beads carried by flow across the epidermis of St.31 *Xenopus laevis* embryos that have been uninjected **(A)** or injected with either Pk2-MO **(B)** or a high dose of *vangl1* mRNA (C). **(D)** Quantification of the flow rate from five beads traced in the movies from which the final frame is shown in **(A-C)**. Error bars indicate Standard Deviation of the mean. Scale bars: 1mm.

PCP patterning, the resulting strength and directionality of flow at the surface of the embryo was severely impaired upon Pk2 morpholino knockdown and Vangl1 overxpression (Figure 23).

2.8: DISCUSSION

The observed behavior of symmetrically distributed PCP complexes later resolving into asymmetric accumulations here is reminiscent of early PCP patterning events in the fly wing (Seifert and Mlodzik, 2007; Strutt and Strutt, 2009; Strutt et al., 2011). In addition, there appears to be a common theme of increasing asymmetry coinciding with increasing polarized cellular behaviors. Here, core PCP asymmetry reflects oriented cilia beating, and in *Drosophila* wings, the degree of aligned asymmetry of core PCP complexes increasing following hinge contraction and reaches a maximum level just prior to trichome formation (Aigouy et al., 2010; Wong and Adler, 1993). Despite this and other behavioral similarities, these reporters also highlight important differences between planar-polarized tissues and proteins encoded by distinct members of PCP gene families. For example, I previously reported that Dvl2 localizes to basal bodies in MCCs (Park et al., 2008), and here I find Dvl1 localizes to asymmetric cortical crescents, a situation similar to that reported in the mouse airway (Vladar et al., 2012). Similarly, I find that while Vangl2 is cortically localized in this tissue it remains symmetrical; Vangl1 on the other hand becomes progressively planar polarized.

A second notable finding in this respect concerns the relationship between PCP protein asymmetry and the direction of ciliary beating. I find that Pk2/Vangl1 complexes are enriched on the "downstream" side of the cell and thus aligned in the direction of the effective stroke, which is consistent with previous functional studies suggesting that Frizzled points "upstream" of flow (Mitchell et al., 2009). This situation is exactly the opposite of that found in MCCs of

64

the mammalian airway and ependyma, where Prickle and/or Vangl mark the "upstream" face of the cell (Guirao et al., 2010; Vladar et al., 2012). This result argues against there being an intrinsic link between cortical enrichment of core PCP protein complexes and basal body orientation. This notion is consistent with the decoupling of Pk2 localization and kinocilia positioning in the mammalian inner ear (Deans et al., 2007), but it is nonetheless curious in light of the known localization of core PCP proteins to basal bodies (Park et al., 2008; Vladar et al., 2012) and the requirement of intact PCP signaling for asymmetry of the MCC microtubule cytoskeleton (Vladar et al., 2012).

Another related observation of note is the basal body localization of Pk2 I found that was not shown in the murine airway (Vladar et al., 2012). The potential limitations of using synthetic GFP protein fusions necessary for live imaging and the chance of mislocalization should not be ignored, though our particular finding that GFP-Pk2 localizes to basal bodies several stages after ciliogenesis is supported by Prickle3 being identified as asymmetrically associating with the more "mature" mother centrioles (but not daughter centrioles) during cell divisions in U-2 OS cells, as well as with the axoneme-associated mother centriole in ciliated hTERT-RPE1 cells (Jakobsen et al., 2011). Determining if Pk2 localization near basal bodies marks or mediates a state in which ciliary orientations are "locked" in place could potentially provide even further insight into the function of this protein in planar polarization.

How the core planar polarity module interfaces with proteins such as Inturned (Intu) and Fritz/Wdpcp, members of the CPLANE complex in vertebrates (Toriyama et al. 2016), remains an important question. In *Drosophila*, these proteins, along with fuzzy, have classically been described as "PCP Effectors," and in the fly wing they exhibit bona fide PCP phenotypes. However, phenotypes vary wildly in vertebrates, ranging from strong to mild to no phenotype at all, depending on the protein in question and the developmental context (Cui et al., 2013; Gray et

al., 2009; Kim et al., 2010; Park et al., 2006; Zeng et al., 2010, Toriyama et al. 2016). Further complicating matters is a recent report of both *frtz* overexpression and *fuzzy/intu* co-overexpression can effect the patterning of core PCP patterns (Wang et al., 2014), though core PCP genes have generally been considered to be upstream based on epistasis experiments (Wong and Adler, 1993) and other genetic studies (Collier et al., 2005; Lee and Adler, 2002). However, Intu overexpression alone did not give a significant phenotype in this study (Wang et al., 2014), consistent with previous data showing normal Fz localization in *intu* mutants (Strutt, 2001), mild convergent extension phenotype upon morpholino knockdown in Xenopus gastrulating mesoderm (Park et al., 2006). Having only modest PCP pattering effect seen here upon Intu-MO treatment sits well with these previous studies. By contrast, Wdpcp knockdown severely inhibits PCP-dependent convergent extension in *Xenopus* (Kim et al. 2010]), consistent with the robust effect on the polarized localization of Pk2 here as well. These data argue that this protein may function independently of Inturned in the control of PCP. Intriguingly, loss of Wdpcp in mice is associated with loss of cortical Vangl2 (Cui et al., 2013).

Additionally, these data shed new light on how mechanisms and relationships identified in *Drosophila* translate to vertebrate PCP signaling, specifically in a multiciliated epithelia consisting of a multi-layered, heterogeneous populations of cells shaped by families of PCP proteins acting at multiple levels. In particular, I expand upon relationships established between Vang and Pk (Bastock et al., 2003) and localization dynamics of Fz dependent upon Dsh (Strutt et al., 2011) to verify that Pk has an analogous affect on Vangl localization dynamics. Beyond this, I demonstrate the activity of the Pk2 LIM domain is likely to be important for this Vangl-enriching behavior, and I also identify the C2 region as critical for asymmetric cortical localization of Pk2 itself. The fact Dvl1 remained asymmetric under conditions when Vangl1 asymmetry was lost is of particular interest due to scenarios where one core PCP protein is

66

visually asymmetric while others are not being extremely rare, a finding which potentially could be attributed to the increased complexity of vertebrate PCP and lack of similar analysis in vertebrate tissues in general. However, data from *Drosophila* cells argue polarization can occur though Stan/Celsr and Frizzled even in the absence of Vang and obvious asymmetric enrichments (Struhl et al., 2012; Strutt and Strutt, 2007). The normal localization of Dvl1 in the face of mislocalized Vangl1 and/or Pk2 could in part be explained by communication from neighboring cells not expressing Pk2 deletions in our mosaic embryos, which would provide further support for Fz/Dsh being the more "dominant" module in comparison to Vangl/Pk (Struhl et al., 2012; Strutt and Strutt, 2007). In addition to providing localization-altering behaviors in the context of previously reported dominant negative activity (Takeuchi et al., 2003), our results provide a cell biological context for previous biochemical data indicating that PET domain function is regulated via intramolecular physical interactions with the LIM domains (Sweede et al., 2008). Ultimately, this work provides a foundation for future studies into the role of vertebrate Prickle proteins and the interface between PCP signaling and vertebrate tissue patterning.

CHAPTER 3: DYNAMIC ENRICHMENTS OF PRICKLE AND VANGL COORDINATE POLARIZED ACTOMYOSIN CONTRACTILITY DURING VERTEBRATE CONVERGENT EXTENSION

3.1: POLARIZED APICAL JUNCTION DYNAMICS FACILITATE MEDIOLATERAL INTERCALATIONS AND CONVERGENT EXTENSION OF THE XENOPUS NEURAL PLATE EPITHELIUM

Xenopus laevis is among premier platforms for studying convergent extension, yet there are still many important unanswered questions regarding core PCP localization and behavior and how they govern coordinated cellular rearrangments. Studies of convergent extension on the cellular and subcellular level and the influence of PCP signaling have primarily been focused on the gastrula mesoderm rather than the neural plate, where apical constriction has been the far more popular topic. And while links to convergent extension go back to the very origin of vertebrate PCP signaling studies, the planar-polarized dynamics of apical junctions, where core PCP proteins are known to localize in the neural plate (Ossipova et al. 2015), have not even been very well described in *Xenopus* compared to other vertebrate models (Nishimura et al. 2012, Williams et al. 2014). So, prior to identifying novel functions and behavior of core PCP proteins during processes that drive vertebrate convergent extension, I needed to first further characterize the associated cellular behaviors that facilitate this process in the neural epithelia.

The neural plate undergoes significant lengthening and narrowing, with the convergence of cells towards the midline, from Stage 11.5 up until the neural folds come into contact with one another at around Stage 15 (Keller et al. 1992) (Figure 25A). Tracking individual cells during this convergent extension process shows cell tend to be displaced medially and widely spread apart along the anterior-posterior access during this timeframe, with cells that are neighboring one another at St.12 often ending up separated by distances ranging over several intervening
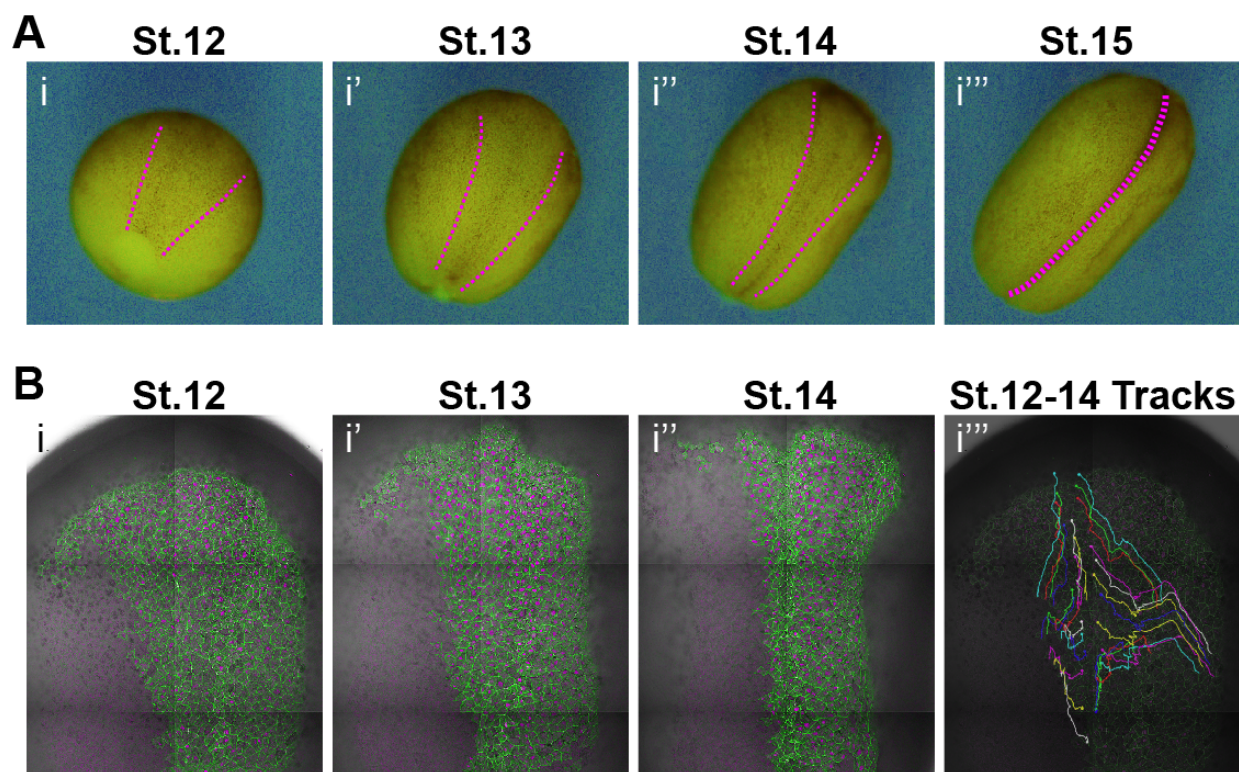
Figure 25: Mediolateral intercalations drive convergent extension of the *Xenopus* neural plate. **(A)** Stereo images from a time-lapse movie of *Xenopus* neural tube morphogenesis from stages 12 to 15. **(B)** Confocal images of dorsal side of embryo from a time-lapse movie of convergent extension of the neural ectoderm from stages 12 to 14. The right neural fold is labeled with membraneGFP and H2B-RFP in its entirety, as is mostly the medial half of the left neural fold. Bi''' shows tracks following cells movements over the duration of the movie capture from Bi-Bi''.

cells by the time the central neural groove matures and the plate begins to significantly bend (Figure 25B). The paths revealed by tracking a significant portion of the cells here very closely resembled results of cell tracing experiments performed by grafting labeled cells onto unlabeled donors (Keller et al. 1992), suggesting the viability of the long-term confocal imaging of this process and the associated cell behaviors *in vivo*.

Similarly to as has been described in chick and mouse models (Nishimura et al. 2012, Williams et al. 2014), the mediolateral cell intercalations that drive convergent extension behavior in the *Xenopus* neural plate appear to be facilitated by the preferential contraction of junctions shared between the anterior face of one cell and the posterior face of another (AP junctions) (Figure 26A). These shrinking anteroposterior junctions are aligned perpendicular to the anterior-posterior axis, while the mediolateral (ML) cell-cell junctions, parallel to the anterior-posterior axis, are elongated along the direction of tissue elongation (Figure 26A). In addition, there is an apparent bias for new junctions emerging from resolving rosettes to be similarly aligned along the axis of extension as well (Figure 26A). Indeed, plotting the change in the length of cell-cell junctions over the course of 30 minutes against the average angle of the junction during this time frame revealed that angles within 45 degrees of the mediolateral axis were generally dramatically reduced in length, whereas junctions with angles closer to being parallel with the anterior-posterior axis tend to become significantly elongated (Figure 26B). In addition, the angles of new junctions that resulted from resolving multicellular rosettes were generally oriented between 45 and 90 degrees from the mediolateral axis, biased towards the dorsal midline (Figure 26C). Together, the tendency for junctions to shrink along the axis of narrowing and elongate along the axis of extension provides foundation for the extent of convergent extension that allows for the fusion of the neural folds later in development.

70
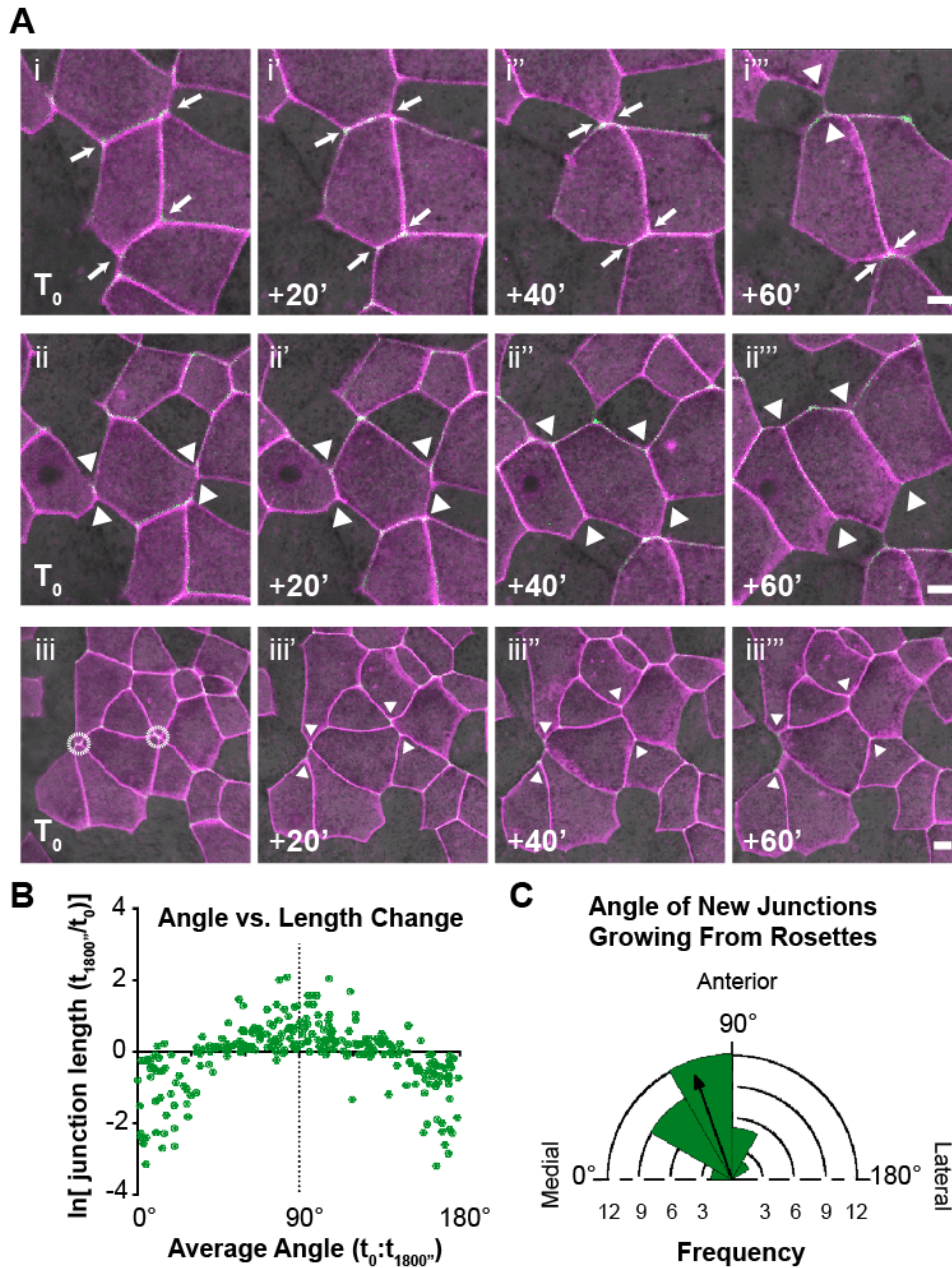
Figure 26: Polarized apical junction dynamics facilitate mediolateral intercalations **(A)** Confocal images of junction dynamics in neural ectoderm mosaically labeled with membraneRFP and GFP-Pk2. Arrows mark the mediolateral ends of shrinking AP junctions, while arrowheads mark the anterior and posterior ends of a new growing mediolateral junctions. Dashed circles in iii are mark multicellular rosettes. Anterior is up. Scale bars = 10μm **(B)** Plot of the average angles of junctions over 1800 seconds against the natural log of the fold increase or decrease in length over the same time frame. Each dot represents on cell-cell junction. n = 267 junctions from 3 embryos across 3 different experiments **(C)** Rose diagram plotting the frequency of new junctions emerging from resolving rosettes growing within a range of 30-degree angle bins. n = 36 new junctions from 3 embryos across 3 separate experiments.

71

3.2: PRICKLE2 AND VANG-LIKE2 ARE ANTERIORLY LOCALIZED AND DYNAMICALLY ENRICHED AT SHRINKING CELL-CELL JUNCTIONS IN THE NEURAL PLATE

To investigate the localization of core PCP proteins in the neural plate and determine relationship of the localization behavior seen to the junctional dynamics that facilitate convergent extension of the tissue observed, I mosaically labeled the neural plate by injecting one cell at 16- or 32-cells stage with mRNA encoding fluorescent fusion proteins (Figure 27A), as this allows for the localization of proteins in single cells of neural plate to be clearly visualized. Examination of GFP-Pk2 revealed it to be clearly restricted to the apicolateral regions of the cells, within roughly 3μm of the apical surface (Figure 28A) and strongly asymmetrically biased towards to the anterior side of the cells here (Figure 28A). The localization of Vangl2 has previously been shown to be similarly strongly biased towards the anterior sides of the cells here (Ossipova et al. 2014), though the polarized localization of GFP-Vangl2 did not require the co-expression of any form of Pk as described previously (Ossipova et al. 2014). However, when GFP-Vangl2 and RFP-Pk2 were simultaneously expressed, it revealed a high degree of overlap between the localization of these two proteins (Figure 28C), and time lapse imaging revealed very similar dynamic behaviors of these proteins during mediolateral cell intercalations.

The observation that Pk2 and Vangl2 localize to the anterior apicolateral regions of the cells of the neural plate here fits well with several known instances of PCP complexes being enriched at the junctions between anterior and posterior cellular faces of neighboring cells in vertebrate tissues that undergo neighbor exchanges (Ciruna et al. 2006, Nishimura et al. 2012, Williams et al. 2014, Ossipova et al. 2015, Roszko et al. 2015, Aw et al. 2016). However, much less is known about core PCP localization dynamics on shorter timescales as junctions are
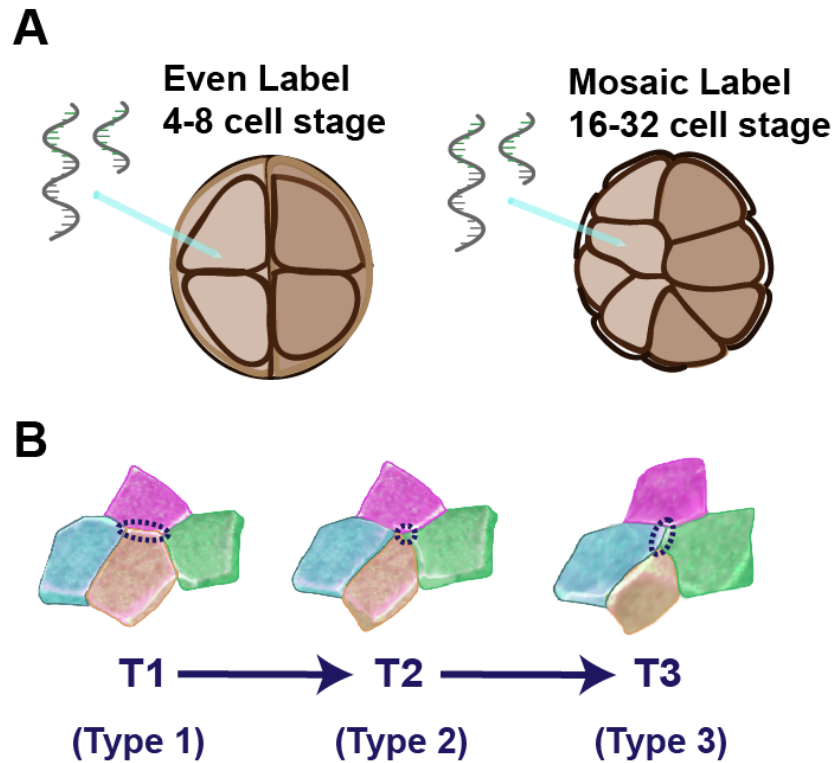
Figure 27: Mosaic labeling the neural plate affords analysis in single cells during collective behaviors **(A)** Methods for even and mosaic labeling of neural plate epithelia. Microinjection of mRNAs into two cells at the 4- or 8-cell stage allows for the even labeling of both the left and right halves of the neural plate and into one cell at the 16- or 32-cell stages results in the mosaic labeling of one side of the neural plate. **(B)** Schematic of the T1 transition process, with the type 1, type 2, and type 3 junctions at each of the three steps marked with a dashed circle.

actively rearranging. As cell-cell junctions shrink in a transition from a type 1 to a type 2 junction (Figure 27B) or in the formation of a multicellular rosette, the intensity of both GFP-Pk2 and -Vangl2 dramatically increase, suggesting they are increasingly enriched at cell-cell junctions as they become shorter (Figure 28D,E). Recording changes along a line draw across two neighboring cell-cell junctions that share a common tricellular junction, one of which shrinks while the other grows, shows that while the average intensity of Pk2 across a junction increases as it shrinks, it remains steady or decreases as a junction grows (Figure 28F). Measuring the changes in intensity in GFP-Pk2 and -Vangl2 normalized the changes in membrane label intensity across several junctions as they shrink or grow reveals a strong negative correlation between the change in junction length and the average intensity of GFP-Pk2 and -Vangl2 along the junction (Figure 28G). The rate at which the average intensity for GFP-Pk2 and -Vangl2 increases at shrinking junctions often appears significantly higher than it decreases along growing junctions (Figure 29A-D), perhaps suggesting that not only is there a mechanism preventing diffusion across tricellular junctions, likely being the linkage to intercellular core PCP complexes (Figure 2C), but for promoting the recruitment or stability of additional core PCP proteins at shrinking junctions and/or removal or reduction from growing junctions.

In order to accommodate dynamic changes in core PCP protein recruitment to rearranging cell-cell junctions, it stands to reason that there might be some level of fluidity to the localization behavior of core PCP complexes. In order to assess the localization stability of such complexes, I measured the recovery of fluorescence intensity after photobleaching enrichments of GFP-Pk2 at the anterior, apicolateral regions of the cell (Figure 30A). Initial studies of core PCP stability in planar-polarized epithelia such as that in the *Drosophila* wing blade (Strutt et al. 2011) and, in vertebrates, in the *Xenopus* epidermis (Figure 20; Butler &
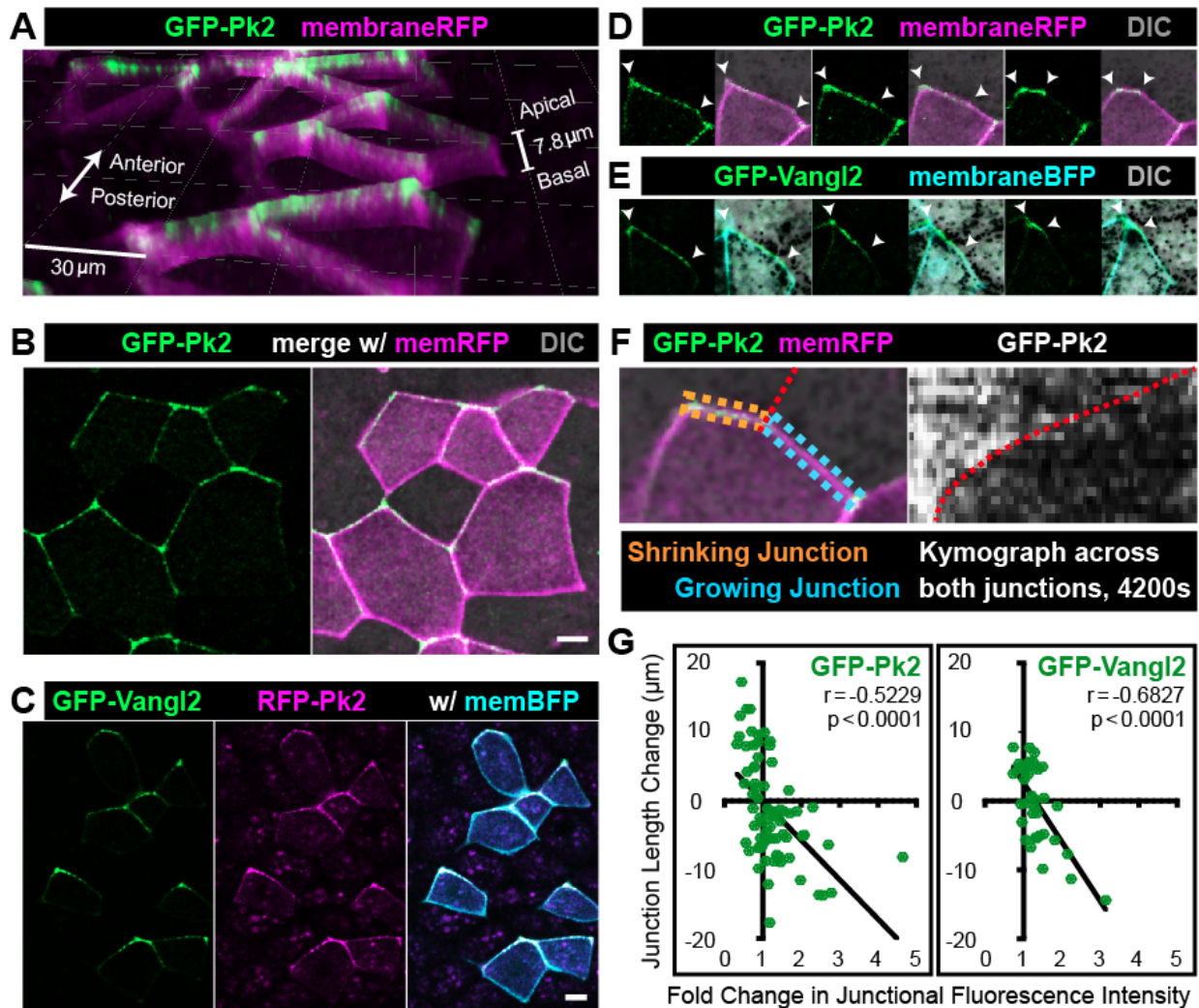
Figure 28: Dynamic Pk2 and Vangl2 accumulations are enriched at anterior, apicolateral junctions in the neural plate. **(A)** Pseudo 3D render of neural epithelium mosaically labeled with GFP-Pk2 and membraneRFP showing Pk2 restricted to the apicolateral cellular regions. **(B)** En face view of neural epithelium mosaically labeled with GFP-Pk2 and membraneRFP showing Pk2 localization is highly planar-polarized towards the anterior cellular junctions. **(C)** Neural epithelium mosaically labeled with GFP-Vangl2, RFP-Pk2, and membraneBFP showing the overlapping localizations of Pk2 and Vangl2. Anterior is up. **(D)** Confocal stills from a movie following changes in GFP-Pk2 localization at a shrinking junction. Roughly 800 sec between each frame. **(E)** Confocal stills from a movie following changes in GFP-Vangl2 localization at a shrinking junction. Roughly 600 sec between each frame. **(F)** Kymograph depicting the simultaneous changes in the lengths of a shrinking and a growing cell-cell junction separated by a shared tricellular junction and changes in GFP-Pk2 fluorescence intensity across these two junctions over the course of 4200s, with the initial time point at the top of the image on the right and the dashed red line tracing the movement of the tricellular junction. **(G)** Graphs showing the correlation between the change in junction length and the change in mean intensity of GFP-Pk2 or GFP-Vangl2 along the junction. Changes in GFP-Pk2 and –Vangl2 Fluorescence intensity were normalized against changes in the intensity of the membrane labeled with a different fluorescent protein. n= 71 junctions for GFP-Pk2 and 37 for GFP-Vangl2. Anterior is up in all images.

75
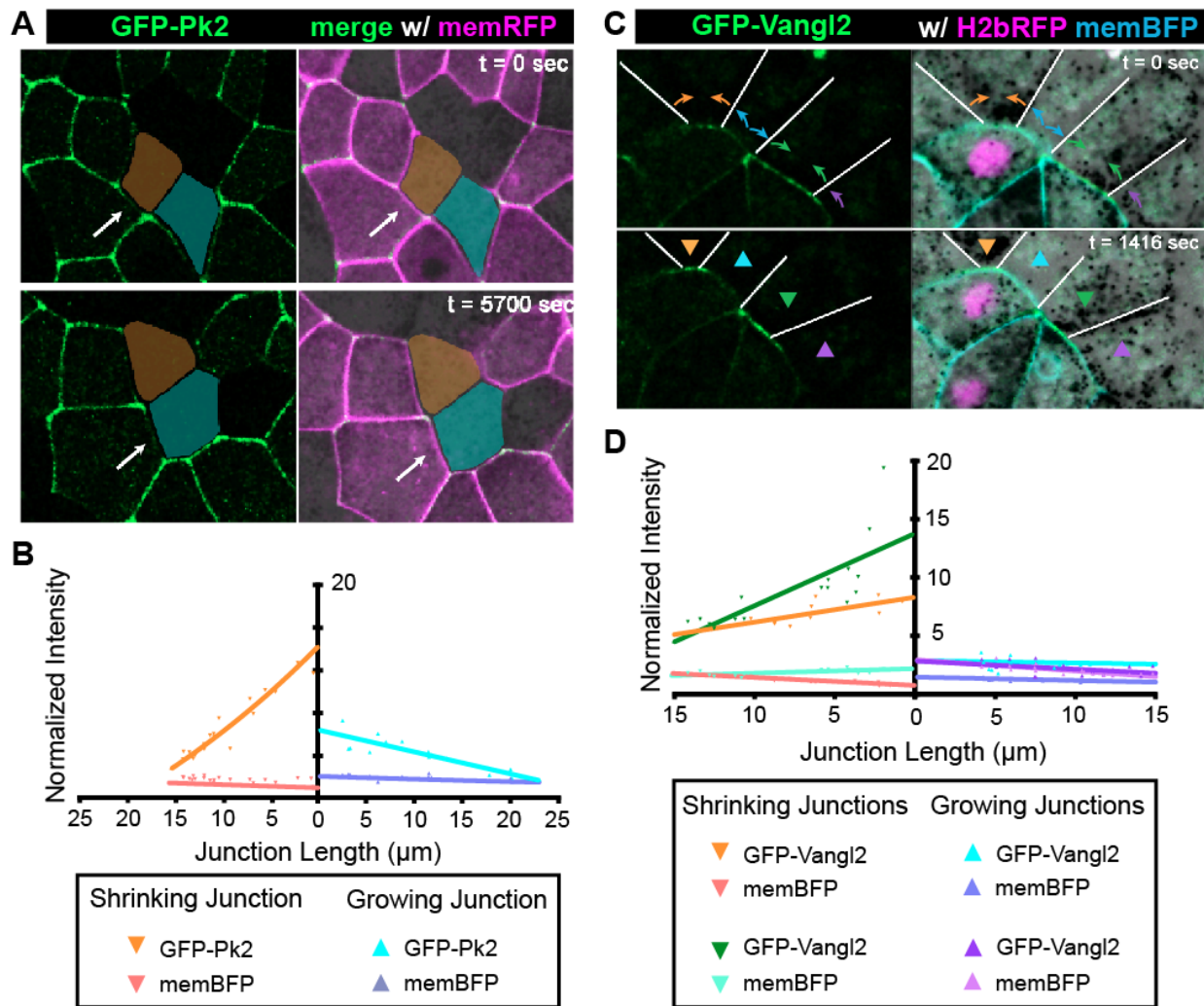
Figure 29: GFP-Pk2 and –Vangl2 are increasingly enriched at shrinking AP junctions. **(A)** Confocal stills of a neural epithelium mosaically labeled with GFP-Pk2 and membraneRFP. Along with the fluorescently labeled cell marked with an arrow, an older cell-cell junction with the pseudocolored cell in orange contracts and new cell-cell junction grows with the pseudocolored cell in blue. **(B)** Graph plotting the changes in GFP-Pk2 intensity at the junction between the cell marked with an arrow in **(A)** and the unlabeled cells marked in orange (left side of the graph) and blue (right side of graph). **(C)** Confocal stills of a neural epithelium mosaically labeled with GFP-Vangl2, H2B-RFP, and membraneBFP. Cell-cell junctions with arrowheads drawn on them either shrink (orange and green) or grow (blue and purple) over the course of the movie. **(D)** Graph plotting the changes in GFP-Vangl2 intensity at the junctions labeled in **(C)** as the cell-cell junction length changes. Lines drawn on graphs in **(B)** and **(D)** are fits of a linear regression model.
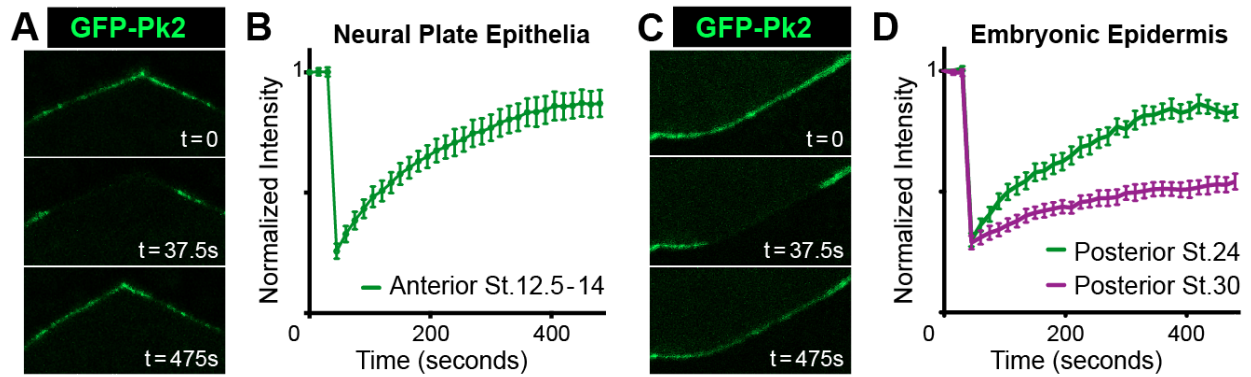
Figure 30: **(A)** Three still images from a time lapse movie captured the before and after photobleaching the anterior apicolateral region of a cell mosaically labeled with GFP-Pk2 in the neural plate. Anterior is up. **(B)** Graph showing the degree of fluorescence intensity recovery over time following the photobleaching of GFP-Pk2 along the anterior apicolateral regions of neuroepithelial cells, such as that shown in **(A)**. n= 39 cells from 7 embryos across 4 experiments. **(C)** Three still images from a time lapse movie captured the before and after photobleaching the ventral-posterior apicolateral region of a cell mosaically labeled with GFP-Pk2 in the embryonic epidermis at Stage 30. For this panel, anterior to the left and dorsal is up. **(K)** Graph showing the degree of fluorescence intensity recovery over time following the photobleaching of GFP-Pk2 along the ventral-posterior apicolateral regions of epidermal cells at two different embryonic stages, such as that shown in **(C)**. Stage 24 prior to complete polarization, while Stage 30 epidermis is completely polarized (See Figure 11H) n= 9 cells from 4 embryos across 2 experiments (St.24) and 16 cell from 4 embryos across 2 experiments (St.30).

77

Wallingford 2015), would seemingly suggest a relatively stable PCP protein population in regions where these proteins are highly asymmetrically localized. However, despite a high degree of asymmetrically planar polarized GFP-Pk2 seen here, there was instead a relatively small stable fraction measured, with recovery up to over 80% of the initial fluorescence intensity on average (Figure 30B). Compared to the embryonic epidermis, where GFP-Pk2 localization is initially symmetric and becomes increasingly asymmetric towards the ventral, posterior regions of the cell (Figure 11C,D,H; Butler and Wallingford 2015), the recovery GFP-Pk2 in the neural plate is more comparable to that in the epidermis at earlier stages, prior to when the tissue exhibits a high degree of asymmetric PCP localization; At later stages when GFP-Pk2 is highly asymmetrically enriched, the stable fraction in the epidermis is significantly higher (Figure 30C,D). Thus, despite highly asymmetric patterning, the more dynamic neural epithelia also has a more dynamic core PCP localization, suggesting that robust mechanisms for PCP trafficking, recycling, or potentially others that could contribute to a relatively fluid yet polarized localization must be in place. Indeed, time lapse movies of single 1-2μm slices show dynamic populations of punctate GFP-Pk2 not only along the junctional regions of the cell, but also slightly further into the cell along the junctions in a population that resembles an endosomal trafficking or recycling network (data not shown).

3.3: Pk2 and Myl9 coordinate polarized junction shrinking in the neural plate

Along with increases in cortical actin, both active, phosphorylated Non-muscle Myosin II (pMyoII) and Myosin regulatory light polypeptide 9 (Myl9) are also enriched at contractile v-junctions in DMZ explants (Shindo & Wallingford, 2014). Considering the known correlations between actin and myosin regulation in the gastrula axial mesoderm, and having documented

increases in Pk2 at shrinking junctions, I next sought to investigate the relationship between Myl9, Pk2 and PCP signaling in the neural ectoderm. The localization of Myl9-GFP does in fact appear to be planar-polarized throughout the neural plate, preferentially enriched along the AP junctions, although not anisotropicly, and instead localizing at both anterior and posterior junctions. Not only this, but time lapse imaging of cells simultaneously labeled with Myl9-GFP and RFP-Pk2 reveals a highly similar localization pattern and behavior at the anterior apicolateral regions of cells here as well (Figure 31A). The fluorescence intensities of Pk2 and Myl9 over time along a contracting cell-cell junction share a nearly identical pattern (Figure 31B), and there was a highly significant correlation between the changes in Pk2 and Myl9 localization across all junctions examined (Figure 31C). In addition, there was a significant positive correlation between the change in Myl9-GFP and actin biosensor Utrophin-RFP and negative correlation between the change in junction length to the intensity of both of these markers (Figure 32A), similarly to that seen with GFP-Pk2 (Figures 28G). These results provide additional evidence for an intricate link between the PCP patterning of the neural plate and the planar polarized recruitment of actomyosin contractile machinery to cellular junctions.

If Pk2 is involved in patterning or localizing Myl9 to AP junctions, then perturbations that increase or decrease levels of Pk2 at cell-cell junctions should have comparable effects on the recruitment of Myl9. To modulate Pk2 localization, I utilized two different dominant negative PCP constructs – a PCP-specific dominant negative Dishevelled, Xdd1, which is missing most of the PDZ domain required for various protein-protein interactions and post-translational modifications (Sokol 1996, Cheyette et al. 2002, Wong et al. 2003, Klein et al. 2006, Strutt et al. 2006, Gao & Chen 2010), and a dominant negative Pk, Pk2DPDL, which is lacking the conserved PET and LIM domains and can prevent the enrichment of Vangl at cell-cell junctions (Butler and Wallingford 2015). Injecting mRNA for GFP-Pk2 and a membrane
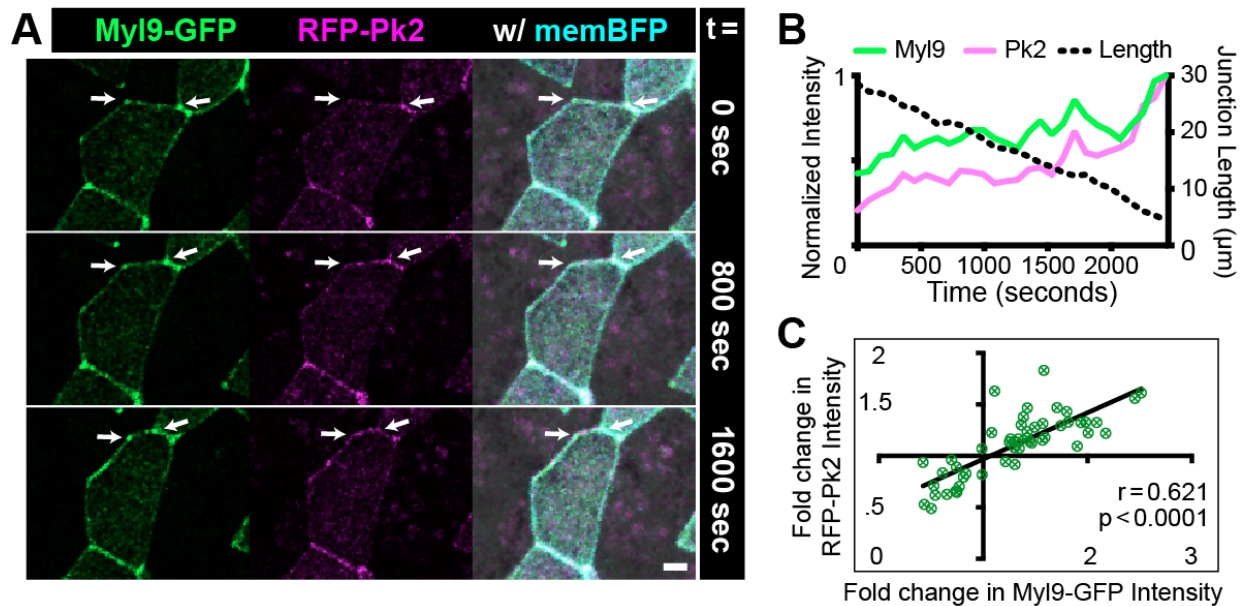
Figure 31: Pk2 and Myl9 coordinate polarized junction shrinking in neural plate in a PCP-dependent fashion. **(A)** Confocal images centered on a shrinking AP junction labeled with Myl9-GFP, RFP-Pk2, and membraneBFP over the course of a 1600s time lapse. Note the increased GFP and RFP intensities as the junction becomes shorter. Scale = 10 μm **(B)** Intensity trace over time of the fraction of the maximum fluorescence intensity as the junction in **(A)** contracts **(C)** Scatter plot and correlation test of the change in RFP-Pk2 intensity plotted against the change in GFP-Myl9 intensity across many dynamic junctions (n= 50 junctions examined).

label at the 4-cell stage and then injecting the same embryos again at the 32 cell stage with mRNA encoding dominant negative protein and a histone label tracer (H2B-RFP) allowed for local comparisons protein localization under different conditions within the same embryo (Figure 27A). While GFP-Pk2 appears planar polarized and strongly localized to AP junctions in control cells, it is instead enriched along almost all junctions in cells expressing Xdd1 (Figure 33A). Conversely, GFP-Pk2 accumulation appears mostly absent from junctions in clones of cells expressing Pk2DPDL, which likely competes with both the endogenous and GFP-tagged Pk constructs for binding to Vangl and other proteins important for stable apicolateral enrichment (Figures 33A, 18C, 21F). Quantification of intensity relative to junction angle reveals that the enrichment of GFP-Pk2 is significantly higher at AP junctions, angled within 45 degrees of the mediolateral axis, than at ML junctions, those angled between 45 and 135 degrees from the mediolateral axis (Figure 33B). Both PCP dominant negatives disrupt the significant difference between enrichment at AP and ML junctions, with the expression of Xdd1 resulting in an increased intensity at ML junctions, while Pk2-DPDL leads to decreased intensity at AP junctions (Figure 33B). By and large, the polarized localization of Myl9-GFP and disrupting effects of dominant-negative PCP protein expression was comparable to that of GFP-Pk2 (Figure 33C,D), suggesting the polarized enrichment of Pk protein to AP junctions may be important for recruiting planar-polarized actomyosin regulatory components.

Because the disruption of PCP patterning appears to have drastic effects on the patterning of actomyosin contractility in the neural plate, defects in polarized cellular behaviors are the likely consequence of such PCP signaling perturbations. A large number of the mediolateral intercalations appear to be mediated through T1 transitions (Figure 27B), which were initially described as major drivers of Drosophila germ band extension (Bertet et al. 2004, Zallen & Wieschaus 2004). This mode of cell intercalation involves the complete contraction of an initial
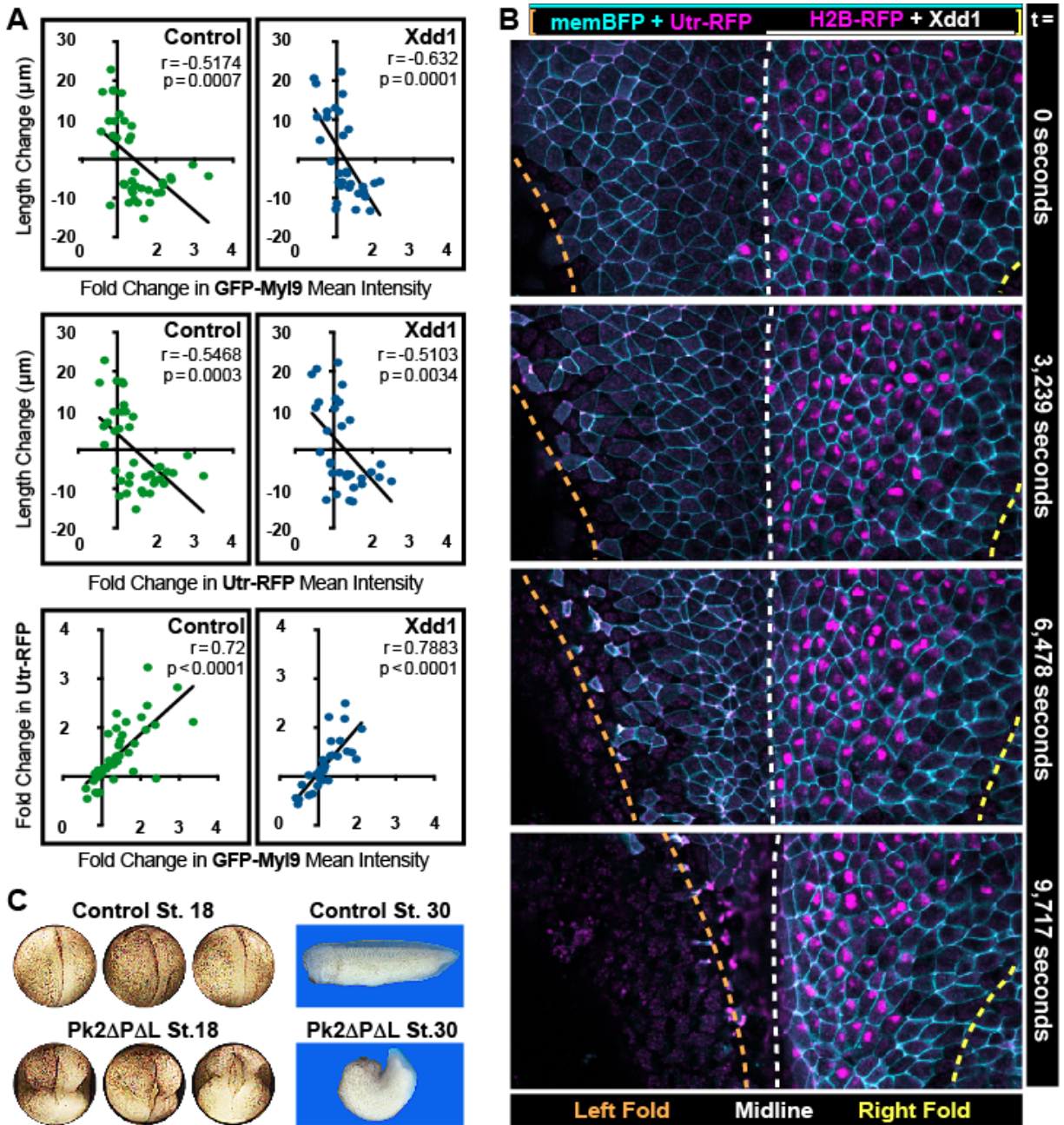
Figure 32: Dominant negative PCP proteins cause convergent extension defects. **(A)** Graphs showing the correlation between normalized changes in Myl9-GFP and Utrophin-RFP (actin biosensor) intensities along with change in length along the junctions these intensities were examined. n=39 junctions (Control), 31 junctions (Xdd1) **(B)** Confocal images from a movie of convergent extension and neural tube closure of an embryo that had the neural plate evenly labeled with membraneBFP and Utr-RFP, but only one half of the neural labeled with H2B-RFP, which is serving as a tracer for Xdd1 expression. The midline and lateral boundaries are marked in each frame and show the extent that Xdd1 expression disrupt the narrowing of the right neural fold in comparison to the control fold on the left. These frames lead up to the result shown in **Figure 34C**. **(C)** Dorsal views of Stage 18 embryos (anterior is up) and lateral views of Stage 30 embryos (anterior is left, dorsal is up), either control or dorsally expressing ~800pg of Pk2-ΔPΔL.
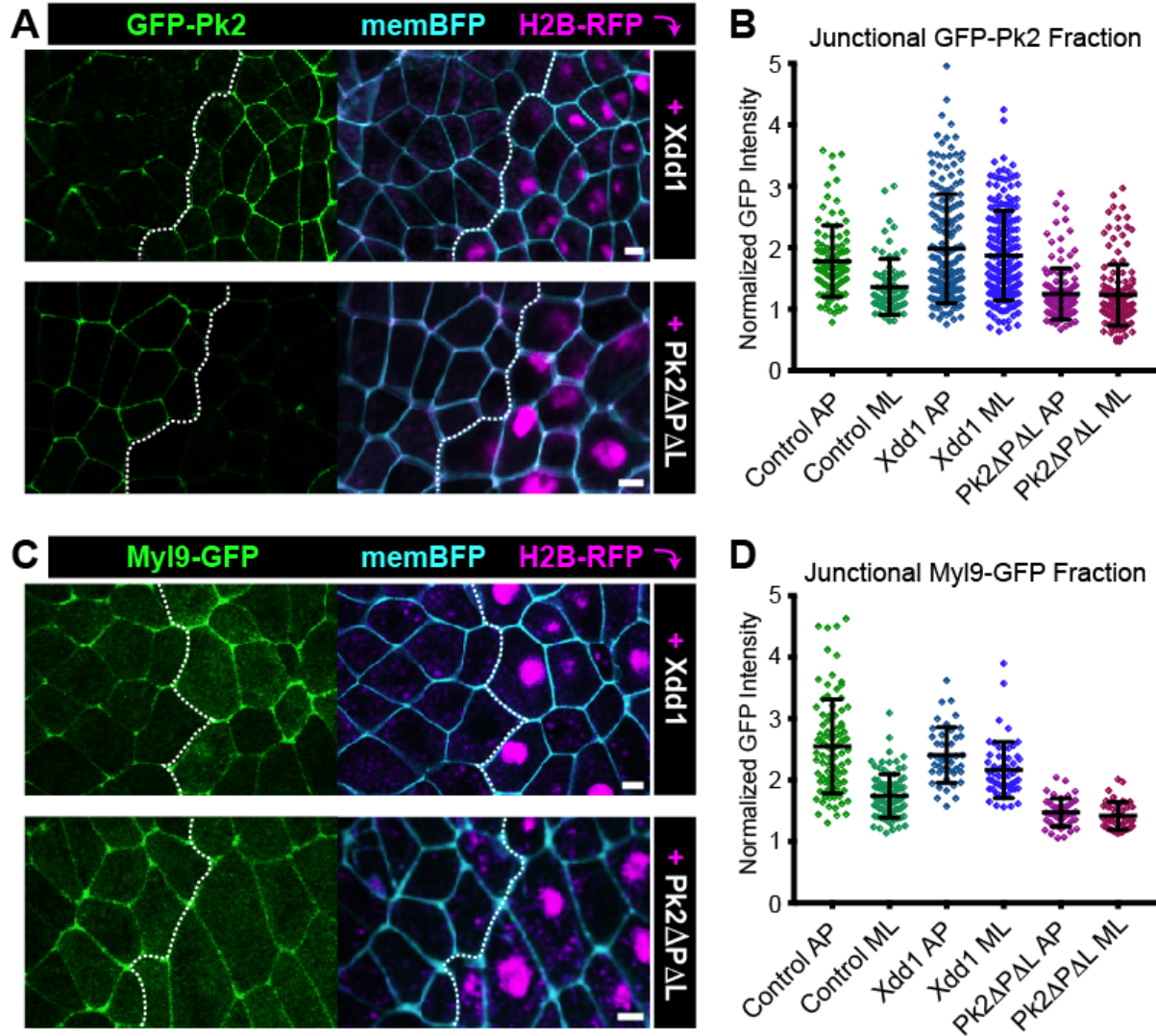
Figure 33: Conditions effecting Pk2 localization have seemingly identical effects on Myl9. **(A)** Confocal images of Xenopus neural epithelia labeled evenly with GFP-Pk2 and membraneBFP and mosaically with H2B-RFP serving as a tracer for either Xdd1 or Pk2-ΔPΔL expression. Scale = 10 μm **(B)** Graph plotting GFP-Pk2 intensity along AP junctions (0-45°, 135-180°) and ML junctions (45-180°) normalized as a ratio to the cytoplasmic intensity in control cells (n=101 AP, 71ML) and cells expressiong Xdd1 (n=171 AP, 199 ML) and Pk2-ΔPΔL (n=128 AP, 142 ML). Ctrl AP vs. ML, p<0.0001; Xdd1 AP vs. ML, p=0.5799; Pk2-ΔPΔL AP vs ML, p=0.173; Ctrl AP vs Xdd1 ML, p=0.5770; Ctrl ML vs Pk2-ΔPΔL AP, p=0.0268 **(C)** Confocal images of Xenopus neural epithelia labeled evenly with Myl9-GFP and membraneBFP and mosaically with H2B-RFP serving as a tracer for either Xdd1 or Pk2-ΔPΔL expression. Scale = 10 μm **(D)** Graph plotting Myl9-GFP intensity along AP junctions (0-45°, 135-180°) and ML junctions (45-180) normalized as a ratio to the cytoplasmic intensity in control cells (n=91 AP, 91ML) and cells expressiong Xdd1 (n=44 AP, 53 ML) and Pk2-ΔPΔL (n=45 AP, 45 ML). Ctrl AP vs. ML, p<0.0001****; Pk2-ΔPΔL AP vs. ML, p=0.2304ns; Xdd1 AP vs. ML, p=0.0022**; Control AP vs. Xdd1 AP, p=0.5826ns; Control ML vs. Xdd1 ML, p <0.0001****; Control ML vs. Pk2-ΔPΔL ML, p<0.0001**** (Mann-Whitney Test for significance)

(Type 1) cell-cell junction down to point, which brings neighboring cells on either side of this junction together and results in the formation of a multicellular Type 2 junction shared by 4 cells. This Type 2 junction then transitions to a Type 3 as a new cell-cell junction grows between the cells that did not initially share one, separating the two cells that initially did (Figure 27B). Because of the orientations of such cell movements relative to the neural plate (Figure 26B), both Pk2 and Vangl2, as well as actin and Myl9, appear to be increasingly accumulated at Type 1 junctions, and they also appear reduced or largely absent from Type 3 junctions. Thus, disrupting the normal localization of these proteins by promoting enrichment at Type 3 junctions (via Xdd1) or reducing enrichment at Type 1 junctions (via Pk2-DPDL) (Figure 33) is likely to have an effect on the dynamics of these junctions.

Monitoring junctional dynamics in the neural plate over several large populations of cells and time points showed that on average, a single Type 1 to Type 2 transition (T1-T2) and Type 2 to Type 3 transition (T2-T3) occurred per hour for roughly every 3-4 cells between Stages 12 and 14. However, when large clones of cells express either Xdd1 or Pk2DPDL, this frequency is greatly reduced, with less than half the number of transitions observed in both conditions (Figure 34A). Thus, the efficiency of cellular rearrangements and degree of convergent extension over comparable timeframes is greatly hindered by defective PCP signaling. Of the junctions that did successfully transition from T1 to T2, they did so at a significantly reduced rate that was roughly half of the rate for control cells examined (Figure 34B). Despite this rate reduction, these contracting junctions did appear to eventually recruit levels of actin and Myl9 that were comparable to the controls as junction length changed (Figure 32A), demonstrating similar contractional machinery was likely driving these transitions under conditions of disrupted PCP signaling.
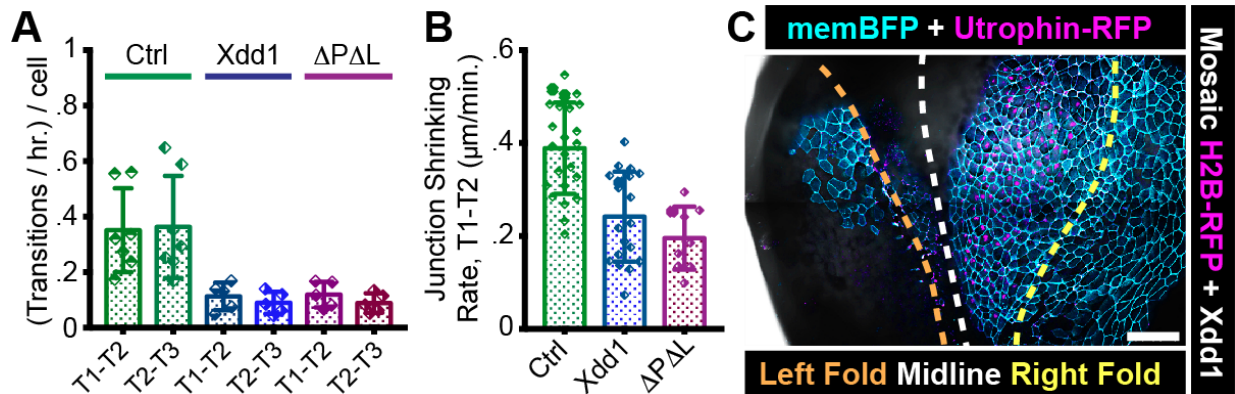
Figure 34: Proper polarization of Pk2 and Myl9 promote efficient cellular rearrangement behavior. **(A)** Graph with the total number of T1 transition events across large patches of embryos and timeframes, presented in the form of number of transitions per hour per cell. For statistical analysis, Control vs. Xdd1, and Control vs. Pk2-ΔPΔL ML, p=0.0025** for both classes of transitions (Mann-Whitney Test for significance). n=4 experiments, 7 embryos, 1,167 cells (Control); 3 experiments, 5 embryos, 560 cells (Xdd1); 3 experiments, 5 embryos, 841 cells (Pk2-ΔPΔL) **(B)** The calculated rate of junction contraction for groups of cells that completely and smoothly transitioned from a Type 1 to Type 2 junction (complete contraction of an AP junction, see Figure 27B). Ctrl vs. Xdd1, p<0.0001****, Ctrl vs. Pk2-ΔPΔL, p<0.0001****, Xdd1 vs. Pk2-ΔPΔL, p=0.2051ns. n=24 (Ctrl), 19 (Xdd1), and 9 (Pk2-ΔPΔL) junctions. (Mann-Whitney statistical test). **(C)** Confocal image demonstrating the open neural fold and wide field of cells on the half of the neural plate expressing Xdd1, as indicated by H2B-RFP coexpression, while the control half of the neural plate is folded over to the midline. Scale = 500 μm. Anterior is up.

3.4 PCP DISRUPTION RESULTS IN FAILURES IN COORDINATED MECHANICS

As a result from the reduction in both the number of cell rearrangements and rate of successful mediolateral intercalations (Figure 34A,B), either a long delay or complete failure in the folding of the neural plate results from the expression of dominant-negative PCP components (Figures 32B and 34C). Neural tube closure defects have long been associated with Xdd1-expressing embryos (Sokol 1996, Wallingford and Harland 2001), but it is interesting to note the drastic effect the cellular phenotypes seemingly have the overall morphogenesis of the tissue. The rate of junction shrinkage and neighbor exchanges is roughly half of that in Xdd1-expressing embryos in comparison to controls, yet the degree to which the tissue undergoes convergent extension seems to occur at a rate significantly less than that even (Figure 32B). With the failure of the neural folds to fuse and severely shortened, curved axes, the phenotypes resulting from dorsal Xdd1 and Pk2ΔPΔL expression appear nearly identical (Wallingford and Harland 2001) (Figure 32C), which is interesting considering the seemingly opposite effects on the localization of Pk2 and Myl9 between Xdd1 and Pk2ΔPΔL expression but similar effects on T-transition rate and frequency. Thus, it seems that a polarization of contractional forces is the defining factor of efficient convergent extension rearrangements than simply the presence or absence of junctional contractional machinery recruitment.

As an alternative to utilizing dominant-negative PCP constructs to probe the function of Pk2 in convergent extension, the effects of knocking down of Pk2 expression via antisense oligonucleotides were also examined. The neural folds tend to fuse together around Stage 20 (Keller et al. 1992), but this fusion can be either delayed or inhibited by the effects of knocking down levels Pk2 in the neural plate (Figure 35A,B). This effect can be partially rescued with the addition of GFP-Pk2 mRNA and is somewhat mimicked by the introduction of the mRNA rescue dose without Pk2 knock down. Similarly, reducing levels of Pk2 disrupts the elongation of
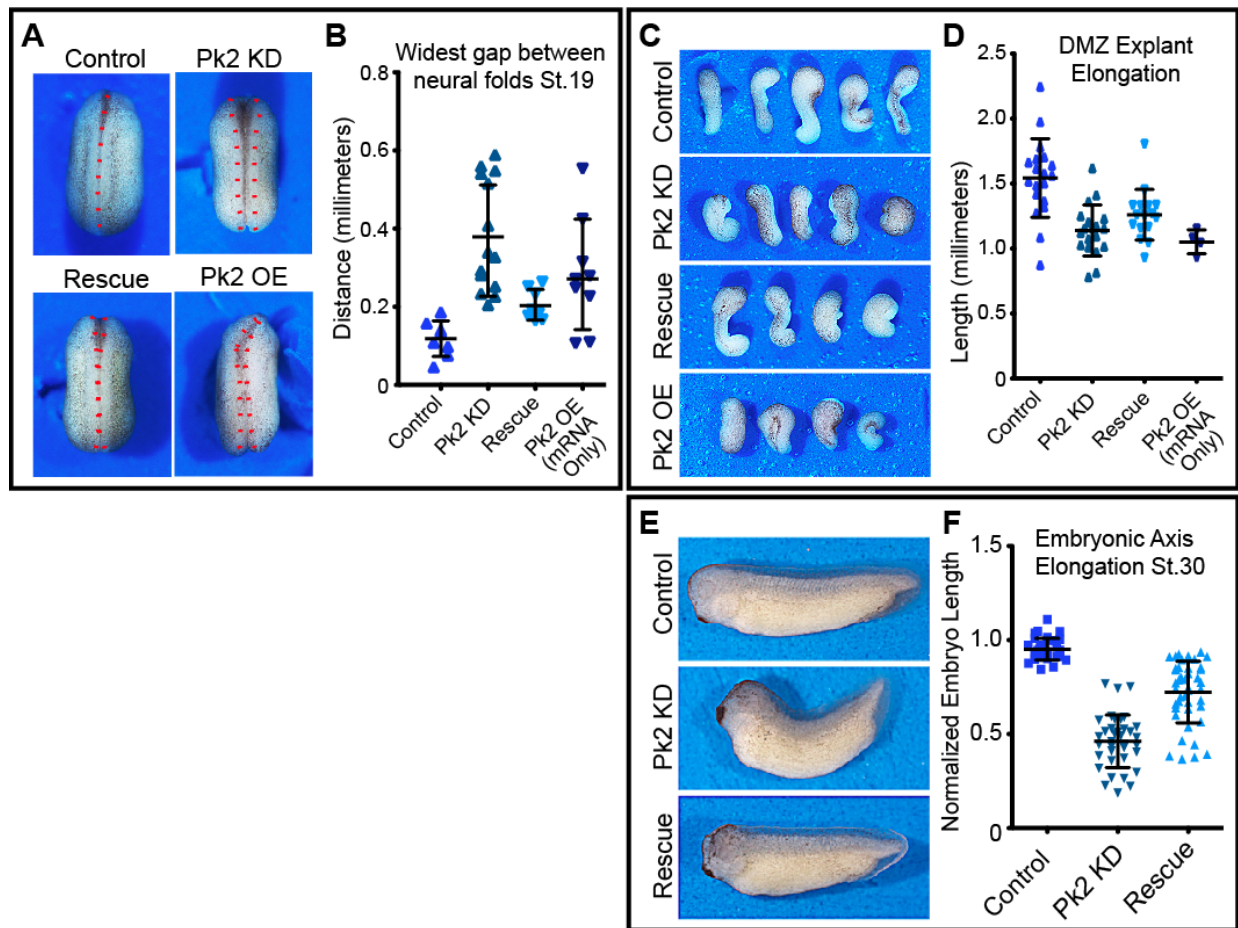
Figure 35: Pk2 knockdown results in embryonic convergent extension phenotypes. **(A)** Dorsal view Stereoscope images of a representative Stage 20 control embryo, embryo that has been injected dorsally with 25ng Pk2 morpholino, embryo that received morpholino plus a 400pg GFP-Pk2 mRNA rescue dose, and embryo that received only the 400pg Pk2 mRNA. Anterior is up **(B)** Graph of the distance between the neural folds at stage 20. n=8 (Control), 14 (Pk2 KD), 8 (Rescue), 9 (RNA/OE). Control vs. KD, $p<0.0001$; vs. Rescue, $p=0.0019$; vs. OE, $p=0.0079$ **(C)** Images of Dorsal marginal zone (DMZ) explants dissected from stage 11.5 embryos of the treated under the same conditions as in **(A)**. **(D)** Graph of DMZ explant length at a time when embryos that had not been dissected had reached Stage 20. n=19 (Control), 19 (Pk2 KD), 16 (Rescue), 4 (RNA/OE). Control vs. KD, $p<0.0001$; vs. Rescue, $p=0.0010$; vs. OE, $p=0.0041$ **(E)** Representative images of Stage 30 embryos that received 30ng Pk2 morpholino, morpholino plus 400pg rescue GFP-Pk2 mRNA, or controls that received neither. Anterior is left and dorsal is up. **(F)** Graph of the length of the dorsal embryonic length of embryos represented by those shown in **(E)**. n=35 (Control), 37 (Pk2 KD), 44 (Rescue). Control vs. KD, $p<0.0001$; vs. Rescue, $p<0.0001$.

explanted dorsal gastrula mesoderm, a tissue that typically elongates despite being dissected from the embryo (Figure 35C,D). This effect of reducing explant elongation can be partially rescued with GFP-Pk2 mRNA as well and inhibited by the rescue dose alone (Figure 35C,D). As a result of inhibiting he convergent extension movements in the neural plate and dorsal gastrula mesoderm, moderate Pk2 knockdown disrupts the elongation of the embryonic axis and results in shorter, wider embryos with considerably curved dorsal axes at the later tailbud stages (Figure 35E,F). Together, these results further demonstrate the importance of Pk function in coordinating vertebrate convergent extension behaviors during gastrulation and neurulation stages.

3.5: Pk2 and Vangl2 are more stable at shrinking junctions, and human NTD mutations disrupt normal localization dynamics

PCP signaling clearly plays an important role in animal models of neural tube morphogenesis, and there is a multitude of mutations in genes encoding several different core PCP family members have been identified in human neural tube defect (NTD) patient studies (De Marco 2014, Butler and Wallingford 2017). Even though the asymmetric localization and control of polarized cell behavior are among the most fundamental properties of core PCP signaling components, there is still a scarcity of information regarding how various PCP alleles implicated human with NTD's can affect the asymmetric localization and behavior of the protein. To study these potential effects, I generated 10 constructs consisting of GFP fused to either Pk2 or Vangl2 harboring different human NTD allele point mutations that have been previously identified in Pk and Vangl family members (Lei 2010, Kibar 2011, Bosoi 2011) and examined their localization (Figure 36).
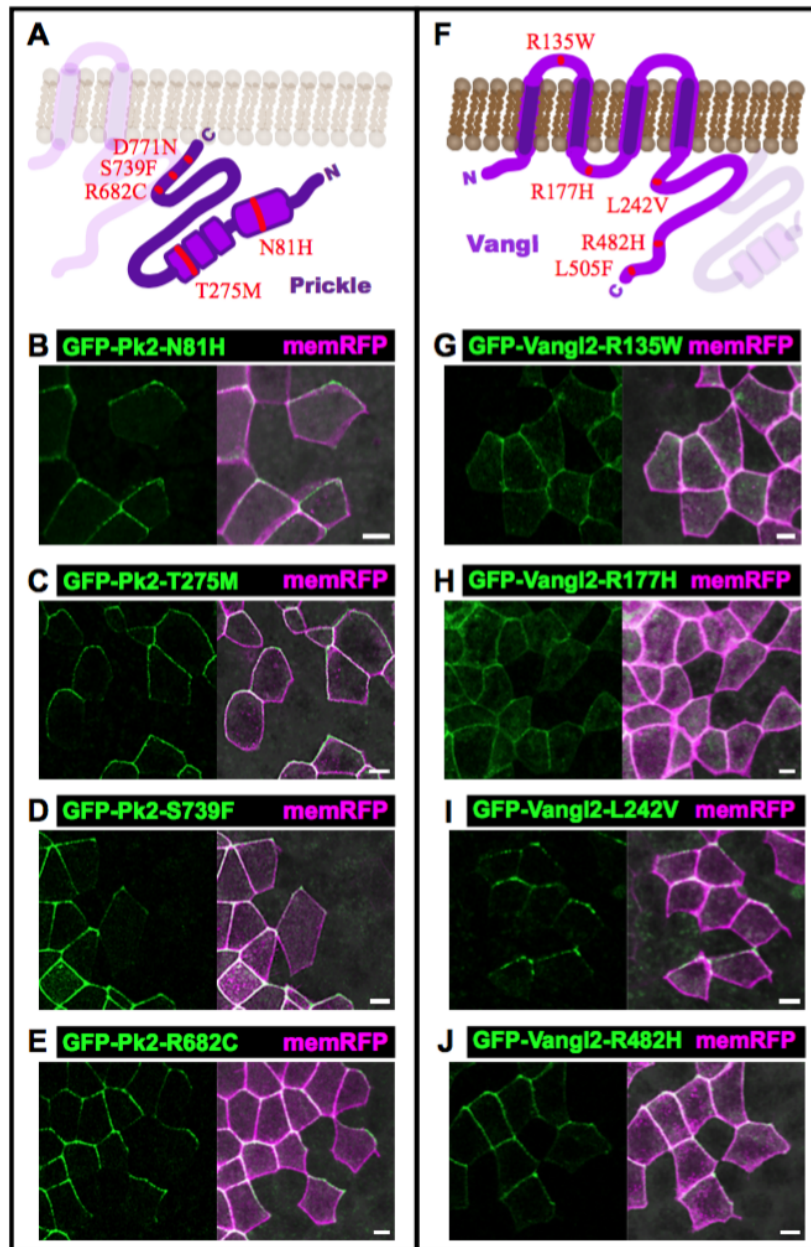
Figure 36: Some PCP point mutations identified in human NTD patient studies disrupt asymmetric localization. **(A)** Schematic of the *Xenopus* Pk2 point mutants prepared analogous to human Pk1 NTD alleles. **(F)** Schematic of the *Xenopus* Vangl2 point mutants prepared analogous to human Vangl2 NTD alleles. **(B-E, G-J)** Confocal images showing localization of GFP fused to the Pk2 **(B-E)** and Vangl2 **(G-J)** point mutants along with membraneRFP in mosaically labeled cell in the *Xenopus* neural plate. Anterior is up, and scale bars = 10μm. Note that the proteins as they are portrayed are not necessarily to scale and merely approximations as there is no high-resolution protein structural data available to support them.

The majority of the Pk2 point mutants appeared to localize normally (Figure 36B-E), with the Pk2 D771N point mutant being the exception due to a seemingly minor increase in intensity at mediolateral and posterior junctions (Figure 37A). In order to characterize the changes in localization caused by the D771N point mutation in more detail, I analyzed the fluorescence recovery after photobleaching the GFP fusion constructs at AP junctions. Initial analysis revealed only minor differences in recovery kinetics between the point mutants and wild type protein; however, separating the recovery curves based on whether the junctions examined were actively contracting (shrinking at least 0.5μm over the course of the experiment) or not revealed significant differences both within and between the different data sets (Figure 37B).

While the D771N point mutation did not appear to significantly alter the mobile fraction for GFP-Pk2, and both fusion proteins exhibited a significant correlation between the change in junction length and nonmobile fraction, there did seem to be difference in the rate of fluorescent recovery between them (Figure 37B,C). These data were interesting for two reasons, then, demonstrating that Pk2 is more stable at actively contracting junctions, and that the D771N point mutation seems to affect the recovery rate at both contracting and noncontracting junctions. Reflecting the difference between the wild type Pk2 protein and point mutant, choosing the best fit for the mean fluorescence recovery curves revealed that while a two-phase association model was preferred for the control recovery curves, one-phase association resulted in a better fit for Pk2 D771N (Figure 38A,B). This further suggests that variable behavior in Pk2 protein localization dynamics is caused by the D771N point mutation.

Similar analyses of localization behavior were also performed with Vangl2 and Vangl2 NTD alleles. Vangl2 L242V and R482H point mutants also appeared to localize normally, but the anterior enrichment at AP junctions appeared reduced with R135W, R177H, and L505F mutations (Figures 36G-J and 37D). The L505F mutant additionally appeared localized to
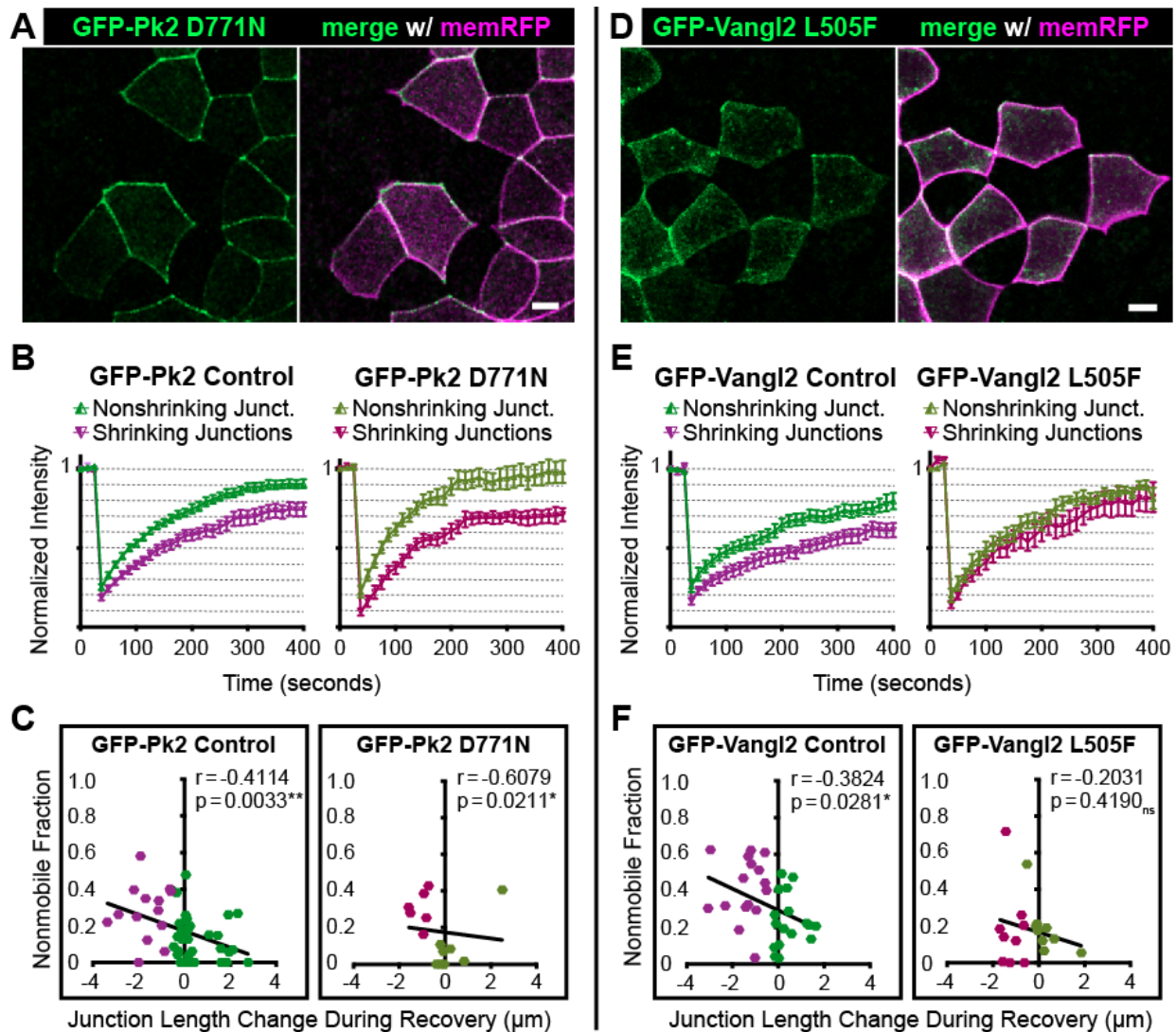
Figure 37: Pk2 and Vangl2 are more stable at shrinking junctions, and human NTD alleles alter protein localization dynamics. **(A)** Confocal images showing the localization of the GFP-Pk2 D771N point mutant. Anterior is up and scale bar = 10μm **(B)** Fluorescence recovery after photobleaching at shrinking and nonshrinking junctions for wild type GFP-Pk2 and GFP-Pk2 D771N. Shrinking juntions are defined as those that were reduced by 0.5μm or more in length over the course of the experiment. n=34 nonshrinking, n=15 shrinking (Control), n=8 nonshrinking, 6 shrinking (D771N) **(C)** Graph plotting the change in junction length during photobleaching and recovery against the calculated nonmobile fraction for each individual junction accounted for in (B), with associated linear regression model and correlation analysis statistics included. n= 49 (Control), 14 (D771N) **(D)** Confocal images showing the localization of the GFP-Vangl2 L505F point mutant. Anterior is up and scale bar = 10μm **(E)** Fluorescence recovery after photobleaching at shrinking and nonshrinking junctions for wild type GFP-Vangl2 and GFP-Vangl2 L505F, as in (B). n= 17 nonshriking, n=16 shrinking (Control), L505F n=8 nonshrinking, n=10 shrinking (L505F) **(F)** Graph plotting the change in junction length during photobleaching and recovery against the calculated nonmobile fraction for each individual junction accounted for in (E), with associated linear regression model and correlation analysis statistics included. n=33 (Control), 18 (L505F).

91
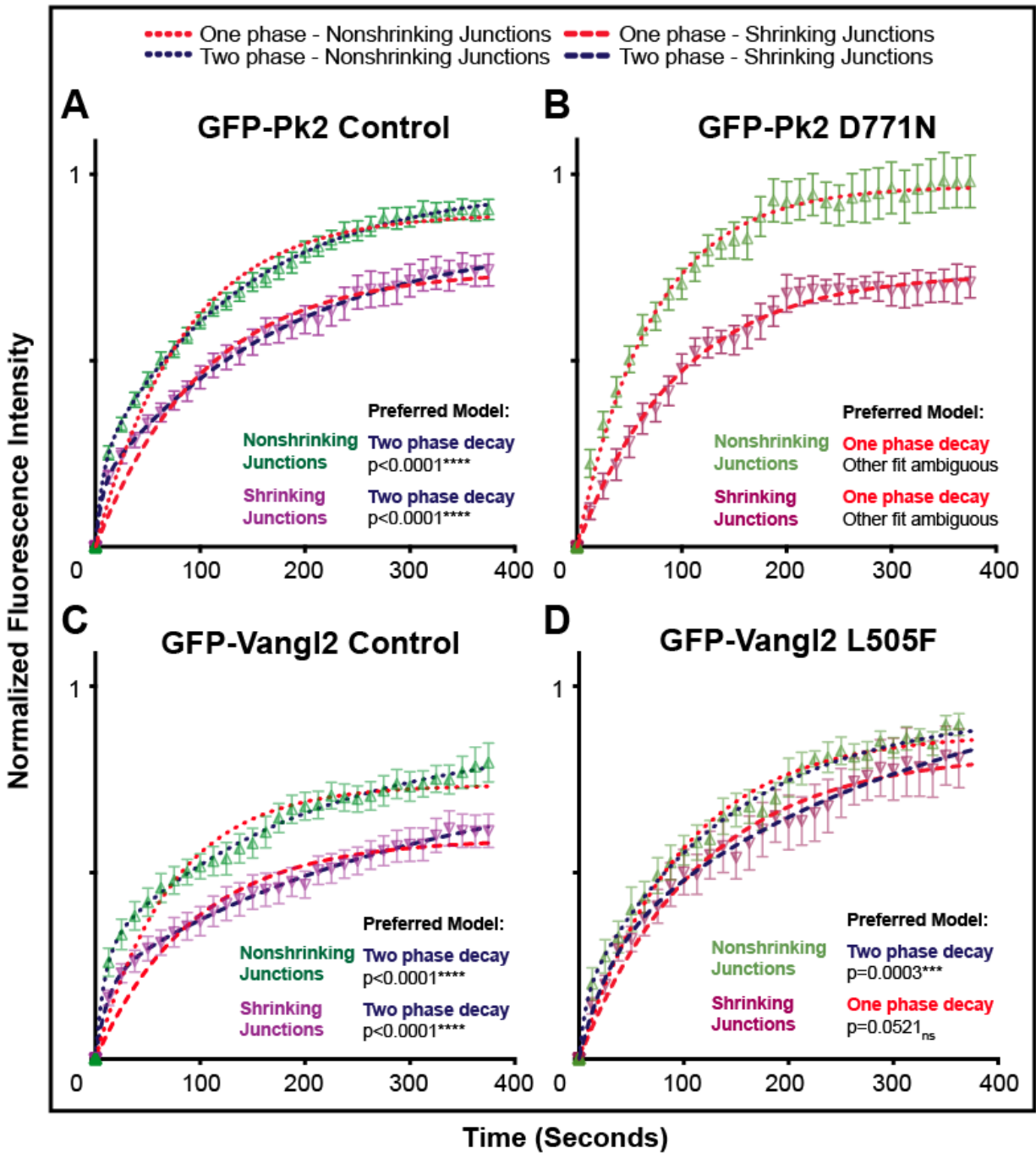
Figure 38: The Pk2-D771N and Vangl2-L505F point mutations alter FRAP recovery kinetics. **(A-D)** Graphs illustrating the results of fitting one-phase and two-phase association models to the mean recovery curves show in Figure 37B and 37E.

cytoplasmic punctae and along posterior and mediolateral junctions to some degree (Figure 37D), thus emerging as potentially the most damaging mutant in the context of localization and behavior disruption and best candidate for further analysis. At nonshrinking junctions, recovery curves for Vangl2 L505F were comparable to wild type, but there appeared to be a significant reduction in the nonmobile fraction at shrinking junctions caused by point mutant (Figure 37E). This eliminated the significant difference seen between shrinking and nonshrinking junctions and the correlation between the change in junction length and nonmobile fraction (Figure 37F). Similar to Pk2, two-phase association curves were better fits for the wild type Vangl2 recovery data at both shrinking and nonshrinking junctions, and while this model was also preferred for Vangl2 L505F at nonshrinking junctions, one phase decay was a better fit at shrinking junctions. These analyses reveal fundamental differences in the localization behavior of Vangl2 caused by a human NTD allele point mutant.

2.6: DISCUSSION

While significant strides have been made in our understanding of PCP in more static epithelial tissues (in particular in the fly), the mechanism of PCP signaling during convergent extension is only now coming into focus. This slow progress likely reflects the dynamic nature of PCP processes, which are more easily visualized in stable tissues. Unlike other epithelia, cells undergoing convergent extension constantly exchange their neighbors. Dynamic analyses of epithelial PCP protein localization with time-lapse imaging and probing localization stability utilizing photobleaching and photoconversion techniques are now providing deeper mechanistic insights into PCP signaling (Butler & Wallingford 2015, Chien et al. 2015, Shi et al. 2016, Strutt

et al. 2011); further studies of PCP involvement in convergent extension, such as that presented here, should also benefit from the application of similar techniques.

In the *Drosophila* wing blade, the junctional accumulation and polarized enrichment of core PCP proteins is reduced during hinge contraction and relatively dynamic cell rearrangements in this tissue (Aigouy et al. 2010fl). However, it is interesting that here, in the *Xenopus* neural plate, that a high degree of asymmetry is maintained during cellular rearrangements, and that Pk2 and Vangl2 are even most asymmetrically enriched at a class of highly dynamic cell-cell junctions. In addition, the high degree of localization asymmetry seen, comparable to the fully polarized epidermal tissue discussed in Chapter 2, is quite surprising given the highly dynamic nature of the Pk2 and Vangl2 examined via FRAP studies. It seems there is potentially more tension in neural plate than in epidermis, as processes such as cell pulling on one another via junction contractions along with the more rapid tissue axis elongation and changes in the tissue landscape occurring here. Such increased mechanical forces could be providing a means for orienting PCP orientation despite lacking quite stable, intercellular PCP complexes (Figure 4C,D).

Several cases of GFP-Pk2 accumulations appearing as punctate structures that laterally diffused along cell-cell junctions were observed, often when imaging thin optical sections with high time resolution (See Figures 28A and 30A for the best examples of this). These could also be observed not only along the junctional regions of the cell, but also slightly further into the cell, but parallel along the junctions in a population that resembles an endosomal trafficking or recycling network (Classen et al. 2005, Strutt et al. 2011, Figure 3). Thus, it could be that the nature of this highly asymmetric yet simultaneously dynamic localization behavior is mediated by tight regulation of vesicular recycling and trafficking mechanisms, a topic that warrants further investigation.

The polarized recruitment of contractile actomyosin machinery to shrinking junctions has been shown to be a conserved mechanism in tissue morphogenesis during gastrulation in both invertebrates and vertebrates (Zallen et al. 2004, Bertet et al. 2004, Blackenship et al. 2006, Nishimura et al. 2012, Shindo & Wallingford 2014), and I now offer evidence to extend this to the *Xenopus* neural plate as well. Although it is clear from this work that Pk2 and Myl9 are enriched together and behave similar during convergent extension, the nature of this association still requires much to be detailed. Perhaps dynamic trafficking or recycling of Pk2 and Vangl2 components could also be a means to facilitate medial myosin flows, which have been described as important for supporting planar polarized contractility of junctions in some contexts (Rauzi et al. 2010) and warrant further study. Additionally, it is not yet clear if accumulations of Pk2 are somehow recruiting actomyosin contractional machinery, or if increased tension at AP junctions is promoting the recruitment of Pk2 and thus Vangl2 (see Figure 4 and section 1.3.4); or perhaps it is even more likely that Pk2 and Myl9 recruitment involves some combination of both involving a feedback loop. PCP signaling components have been shown to activate cytoskeletal machinery such as RhoA and ROCK (Strutt et al. 1997, Winter et al. 2001), though these studies were associated with components of the Frizzled and Dishevelled side of the asymmetric pattern, which could theoretically contract one side of the cell-cell junction causing Pk2 and Myl9 to be stabilized on the other side. Unfortunately I failed to identify a robust asymmetric marker from the Fzd and Dvl constructs tested in the epidermis, thought Dvl1 did exhibit a very minor posterior enrichment (data not shown).

Among the first vertebrate PCP phenotypes described, defective PCP signaling has long been know to disrupt the convergent extension movements during gastrulation and neurulation. The PCP-specific Xdd1 construct was unique in that it did not appear to disrupt canonical Wnt signaling, in which Dishevelled and Frizzled proteins play key roles (Sokol 1996, Axelrod et al.

1998). The effects of Xdd1 have long been described to lead to failure to bring neural folds close enough to fold by disrupting tissue elongation. In imaging the cellular behaviors involved, my data extends upon this and offers the notion that less efficient cellular rearrangments leads less cells aligned along the hinge points along which apical constriction drive neural plate folding, so that ultimately fewer cells are constricting, providing the force to fold the plate, and more cells are lateral to the hinge point, leading to more cellular mass to fold inwards.

Lastly, work detailed in this chapter provides some of the first evidence for how mutations identified in PCP genes in human patients studies might impact protein localization and behavior. Previous studies examining the effects of such mutations have generally utilized mammalian cell culture systems (eg. Iliescu et al. 2014), which lack the necessary inputs for developmental patterning of PCP signaling components. One issue with using *Xenopus* as presented here is the potential for proteins encoded by damaging alleles to be recruited or enriched by the endogenous proteins, something that could potentially be corrected as the techniques to knock mutant alleles into the endogenous loci of *Xenopus* improve. I consider this and techniques for tagging endogenous loci with markers such as fluorescent proteins to be an essential focus of future work utilizing this strong platform.

CHAPTER 4: CONCLUDING REMARKS ON CONTEXT AND SIGNIFICANCE

PCP signaling is a ubiquitous mechanism of tissue patterning, with particular importance for animal development. Understanding the dynamics of PCP patterning events in vivo provides potential insights regarding the function and interactions of the molecular players involved, yet studies in vertebrates have been limited in this respect. As development is such a dynamic process, there is a wealth of knowledge to be gained from highly quantitative analysis time resolution time lapse imaging capture. In addition, there is often a loss of contextual inputs, whether mechanical or molecular, in cell culture and explants that can only be maintained in intact living embryos. I describe here the use of novel reporters and techniques for in vivo imaging of the dynamic localization of vertebrate core PCP proteins in Xenopus, further supplementing this established rapid and tractable vertebrate PCP model. The relative ease of observing epidermal MCCs has contributed to them being an excellent platform for analysis of planar polarization for decades (König and Hausen, 1993; Twitty, 1928). Early studies of the role for PCP signaling in MCC directional beating were performed in these cells, prefiguring the work in mammals (Mitchell et al., 2009; Park et al., 2008). In addition, some of groundbreaking original studies of vertebrate PCP signaling were in context of convergent extension in Xenopus, and the use of labeling and imaging the neural plate epithelia with the markers and methods I describe here has the potential to substantiate the value of this platform moving forward.

Many of the initial studies that have contributed a large portion to our understanding of PCP protein patterning dynamics were carried out using *Drosophila* as a model system, which is in part due to the relative ease of creating genetic mosaics and live imaging PCP proteins *in vivo* here. Similar techniques have been employed in vertebrate models, but further development of

the tools and methods for studying the dynamics of vertebrate PCP pattering and signaling are particularly important due to the increased complexity of multiple PCP family members and the wide array of interesting, PCP-patterned tissues that are more specific to vertebrates (e.g. multicilated epithelia, tissues of the inner ear, etc.). As different PCP family members can behave differently in varying contexts, having been shown to clearly have cell-type and tissue-specific localizations and functions, comprehensive analysis should continue to be conducted without assuming redundancy between these PCP signaling components outright. I present here work from the first published study of core PCP FRAP kinetics in a vertebrate model, a tool that has maintained significant value throughout my dissertation studies, as has my approach to quantifying asymmetric enrichment of PCP markers along different faces of the cell (PCP enrichment). Disseminating my PCP markers and methods has already allowed for similar PCP enrichment analyses in the characterization of at least one novel vertebrate gene (Jaffe et al. 2016), with additional studies that benefit from using the methods presented hopefully to come.

Lastly, I provide here an in depth study of how a vertebrate Prickle participates in PCP patterning and signaling, providing novel insights in the function and structure of this arguably under studied gene (at least compared to other core PCP family members). Pk occupies an interesting space among PCP genes, having uniquely shown to have multiple isoforms that interface with Ft-Ds-Fj signaling and impact PCP directionality in *Drosophila* (Gubb et al. 1999, Ayukawa et al. 2014) on one hand, and having been associated with the establishment of apical-basal polarity during mouse epiblast formation, along with a functional nuclear localization (Tao et al. 2012) on the other. Additionally, including links to the many human disorders mentioned previously, Pk specifically has been shown to be potentially associated human neurological disorders, such as epilepsy, and possibly autism (Okumura et al., 2014; Sowers et al., 2013; Tao

et al., 2011). Further work with this interesting gene is warranted to uncover its potential role in these and potentially other developmental disorders.

APPENDIX: MATERIALS AND METHODS

A.1: *XENOPUS* MANIPULATIONS

Eggs were collected and fertilized according to standard protocols (Sive et al. 1998). The jelly coat was removed from embryos at the 2-cell stage by bathing in a solution of 2% cysteine (pH 7.9). The embryos were then washed in 1/3x Marc's Modified Ringer's (MMR) solution and microinjected in a solution of 1/3x MMR with 2% Ficoll using an Oxford manipulator. The mRNAs coding for fluorescent protein fusions were synthesized using mMessage mMachine kits (Ambion). For all manipulations, developmental stages were determined according to Nieuwkoop and Faber (1967).

A.2: MORPHOLINO AND PLASMID DESIGN

The splice-blocking Pk2 morpholino oligonucleotide was designed based on the longest mRNA sequence obtained from the UTexas Oktoberfest gene models available from Xenbase.org. The sequence for splice-blocking Pk2 Morpholino #1 is GATTGGACAAAGGATTCTCACCTCA and complementary to the region spanning the 3' end of exon 4 and 5' end of intron 4 of sequence JGIv6.000014371_26644_262472 and was prepared by GeneTools, LLC. The second splicing morpholino Pk2-MO#2 has the sequence GAACCCAAACAAACACTTACCTGTT and is complementary to the region spanning the 3' end of exon 3 and 5' end of intron 3.

The Pk2 Primers used for cloning the CDS into Pk2 CS107-GFP using StuI and NotI were:

5'-ATAGGCCTATGTTTAACCGGAGCTCTTGGACAAGGGCTTC -3'
5'-ATGCGGCCGCCTAGGAGATGATGCAATTTTTGCTTTTTCGCCTTT -3'

The CDS following list of genes were cloned into Gateway entry vectors using the Invitrogen

pENTR™/D-TOPO® cloning system for recombination of coding sequences into pCSDest GFP

or RFP vectors. The sequences and primers used are as follows:

Pk2 for RFP-Pk2
5'-CACCATGTTTAACCGGAGCTCTTGGACAAGGGCTTCCAGC -3'
5'-CTAGGAGATGATGCAATTTTTGCTTTTTCGCCTTTTTCTG -3'

Dvl1 Sequence Genbank BC074103.1 and Primers:
5'-CACCATGGCTGAGACCAAAATCATCTACCATATAGATGAA -3'
5'-CATGATGTCAACAAAGAATTCACAAGGGTTCCCCA -3'

Dvl3 Sequence NCBI ref NM_001092629.1 and Primers:
5'-CACCATGGGGGAGACCAAGGTCATCTACCACCTGGATGAA-3'
5'-AACACCCCAGAATTCTTTGATAACATCCACAAAGAACTCA-3'

Fzd6 Sequence JGIv7b.000063404_134470-165935+ and Primers:
5'-CACCATGGATCTGATTGGCTGCTGCCTCCAAGCTCCGAGC-3'
5'-TCACGCACTTGTCGTATTAATATTAATGTCATTGGCATGG-3'

Vangl1 Sequence JGIv7b.000169011_589431-599179+ and Primers:
5'-CACCATGGACACGGAATCCAACCACTCGGGATATTCACAT-3'
5'-TCACAGGTTGGTCTCAGGTTTGCTACTCACAATGAGACGA-3'

Pk2 deletion constructs were amplified by fusing 2 PCR products generated with the above and

following primers:

ΔPET-1
5'-AGATGGCACCAGTCATGGTTACTGGGAAAAAGTCAAACATCAGCTTGTTC-3'

ΔPET-2
5'-AACTATGAACAAGCTGATGTTTGACTTTTTCCCAGTAACCATGACTGGTG-3'

ΔPETΔLIM-1
5'-AGGCGGAATCTGAAGAGTCCGAGCCATTAAAGTCAAACATCAGCTTGTTC-3'

ΔPETΔLIM-2

101

5'-AACTATGAACAAGCTGATGTTTGACTTTAATGGCTCGGACTCTTCAGATT-3'

ΔC2-1
5'-CCGTGATAATGAGCAACACTATCGACATTCTTCAGAGTCTGACAATGAAG-3'

ΔC2-2
5'- AGTATCCTTCATTGTCAGACTCTGAAGAATGTCGATAGTGTTGCTCATTA-3'

These fusions resulted in the removal of amino acids 77-176 for Pk2-ΔPET, 77-382 for Pk2-ΔPETΔLIM, and 734-827 for Pk2-ΔC2.

Dvl1-ΔPDZ$_{partial}$ was amplified by fusing 2 PCR products generated with the above and following primers:

5'-TGTAGCAGCGGATGGGCGTATTGAACCTATGGGCCCCTCCATGAGCATCATCACAT-3'
5'-ATGTGATGATGCTCATGGAGGGGCCCATAGGTTCAATACGCCCATCCGCTGCTACA-3'

This fusion resulted in the removal of amino acids 300-380.

Plasmids encoding GFP fused to Pk2 and Vangl2 variants harboring point mutations identified in human NTD patients were constructed via NEB Hifi assembly reactions, using pCSDest-Nterm-GFP as the vector backbone fragment prepared via restriction enzyme digest using NheI and KpnI and two insert fragments that centrally overlap the point mutation of interest. Primers were used to amplify the DNA insert fragments using the wild type GFP fusion constructs used previously (Butler and Wallingford 2015) as the template, with sequences:

pCSDest-NtermGFP Backbone Forward Primer
5'-CGATTCGAATTCAAGGCTAGCGCTACCGGTCGCCACCATG-3'

pCSDest-NtermGFP Backbone Reverse Primer
5'-CTAAAGGGAACAAAAGCTGGGTACCGGGCCCAATGCATTG-3'

GFP-Pk2 N81H
5'-CAGCTGCCTCCGCATGACCATGAGGTCCGGTATTGCAATT-3'
5'-AATTGCAATACCGGACCTCATGGTCATGCGGAGGCAGCTG-3'

GFP-Pk2 T275M

5'-GGCCAACACTGGCATGCAATGGAGAACTGTTTCTGTTGCG-3'
5'-GCAACAGAAACAGTTCTCCATTGCATGCCAGTGTTGGCC-3'

GFP-Pk2 R682C
5'-GAGAAGGTCAAGGCGTTCCTGTTCTGATAACGCCCTCCAC-3'
5'-GTGGAGGGCGTTATCAGAACAGGAACGCCTTGACCTTCTC-3'

GFP-Pk2 S739F
5'-CGTTATCAAAAGACTGCTTTCGACCTTGCTTTACAAAACC-3'
5'-GGTTTTGTAAAGCAAGGTCGAAAGCAGTCTTTTGATAACG-3'

GFP-Pk2 D771N
5'-CTCCTCCTCTTCAGAGTCCAACAATGAAGGATATTTCTTA-3'
5'-TAAGAAATATCCTTCATTGTTGGACTCTGAAGAGGAGGAG-3'

GFP-Vangl2 R135W
5'-TGCTGCCCCAGATCCTATGG**T**GGGAGGACTTGGAGCAATG-3'
5'-CATTGCTCCAAGTCCTCCCACCATAGGATCTGGGGCAGCA-3'

GFP-Vangl2 R177H
5'-CCAAAAGCCTTCTTCCCACACGTGTTTGTTTTTCGAGCCC-3'
5'-GGGCTCGAAAAACAAACACGTGTGGGAAGAAGGCTTTTGG-3'

GFP-Vangl2 L242V
5'-CCTTCTGGAGTTGAGGCAGGTCCAGCCTCAGTTTACCATC-3'
5'-GATGGTAAACTGAGGCTGGACCTGCCTCAACTCCAGAAGG-3'

GFP-Vangl2 R482H
5'-CGTTGTGTTCGAATTGAAGCACCAAGACTTTAGCCTCGTG-3'
5'-CACGAGGCTAAAGTCTTGGTGCTTCAATTCGAACACAACG-3'

GFP-Vangl2 L505F
5'-ATAAGTTTGTCATGAGATTTCAATCAGAGACCTCGGTTTG-3'
5'-CAAACCGAGGTCTCTGATTGAAATCTCATGACAAACTTAT-3'

Verification of new plasmid sequences was carried out via DNA sequencing data obtained from the services of the UT Austin DNA core facility.

A.3: MORPHOLINO AND MRNA INJECTIONS

For ventral injections targeting the epidermis, 20-25ng of Pk2 morpholino was injected into one cell at the sixteen-cell stage for mosaic analysis. For dorsal rescues experiments, an

amount of 30ng was injected at the four-cell stage, and Pk2 was overexpressed at 600-750pg at the sixteen- cell stage (for determining PCP localization defects) or upwards of 1ng of mRNA at the four-cell stage (for determining ciliary orientation defects). About 22ng was injected for both Wdpcp/Fritz and Inturned morpholinos at the 16-cell stage. Core PCP fluorescent protein fusion mRNA was injected into one of sixteen or thirty-two cells along with ~50pg of memRFP mRNA, with approximate amounts being 20-30pg for Dvl1-GFP, Dvl2-GFP, and Dvl3-GFP, 60-80pg Fzd6-GFP, Fzd7-GFP, and Fzd8-GFP, ~150pg for GFP/RFP-Pk2, and 50-60pg for GFP-Vangl1 and GFP-Vangl2. Pk2 deletion constructs were injected at 125-150pg for localization of GFP fused constructs and 700-800pg for overexpression of non-GFP fused constructs at the sixteen-cell stage. This amount was increased to 1ng at the 4-cell stage for the determination of effects on ciliary orientation. For Vangl1 and Dvl-ΔPDZ$_{partial}$ constructs injected at the 4 cell stage, 880pg were introduced. Centrin-RFP, CLAMP-GFP and GFP-Pk2 were co-injected into one of four cells at 60pg, 60pg, and 150pg, respectively.

For dorsal injections targeting the neural plate, Pk2 morpholino treatments was injected at 20-25ng per each of the two blastomeres that will give rise to dorsal ectoderm at the eight-cell stage, and 400pg of GFP-Pk2 were used to rescue the morpholino phenotypes. Synthetic mRNA was injected into one of eight dorsal blastomeres for even labeling at the following concentrations: 50pg membraneGFP, 60pg of membraneRFP, 80pg of membraneBFP, 200pg for GFP- or RFP-Pk2 and human NTD point mutants, 60pg for GFP-Vangl2 and human NTD point mutants, 50pg for H2B-RFP, and 30pg for Myl9-GFP. For mosaically labeled tissues, mRNAs were injected at the sixteen- or thirty-two-cell stages with approximately 70% of the totals amounts listed above. Dominant-negative Pk2 (Pk2ΔPETΔLIM) was injected at 700-800pg for overexpression at the eight-cell stage, as was the dominant-negative Dvl (Xdd1), and both were similarly reduced by around 70% for injections at later stages for mosaics.

104

A.4: LIVE IMAGING OF EMBRYOS

All confocal imaging was done using live embryos gently sandwiched between coverglasses using silicon grease as an adhesive spacer and carried out with a Zeiss LSM700 confocal microscope. For time lapse imaging of neural tube closure, imaging of embryonic phenotypes and assessment of flow across the epidermis, embryos were placed on modeling clay submerged in 1/3x MMR and photographed or filmed using Zeiss AXIO Zoom.V16 Stereomicroscope and associated Zen software. For flow analysis, blue latex beads were loaded into the medium.

A.5: IMAGE QUANTIFICATION AND DATA ANALYSIS

Images were processed with the Fiji distribution of ImageJ, Imaris (Bitplane) and Photoshop (Adobe) software suites, and figures were assembled in Illustrator (Adobe). For PCP enrichment measures, freehand lines (3-5 pixels wide, depending on image zoom) were drawn over dorsoanterior and ventroposterior memRFP-labeled cell membranes with unlabeled neighbors on images in the Fiji distribution of ImageJ for mean intensity measurements. PCP enrichment was calculated by taking the natural log of the final value obtained after dividing the dorsoanterior measurements by the ventroposterior measurements, both of which were normalized values of PCP-GFP average intensity divided by the membraneRFP intensity at the same region. Statistical analyses were carried out using Graphpad Prism software with Mann Whitney tests for significance. For junction length and protein enrichment measures, freehand lines (3-5 pixels wide, depending on image zoom) were similarly drawn over cell membranes,

while cytoplasmic measures were taken with the freehand shapes tools. Statistical analyses were carried out using Graphpad Prism software with Mann Whitney tests for significance.

For FRAP analysis, junctional intensity measurements were performed in Fiji similarly to above, with recordings for each time point taken individually from each frame captured at bleached regions and normalized as detailed in (Goldman et al., 2005). Recovery trend lines were calculated and plotted in Graphpad Prism software with one phase decay or two phase decay exponential association curve fitting.

Ciliary orientations were determined manually in Fiji, and Mean Polarity Vectors and Mean Vector lengths were calculated with the CircStat Matlab circular statistics toolbox (Berens, 2009) before values were plotted with Oriana software (Kovach Computing Services). Angles of new junctions emerging from resolving rosettes were similarly determined manually in Fiji and plotted as rose diagrams with Oriana software (Kovach Computing Services).

Bead traces for flow analysis and cell tracking during neural convergent extension was performed with the Fiji manual tracking plug-in.

Wallingford Lab Plasmids

Record number	Plasmid name	Record number	Plasmid name
2948	pCS107-Prickle2 (L)	2937	Dvl3-eGFP
2949	a-tub-promoter-GFP-Prickle2 (L)	2938	CS107-Prickle3
3079	pENTR-Pk2L CTerm dC2	2939	eGFP-Prickle3
3080	pCSDEST GFP-Pk2L CTerm dC2	2940	Prickle2-eGFP (S)
3115	pCS10R-Dvl1-PA-GFP	2942	Prickle2-eGFP (L)
3397	GFP-Vangl1 (Long)	2951	pENTR-Vangl2
3411	pCSDest-mEos2 No Stop	2952	pENTR-PK2 (S)
3412	pCSDest-mEos2 Stop	2953	pENTR-Pk2 (L)
3413	pCSDest mEos2-Pk2	2954	pENTR-Dvl1 (New, topo)
3414	pCSDest mEos2-Vangl1	2973	pCS/GW-Dvl1-RFP
3415	pCSDest Dvl1-mEos2	2974	pCS/GW-RFP-Pk2 (L)
3416	pCSDest Fzd6-mEos2	2996	pENTR-Dvl2 (New, topo)
3418	pENTR-Wdpcp (no stop)	2997	pENTR-Dvl3 (New, topo)
3419	pENTR-Wdpcp (stop)	3054	pENTR-Nktr
3420	pENTR-Inturned (stop)	3055	pENTR-Sestd1
3421	pENTR-Inversin-a (no stop)	3056	pCSDest GFP-Sestd1
3422	pCSDest-Wdpcp-GFP	3057	pENTR-Vangl1 (short)
3423	pCSDest-GFP-Wdpcp	3058	pCSDest GFP-Vangl1 (Short)
3424	pCSDest-GFP-Inturned	3059	pENTR-Pk2L dPETdLIM
3425	pCSDest-Inversin-a-GFP	3060	pCSDest Pk2L dPETdLIM
3469	RFP-Vangl1	3061	pCSDest GFP-Pk2L dPETdLIM
3210	pENTR-Gli3 Truncated	3062	pCSDest Dvl2-GFP
2877	P2 - enpep promoter	3063	pCSDest GFP-Vangl2
2878	P2 - otx2 promoter	3068	pCSDest Fzd6-GFP
2879	CS107-mCherry-Vinculin-23	3069	pENTR-Pk2L dPET
2880	CS107-eGFP-Vinculin-13	3070	pENTR-Fzd6 STOP
2916	P2-Pax8 P/E	3071	pCSDest Nktr-GFP
2917	Pax8-memRFP Gateway Tg	3072	pCSDest Pk2L dPET
2918	enpep-memRFP Gateway Tg	3073	pCSDest GFP-Pk2L dPET
2924	CS107-Prickle2 (S)	3078	pENTR-Fzd6 NO STOP
2925	pENTR-PA-GFP (No Stop)	3219	Dest-Gli3 Trunc
2926	pENTR-Dvl1 (No Stop)	3220	Dest-Gli3(Trunc)-GFP
2930	pENTR-Dvl2 (No Stop)	2941	eGFP-Prickle2 (S)
2931	pENTR-Dvl3 (No Stop)	2944	Dvl1-eGFP

107

LIST OF ABBREVIATIONS

AP – anteroposterior or anterior-posterior

ML – mediolateral

NTD – Neural tube defect

MCC – Multiciliated cell

MO – Morpholino Oligonucleotide

KD – Knock down

OE – Over expression

Xdd1 – Dishevelled2-ΔPDZ$_{partial}$

Pk2-ΔPΔL – Prickle2-ΔPETΔLIM

PCP – Planar Cell Polarity

CE – Convergent extension

GFP – Green fluorescent protein

RFP – Red fluorescent protein

BFP – Blue fluorescent protein

FRAP – Fluorescence Recovery After Photobleaching (proxy for protein localization stability)

REFERENCES

Adler, P. N., Krasnow, R. E. and Lui, J. (1997). Tissue polarity points from cells that have higher Frizzled levels towards cells that have lower Frizzled levels. *Current Biology* 7, 940–949.

Adler, P. N., Taylor, J. and Charlton, J. (2000). The domineering non-autonomy of frizzled and van Gogh clones in the Drosophila wing is a consequence of a disruption in local signaling. *Mech Dev* 96, 197–207.

Adler PN. 2012. The frizzled/stan pathway and planar cell polarity in the Drosophila wing. *Curr Top Dev Biol*. 101:1–31

Afzal AR, Rajab A, Fenske CD, Oldridge M, Elanko N, et al. 2000. Recessive Robinow syndrome, allelic to dominant brachydactyly type B, is caused by mutation of ROR2. *Nature Genetics*. 25(4):419–22

Aigouy B, Farhadifar R, Staple DB, Sagner A, Röper J-C, et al. 2010. Cell Flow Reorients the Axis of Planar Polarity in the Wing Epithelium of Drosophila. *Cell*. 142(5):773–86

Ambegaonkar AA, Irvine KD. 2015. Coordination of planar cell polarity pathways through Spiny legs. *eLife*. 4:

Ambegaonkar AA, Pan G, Mani M, Feng Y, Irvine KD. 2012. Propagation of Dachsous-Fat planar cell polarity. *Curr Biol*. 22(14):1302–8

Andersen MR, Farooq M, Koefoed K, Kjaer KW, Simony A, et al. 2016. Mutation of the planar cell polarity gene VANGL1 in adolescent idiopathic scoliosis. *Spine (Phila Pa 1976)*

Andreeva A, Lee J, Lohia M, Wu X, Macara IG, Lu X. 2014. PTK7-Src Signaling at Epithelial Cell Contacts Mediates Spatial Organizationof Actomyosin and Planar Cell Polarity. *Developmental Cell*. 29(1):20–33

Antic D, Stubbs JL, Suyama K, Kintner C, Scott MP, Axelrod JD. 2010. Planar Cell Polarity Enables Posterior Localization of Nodal Cilia and Left-Right Axis Determination during Mouse and Xenopus Embryogenesis. *PLoS ONE*. 5(2):e8999

Aw WY, Heck BW, Joyce B, Devenport D. 2016. Transient Tissue-Scale Deformation Coordinates Alignment of Planar Cell Polarity Junctions in the Mammalian Skin. *Curr Biol*. 1–12

Axelrod JD. 2001. Unipolar membrane association of Dishevelled mediates Frizzled planar cell polarity signaling. *Genes & Development*. 15(10):1182–87

Axelrod JD, Miller JR, Shulman JM, Moon RT, Perrimon N. 1998. Differential recruitment of Dishevelled provides signaling specificity in the planar cell polarity and Wingless signaling pathways. *Genes & Development*. 12(16):2610–22

Ayukawa T, Akiyama M, Mummery-Widmer JL, Stoeger T, Sasaki J, et al. 2014. Dachsous-Dependent Asymmetric Localization of Spiny-Legs Determines Planar Cell Polarity Orientation in Drosophila. *CELREP*. 8(2):610–21

Bastock R, Strutt H, Strutt D. 2003. Strabismus is asymmetrically localised and binds to Prickle and Dishevelled during Drosophila planar polarity patterning. *Development*. 130(13):3007–14

Berens, P. (2009). CircStat: A MATLAB Toolbox for Circular Statistics. 31, 1–21.

Bertet C, Sulak L, Lecuit T. 2004. Myosin-dependent junction remodelling controls planar cell intercalation and axis elongation. *Nature*. 429(6992):667–71

Blair A, Tomlinson A, Pham H, Gunsalus KC, Goldberg ML, Laski FA. 2006. Twinstar, the Drosophila homolog of cofilin/ADF, is required for planar cell polarity patterning. *Development*. 133(9):1789–97

Blankenship JT, Backovic ST, Sanny JSP, Weitz O, Zallen JA. 2006. Multicellular Rosette Formation Links Planar Cell Polarity to Tissue Morphogenesis. *Developmental Cell*. 11(4):459–70

Billett, F. S. and Gould, R. P. (1971). Fine structural changes in the differentiating epidermis of Xenopus laevis embryos. *J Anat* 108, 465–480.

Bosoi CM, Capra V, Allache R, Trinh VQ-H, De Marco P, et al. 2011. Identification and characterization of novel rare mutations in the planar cell polarity gene PRICKLE1 in human neural tube defects. *Hum. Mutat*. 32(12):1371–75

Bosveld F, Bonnet I, Guirao B, Tlili S, Wang Z, et al. 2012. Mechanical control of morphogenesis by Fat/Dachsous/Four-jointed planar cell polarity pathway. *Science*. 336(6082):724–27

Boutin C, Labedan P, Dimidschstein J, Richard F, Cremer H, et al. 2014. A dual role for planar cell polarity genes in ciliated cells. *Proceedings of the National Academy of Sciences*

Brittle A, Thomas C, Strutt D. 2012. Planar Polarity Specification through Asymmetric Subcellular Localization of Fat and Dachsous. *Curr Biol*. 22(10):907–14

Brittle AL, Repiso A, Casal J, Lawrence PA, Strutt D. 2010. Four-Jointed Modulates Growth and Planar Polarity by Reducing the Affinity of Dachsous for Fat. *Curr Biol*. 20(9):803–10

Brooks ER, Wallingford JB. 2014. Multiciliated Cells. *Curr Biol*. 24(19):R973–82

Bryant DM, Mostov KE. 2008. From cells to organs: building polarized tissue. *Nat Rev Mol Cell Biol*. 9(11):887–901

Brzoska HL, d'Esposito AM, Kolatsi-Joannou M, Patel V, Igarashi P, et al. 2016. Planar cell polarity genes Celsr1 and Vangl2 are necessary for kidney growth, differentiation, and rostrocaudal patterning. *Kidney Int*

Bunn KJ, Daniel P, Rösken HS, O'Neill AC, Cameron-Christie SR, et al. 2015. Mutations in DVL1 Causean Osteosclerotic Form of Robinow Syndrome. *The American Journal of Human Genetics*. 96(4):623–30

Butler MT, Wallingford JB. 2015. Control of vertebrate core planar cell polarity protein localization and dynamics by Prickle 2. *Development*. 142(19):3429–39

Carvajal-Gonzalez JM, Balmer S, Mendoza M, Dussert A, Collu G, et al. 2015. The clathrin adaptor AP-1 complex and Arf1 regulate planar cell polarity in vivo. *Nature Communications*. 6:6751–15

Casal J, Lawrence PA, Struhl G. 2006. Two separate molecular systems, Dachsous/Fat and Starry night/Frizzled, act independently to confer planar cell polarity. *Development*. 133(22):4561–72

Cervenka, I. *et al*. 2016. Dishevelled is a NEK2 kinase substrate controlling dynamics of centrosomal linker proteins. *Proc. Natl Acad. Sci. USA* **113**, 9304–9309

Chacon-Heszele, M., Ren, D., Reynolds, A., Chi, F., Chen, P. 2010. Regulation of cochlear convergent extension by the vertebrate planar cell polarity pathway is dependent on p120-catenin. *Development* 139: 968–978.

Chen W-S, Antic D, Matis M, Logan CY, Povelones M, et al. 2008. Asymmetric Homotypic Interactions of the Atypical Cadherin Flamingo Mediate Intercellular Polarity Signaling. *Cell*. 133(6):1093–1105

Chesarone MA, DuPage AG, Goode BL. 2009. Unleashing formins to remodel the actin and microtubule cytoskeletons. *Nat Rev Mol Cell Biol*. 11(1):62–74

Cheyette BNR, Waxman JS, Miller JR, Takemaru K-I, Sheldahl LC, et al. 2002. Dapper, a Dishevelled-associated antagonist of beta-catenin and JNK signaling, is required for notochord formation. *Developmental Cell*. 2(4):449–61

Chien Y-H, Keller R, Kintner C, Shook DR. 2015. Mechanical Strain Determines the Axis of Planar Polarity in Ciliated Epithelia. *Curr Biol*. 1–12

Cho B, Pierre-Louis G, Sagner A, Eaton S, Axelrod JD. 2015. Clustering and Negative Feedback by Endocytosis in Planar Cell Polarity Signaling Is Modulated by Ubiquitinylation of Prickle. *PLoS Genet*. 11(5):e1005259

Chu C-W, Sokol SY. 2016. Wnt proteins can direct planar cell polarity in vertebrate ectoderm. *eLife*. 5:e16463–33

Chung, M. I., Kwon, T., Tu, F., Brooks, E. R., Gupta, R., Meyer, M., Baker, J. C., Marcotte, E. M. and Wallingford, J. B. 2014. Coordinated genomic control of ciliogenesis and cell movement by RFX2. *eLife* 3, e01439–e01439.

Ciruna B, Jenny A, Lee D, Mlodzik M, Schier AF. 2006. Planar cell polarity signaling couples cell division and morphogenesis during neurulation. *Nature Cell Biology*. 439(7073):220–24

Collier, S., Lee, H., Burgess, R. and Adler, P. 2005. The WD40 Repeat Protein Fritz Links Cytoskeletal Planar Polarity to Frizzled Subcellular Localization in the Drosophila Epidermis. *Genetics* 169, 2035–2045

Cui, C., Chatterjee, B., Lozito, T. P., Zhang, Z., Francis, R. J., Yagi, H., Swanhart, L. M., Sanker, S., Francis, D., Yu, Q., et al. 2013. Wdpcp, a PCP Protein Required for Ciliogenesis, Regulates Directional Cell Migration and Cell Polarity by Direct Modulation of the Actin Cytoskeleton. *PLoS Biol* 11, e1001720

Curtin JA, Quint E, Tsipouri V, Arkell RM, Cattanach B, et al. 2003. Mutation of Celsr1 disrupts planar polarity of inner ear hair cells and causes severe neural tube defects in the mouse. *Curr Biol*. 13(13):1129–33

Classen A-K, Anderson KI, Marois E, Eaton S. 2005. Hexagonal Packing of Drosophila Wing Epithelial Cells by the Planar Cell Polarity Pathway. *Developmental Cell*. 9(6):805–17

Das G, Jenny A, Klein TJ, Eaton S, Mlodzik M. 2004. Diego interacts with Prickle and Strabismus/Van Gogh to localize planar cell polarity complexes. *Development*. 131(18):4467–76

Daulat AM, Luu O, Sing A, Zhang L, Wrana JL, et al. 2011. Mink1 regulates beta-catenin-independent Wnt signaling via Prickle phosphorylation. *Molecular and Cellular Biology*. 32(1):173–85

Davis CW, Dickey BF. 2008. Regulated Airway Goblet Cell Mucin Secretion. *Annu Rev Physiol*.

70(1):487–512

De Marco P, Merello E, Piatelli G, Cama A, Kibar Z, Capra V. 2014. Planar cell polarity gene mutations contribute to the etiology of human neural tube defects in our population. *Birth Defects Research Part A: Clinical and Molecular Teratology*. 100(8)

Deans, M. R., Antic, D., Suyama, K., Scott, M. P., Axelrod, J. D. and Goodrich, L. V. 2007. Asymmetric Distribution of Prickle-Like 2 Reveals an Early Underlying Polarization of Vestibular Sensory Epithelia in the Inner Ear. *Journal of Neuroscience* 27, 3139–3147

Devenport D. 2016. Tissue morphodynamics: Translating planar polarity cues into polarized cell behaviors. *Seminars in Cell and Developmental Biology*. 1–12

Devenport D, Oristian D, Heller E, Fuchs E. 2011. Mitotic internalization of planar cell polarity proteins preserves tissue polarity. *Nat Cell Biol*. 13(8):893–902

Dollar G, Gombos R, Barnett AA, Sanchez Hernandez D, Maung SMT, et al. 2016. Unique and Overlapping Functions of Formins Frl and DAAM During Ommatidial Rotation and Neuronal Development in Drosophila. *Genetics*. 202(3):1135–51

Drysdale, T. A. and Elinson, R. P. 1992. Cell migration and induction in the development of the surface ectodermal pattern of the Xenopus laevis tadpole. *Develop. Growth Differ*. 34, 51–59

Dubaissi, E. and Papalopulu, N. 2011. Embryonic frog epidermis: a model for the study of cell-cell interactions in the development of mucociliary disease. *Disease Models & Mechanisms* 4, 179–192

Dubaissi, E., Rousseau, K., Lea, R., Soto, X., Nardeosingh, S., Schweickert, A., Amaya, E., Thornton, D. J. and Papalopulu, N. 2014. A secretory cell type develops alongside multiciliated cells, ionocytes and goblet cells, and provides a protective, anti-infective function in the frog embryonic mucociliary epidermis. *Development* 141, 1514–1525

Eaton S, Wepf R, Simons K. 1996. Roles for Rac1 and Cdc42 in planar polarization and hair outgrowth in the wing of Drosophila. *The Journal of Cell Biology*. 135(5):1277–89

Etheridge SL, Ray S, Li S, Hamblet NS, Lijam N, et al. 2008. Murine Dishevelled 3 Functions in Redundant Pathways with Dishevelled 1 and 2 in Normal Cardiac Outflow Tract, Cochlea, and Neural Tube Development. *PLoS Genet*. 4(11):e1000259

Gao B, Song H, Bishop K, Elliot G, Garrett L, et al. 2011. Wnt Signaling Gradients Establish Planar Cell Polarity by Inducing Vangl2 Phosphorylation through Ror2. *Developmental Cell*. 20(2):163–76

Gao C, Chen Y-G. 2010. Cellular Signaling. *Cellular Signaling*. 22(5):717–27

Goldman, R. D., Spector, D. L. and Swedlund, A. C. 2005. *Live cell imaging: a laboratory manual*. Cold Spring Harbor Laboratory Press Cold Spring Harbor, NY:

Goodrich LV, Strutt D. 2011. Principles of planar polarity in animal development. *Development*. 138(10):1877–92

Gray, R. S., Abitua, P. B., Wlodarczyk, B. J., Szabo-Rogers, H. L., Blanchard, O., Lee, I., Weiss, G. S., Liu, K. J., Marcotte, E. M., Wallingford, J. B., et al. 2009. The planar cell polarity effector Fuz is essential for targeted membrane trafficking, ciliogenesis and mouse embryonic development. *Nature Cell Biology* 11, 1225–1232

Grimes DT, Boswell CW, Morante NFC, Henkelman RM, Burdine RD, Ciruna B. 2016. Zebrafish models of idiopathic scoliosis link cerebrospinal fluid flow defects to spine

curvature. *Science*. 352(6291):1341–44

Gubb D, Green C, Huen D, Coulson D, Johnson G, et al. 1999. The balance between isoforms of the prickle LIM domain protein is critical for planar polarity in Drosophila imaginal discs. *Genes & Development*. 13(17):2315–27

Guirao B, Meunier A, Mortaud S, Aguilar A, Corsi J-M, et al. 2010. Coupling between hydrodynamic forces and planar cell polarity orients mammalian motile cilia. *Nature Cell Biology*. 12(4):341–50

Guo, Y., Zanetti, G. and Schekman, R. 2013. A novel GTP-binding protein-adaptor protein complex responsible for export of Vangl2 from the trans Golgi network. *eLife* 2, e00160–e00160

Habas R, Kato Y, He X. 2001. Wnt/Frizzled activation of Rho regulates vertebrate gastrulation and requires a novel Formin homology protein Daam1. *Cell*. 107(7):843–54

Habas R, Dawid IB, He X. 2003. Coactivation of Rac and Rho by Wnt/Frizzled signaling is required for vertebrate gastrulation. *Genes & Development*. 17(2):295–309

Hale R, Brittle AL, Fisher KH, Monk NAM, Strutt D. 2015. Cellular interpretation of the long-range gradient of Four-jointed activity in the Drosophila wing. *eLife*. 4:1–21

Hannus M, Feiguin F, Heisenberg C-P, Eaton S. 2002. Planar cell polarization requires Widerborst, a B' regulatory subunit of protein phosphatase 2A. *Development*. 129(14):3493–3503

Hayes M, Gao X, Yu LX, Paria N, Henkelman RM, et al. 2014. ptk7 mutant zebrafish models of congenital and idiopathic scoliosis implicate dysregulated Wnt signaling in disease. *Nature Communications*. 5:4777–11

Hayes M, Naito M, Daulat A, Angers S, Ciruna B. 2013. Ptk7 promotes non-canonical Wnt/PCP-mediated morphogenesis and inhibits Wnt/ -catenin-dependent cell fate decisions during vertebrate development. *Development*. 140(10):2245–45

Hegan PS, Ostertag E, Geurts AM, Mooseker MS. 2015. Myosin Id is required for planar cell polarity in ciliated tracheal and ependymal epithelial cells. *Cytoskeleton*. 72(10):n/a–n/a

Heisenberg CP, Tada M, Rauch GJ, Saude L, Concha ML, et al. 2000. Silberblick/Wnt11 mediates convergent extension movements during zebrafish gastrulation. *Nature*. 405(6782):76–81

Iliescu A, Gravel M, Horth C, Gros P. 2014. Independent Mutations at Arg181 and Arg274 of Vangl Proteins That Are Associated with Neural Tube Defects in Humans Decrease Protein Stability and Impair Membrane Targeting. *Biochemistry*. 53(32):5356–64

Ishikawa HO, Takeuchi H, Haltiwanger RS, Irvine KD. 2008. Four-jointed is a Golgi kinase that phosphorylates a subset of cadherin domains. *Science*. 321(5887):401–4

Jakobsen, L., Vanselow, K., Skogs, M., Toyoda, Y., Lundberg, E., Poser, I., Falkenby, L. G., Bennetzen, M., Westendorf, J., Nigg, E. A., et al. 2011. Novel asymmetrically localizing components of human centrosomes identified by complementary proteomics methods. *The EMBO Journal* 30, 1520–1535

Jaffe KM, Grimes DT, Schottenfeld-Roames J, Werner ME, Ku T-SJ, et al. 2016. c21orf59/kurly Controls Both Cilia Motility and Polarization. *CELREP*. 1–10

Jenny A. 2010. Planar Cell Polarity Signaling in the Drosophila Eye. *Curr Top Dev Biol*. 93:189

Jenny A, Darken RS, Wilson PA, Mlodzik M. 2003. Prickle and Strabismus form a functional complex to generate a correct axis during planar cell polarity signaling. *The EMBO Journal*. 22:4409–20

Jenny A, Reynolds-Kenneally J, Das G, Burnett M, Mlodzik M. 2005. Diego and Prickle regulate Frizzled planar cell polarity signaling by competing for Dishevelled binding. *Nature Cell Biology*. 7(7):691–97

Jiang D, Munro EM, Smith WC. 2005. Ascidian prickle regulates both mediolateral and anterior-posterior cell polarity of notochord cells. *Curr Biol*. 15(1):79–85

Juriloff DM, Harris MJ. 2012. A consideration of the evidence that genetic defects in planar cell polarity contribute to the etiology of human neural tube defects. *Birth Defects Research Part A: Clinical and Molecular Teratology*. 94(10):824–40

Keller R, Shih J, Sater A. 1992. The cellular basis of the convergence and extension of the Xenopus neural plate. *Dev. Dyn*. 193(3):199–217

Kibar Z, Torban E, McDearmid JR, Reynolds A, Berghout J, et al. 2007. Mutations in VANGL1 Associated with Neural-Tube Defects. *N Engl J Med*. 356(14):1432–37

Kibar Z, Vogan KJ, Groulx N, Justice MJ, Underhill DA, Gros P. 2001. Ltap, a mammalian homolog of Drosophila Strabismus/Van Gogh, is altered in the mouse neural tube mutant Loop-tail. *Nature Genetics*. 28(3):251–55

Kim SK, Shindo A, Park TJ, Oh EC, Ghosh S, et al. 2010. Planar Cell Polarity Acts Through Septins to Control Collective Cell Movement and Ciliogenesis. *Science*. 329(5997):1337–40

Klein TJ, Jenny A, Djiane A, Mlodzik M. 2006. CKIε/discs overgrown Promotes Both Wnt-Fz/β-Catenin and Fz/PCP Signaling in Drosophila. *Current Biology*. 16(13):1337–43

Kochanek KD, Murphy SL, Xu J, Tejada-Vera B. 2016. Deaths: Final Data for 2014. *Natl Vital Stat Rep*. 65(4):1–122

König, G. and Hausen, P. 1993. Planar Polarity in the Ciliated Epidermis of *Xenopus* Embryos. *Developmental Biology* 160, 355–368

Kunimoto K, Yamazaki Y, Nishida T, Shinohara K, Ishikawa H, et al. 2012. Coordinated ciliary beating requires Odf2-mediated polarization of basal bodies via basal feet. *Cell*. 148(1-2):189–200

Lawrence PA, Casal J. 2013. The mechanisms of planar cell polarity, growth and the Hippo pathway: some known unknowns. *Developmental Biology*. 377(1):1–8

Lawrence PA, Casal J, Struhl G. 2004. Cell interactions and planar polarity in the abdominal epidermis of Drosophila. *Development*. 131(19):4651–64

Lee, H. and Adler, P. N. 2002. The function of the frizzled pathway in the Drosophila wing is dependent on inturned and fuzzy. *Genetics* 160, 1535–1547

Lee J, Andreeva A, Sipe CW, Liu L, Cheng A, Lu X. 2012. PTK7 regulates myosin II activity to orient planar polarity in the mammalian auditory epithelium. *Curr Biol*. 22(11):956–66

Lei Y, Zhu H, Yang W, Ross ME, Shaw GM, Finnell RH. 2014. Identification of novel CELSR1 mutations in spina bifida. *PLoS ONE*. 9(3):e92207–8

Lienkamp SS, Liu K, Karner CM, Carroll TJ, Ronneberger O, et al. 2012. Vertebrate kidney tubules elongate using a planar cell polarity–dependent, rosette-based mechanism of convergent extension. *Nature Genetics*. 44(12):1382–87

Lin, Y.-Y. and Gubb, D. 2009. Molecular dissection of Drosophila Prickle isoforms distinguishes their essential and overlapping roles in planar cell polarity. *Developmental Biology* 325, 386–399

Liu, C., Lin, C., Gao, C., May-Simera, H., Swaroop, A. and Li, T. 2014. Null and hypomorph Prickle1 alleles in mice phenocopy human Robinow syndrome and disrupt signaling downstream of Wnt5a. *Biology Open*

Lu Q, Yan J, Adler PN. 2010. The Drosophila planar polarity proteins inturned and multiple wing hairs interact physically and function together. *Genetics*. 185(2):549–58

Lu X, Borchers AGM, Jolicoeur C, Rayburn H, Baker JC, Tessier-Lavigne M. 2004. PTK7/CCK-4 is a novel regulator of planar cell polarity in vertebrates. *Nature*. 430(6995):93–98

Luxenburg C, Heller E, Pasolli HA, Chai S, Nikolova M, et al. 2015. Wdr1-mediated cell shape dynamics and cortical tension are essential for epidermal planar cell polarity. *Nature Publishing Group*. 17(5):592–604

Ma D, Yang C-H, McNeill H, Simon MA, Axelrod JD. 2003. Fidelity in planar cell polarity signaling. *Nature*. 421(6922):543–47

Mahaffey JP, Grego-Bessa J, Liem KF, Anderson KV. 2013. Cofilin and Vangl2 cooperate in the initiation of planar cell polarity in the mouse embryo. *Development*. 140(6):1262–71

Mao Y, Kuta A, Crespo-Enriquez I, Whiting D, Martin T, et al. 2016. Dchs1-Fat4 regulation of polarized cell behaviors during skeletal morphogenesis. *Nat Commun*. 7 SP -:1–10

Mao Y, Mulvaney J, Zakaria S, Yu T, Morgan KM, et al. 2011. Characterization of a Dchs1 mutant mouse reveals requirements for Dchs1-Fat4 signaling during mammalian development. *Development*. 138(5):947–57

Marlow F, Topczewski J, Sepich D, Solnica-Krezel L. 2002. Zebrafish Rho kinase 2 acts downstream of Wnt11 to mediate cell polarity and effective convergence and extension movements. *Curr Biol*. 12(11):876–84

Matakatsu H, Blair SS. 2004. Interactions between Fat and Dachsous and the regulation of planar cell polarity in the Drosophila wing. *Development*. 131(15):3785–94

Matis M, Axelrod JD. 2013. Regulation of PCP by the Fat signaling pathway. *Genes & Development*. 27(20):2207–20

Matis M, Russler-Germain DA, Hu Q, Tomlin CJ, Axelrod JD. 2014. Microtubules provide directional information for core PCP function. *eLife*. 3:e02893

Merkel M, Sagner A, Gruber FS, Etournay R, Blasse C, et al. 2014. The Balance of Prickle/Spiny-Legs Isoforms Controls the Amount of Coupling between Core and Fat PCP Systems. *Curr Biol*. 1–13

Merte, J., Jensen, D., Wright, K., Sarsfield, S., Wang, Y., Schekman, R. and Ginty, D. D. 2009. Sec24b selectively sorts Vangl2 to regulate planar cell polarity during neural tube closure. *Nature Cell Biology* 12, 41–46

Mitchell B, Jacobs R, Li J, Chien S, Kintner C. 2007. A positive feedback mechanism governs the polarity and motion of motile cilia. *Nature*. 447(7140):97–101

Mitchell B, Stubbs JL, Huisman F, Taborek P, Yu C, Kintner C. 2009. The PCP Pathway Instructs the Planar Orientation of Ciliated Cells in the Xenopus Larval Skin. *Current*

Biology. 19(11):924–29

Mottola G, Classen AK, Gonzalez-Gaitan M, Eaton S, Zerial M. 2010. A novel function for the Rab5 effector Rabenosyn-5 in planar cell polarity. *Development*. 137(14):2353–64

Murdoch JN, Doudney K, Paternotte C, Copp AJ, Stanier P. 2001. Severe neural tube defects in the loop-tail mouse result from mutation of Lpp1, a novel gene involved in floor plate specification. *Human Molecular Genetics*. 10(22):2593–2601

Narimatsu M, Bose R, Pye M, Zhang L, Miller B, et al. 2009. Regulation of Planar Cell Polarity by Smurf Ubiquitin Ligases. *Cell*. 137(2):295–307

Nishimura T, Honda H, Takeichi M. 2012. Planar Cell Polarity Links Axes of Spatial Dynamics in Neural-Tube Closure. *Cell*. 149(5):1084–97

Nieuwkoop P, Faber J. 1967. *Normal Table of Xenopus Laevis (Daudin): a Systematic and Chronological Survey of the Development From the Fertilized Egg Till the End of Metamorphosis*. North-Holland

Ohata S, Nakatani J, Herranz-Pérez V, Cheng J, Belinson H, et al. 2014. Loss of Dishevelleds Disrupts Planar Polarity in Ependymal Motile Cilia and Results in Hydrocephalus. *Neuron*. 83(3):558–71

Okumura, A., Yamamoto, T., Miyajima, M., Shimojima, K., Kondo, S., Abe, S., Ikeno, M. and Shimizu, T. 2014. 3p Interstitial Deletion Including PRICKLE2 in Identical Twins With Autistic Features. *Pediatr Neurol*.

Olofsson J, Sharp KA, Matis M, Cho B, Axelrod JD. 2014. Prickle/spiny-legs isoforms control the polarity of the apical microtubule network in planar cell polarity. *Development*. 141(14):2866–74

Ossipova O, Kim K, Lake BB, Itoh K, Ioannou A, Sokol SY. 2014. Role of Rab11 in planar cell polarity and apical constriction during vertebrate neural tube closure. *Nature Communications*. 5:1–8

Ossipova O, Kim K, Sokol SY. 2015. Planar polarization of Vangl2 in the vertebrate neural plate is controlled by Wnt and Myosin II signaling. *Biology Open*. 4(6):722–30

Park M, Moon RT. 2002. The planar cell-polarity gene stbm regulates cell behavior and cell fate in vertebrate embryos. *Nat Cell Biol*. 4(1):20–25

Park, T. J., Haigo, S. L. and Wallingford, J. B. 2006. Ciliogenesis defects in embryos lacking inturned or fuzzy function are associated with failure of planar cell polarity and Hedgehog signaling. *Nature Genetics* 38, 303–311

Park TJ, Mitchell BJ, Abitua PB, Kintner C, Wallingford JB. 2008. Dishevelled controls apical docking and planar polarization of basal bodies in ciliated epithelial cells. *Nature Genetics*. 40(7):871–79

Peng Y, Axelrod JD. 2012. Asymmetric protein localization in planar cell polarity: Mechanisms, puzzles and challenges. *Curr Top Dev Biol*. 101:33

Person AD, Beiraghi S, Sieben CM, Hermanson S, Neumann AN, et al. 2010. WNT5A mutations in patients with autosomal dominant Robinow syndrome. *Dev. Dyn*. 239(1):327–37

Quigley, I. K., Stubbs, J. L. and Kintner, C. 2011. Specification of ion transport cells in the Xenopus larval skin. *Development* 138, 705–714

Rauzi M, Lenne P-F, Lecuit T. 2010. Planar polarized actomyosin contractile flows control epithelial junction remodelling. *Nature*. 468(7327):1110–14

Rida PCG, Chen P. 2009. Line up and listen: Planar cell polarity regulation in the mammalian inner ear. *Seminars in Cell and Developmental Biology*. 20(8):978–85

Robinson A, Escuin S, Doudney K, Vekemans M, Stevenson RE, et al. 2012. Mutations in the planar cell polarity genes CELSR1 and SCRIB are associated with the severe neural tube defect craniorachischisis. *Hum. Mutat*. 33(2):440–47

Rock R, Schrauth S, Gessler M. 2005. Expression of mouse dchs1, fjx1, and fat-jsuggests conservation of the planar cell polarity pathway identified in drosophila. *Dev. Dyn*. 234(3):747–55

Rodriguez-Boulan E, Macara IG. 2014. Organization and execution of the epithelial polarity programme. *Nat Rev Mol Cell Biol*. 15(4):225–42

Roszko I, S Sepich D, Jessen JR, Chandrasekhar A, Solnica-Krezel L. 2015. A dynamic intracellular distribution of Vangl2 accompanies cell polarization during zebrafish gastrulation. *Development*. 142(14):2508–20

Saburi S, Hester I, Fischer E, Pontoglio M, Eremina V, et al. 2008. Loss of Fat4 disrupts PCP signaling and oriented cell division and leads to cystic kidney disease. *Nature Genetics*. 40(8):1010–15

Seifert, J. R. K. and Mlodzik, M. 2007. Frizzled/PCP signaling: a conserved mechanism regulating cell polarity and directed motility. *Nat Rev Genet* 8, 126–138

Seo JH, Zilber Y, Babayeva S, Liu J, Kyriakopoulos P, et al. 2011. Mutations in the planar cell polarity gene, Fuzzy, are associated with neural tube defects in humans. *Human Molecular Genetics*. 20(22):4324–33

Sepich DS, Usmani M, Pawlicki S, Solnica-Krezel L. 2011. Wnt/PCP signaling controls intracellular position of MTOCs during gastrulation convergence and extension movements. *Development*. 138(3):543–52

Shafer B, Onishi K, Lo C, Colakoglu G, Zou Y. 2011. Vangl2 Promotes Wnt/Planar Cell Polarity-like Signaling by Antagonizing Dvl1-Mediated Feedback Inhibition in Growth Cone Guidance. *Developmental Cell*. 20(2):177–91

Sharpey W. 1836. *Cilia*. Marchant, printer

Shi D, Komatsu K, Hirao M, Toyooka Y, Koyama H, et al. 2014. Celsr1 is required for the generation of polarity at multiple levels of the mouse oviduct. *Development*. 141(23):4558–68

Shi D, Usami F, Komatsu K, Oka S, Abe T, et al. 2016. Dynamics of planar cell polarity protein Vangl2 in the mouse oviduct epithelium. *MOD*. 1–52

Shih J, Keller R. 1992. Cell motility driving mediolateral intercalation in explants of Xenopus laevis. *Development*. 116(4):901–14

Shimada Y, Yonemura S, Ohkura H, Strutt D, Uemura T. 2006. Polarized Transport of Frizzled along the Planar Microtubule Arrays in Drosophila Wing Epithelium. *Developmental Cell*. 10(2):209–22

Shindo A, Wallingford JB. 2014. PCP and septins compartmentalize cortical actomyosin to direct collective cell movement. *Science*. 343(6171):649–52

117

Shrestha R, Little KA, Tamayo JV, Li W, Perlman DH, Devenport D. 2015. Mitotic Control of Planar Cell Polarity by Polo-like Kinase 1. *Developmental Cell*. 33(5):522–34

Simon MA, Xu A, Ishikawa HO, Irvine KD. 2010. Modulation of Fat:Dachsous Binding by the Cadherin Domain Kinase Four-Jointed. *Curr Biol*. 20(9):811–17

Simons M, Gault WJ, Gotthardt D, Rohatgi R, Klein TJ, et al. 2009. Electrochemical cues regulate assembly of the Frizzled/Dishevelled complex at the plasma membrane during planar epithelial polarization. *Nature Publishing Group*. 11(3):286–94

Sive HL, Grainger RM, Harland RM. 2000. Early development of Xenopus laevis: a laboratory manual

Sokol, S. Y. 1996. Analysis of Dishevelled signaling pathways during Xenopus development. *Curr Biol* 6, 1456–1467

Sokol SY. 2015. Spatial and temporal aspects of Wnt signaling and planar cell polarity during vertebrate embryonic development. *Seminars in Cell and Developmental Biology*. 42 IS -(0 SP - EP - PY - T2 -):78–85

Song, H., Hu, J., Chen, W., Elliott, G., Andre, P., Gao, B. and Yang, Y. 2010. Planar cell polarity breaks bilateral symmetry by controlling ciliary positioning. *Nature* 466, 378–382

Sowers, L. P., Loo, L., Wu, Y., Campbell, E., Ulrich, J. D., Wu, S., Paemka, L., Wassink, T., Meyer, K., Bing, X., et al. 2013. Disruption of the non-canonical Wnt gene PRICKLE2 leads to autism-like behaviors with evidence for hippocampal synaptic dysfunction. *Mol Psychiatry* 18, 1077–1089

Stramer B, Mayor R. 2016. Mechanisms and in vivo functions of contact inhibition of locomotion. *Nat Rev Mol Cell Biol*. 1–13

Struhl G, Casal J, Lawrence PA. 2012. Dissecting the molecular bridges that mediate the function of Frizzled in planar cell polarity. *Development*. 139(19):3665–74

Strutt D, Strutt H. 2007. Differential activities of the core planar polarity proteins during Drosophila wing patterning. *Developmental Biology*. 302(1):181–94

Strutt DI. 2001. Asymmetric localization of frizzled and the establishment of cell polarity in the Drosophila wing. *Molecular Cell*. 7(2):367–75

Strutt DI, Weber U, Mlodzik M. 1997. The role of RhoA in tissue polarity and Frizzled signaling. *Nature*. 387(6630):292–95

Strutt H, Searle E, Thomas-MacArthur V, Brookfield R, Strutt D. 2013a. A Cul-3-BTB ubiquitylation pathway regulates junctional levels and asymmetry of core planar polarity proteins. *Development*. 140(8):1693–1702

Strutt, H. and Strutt, D. 2009. Asymmetric localisation of planar polarity proteins: Mechanisms and consequences. *Seminars in Cell and Developmental Biology* 20, 957–963

Strutt H, Strutt D. 2002. Nonautonomous planar polarity patterning in Drosophila: dishevelled-independent functions of frizzled. *Developmental Cell*. 3(6):851–63

Strutt H, Strutt D. 2003. EGF Signaling and Ommatidial Rotation in the Drosophila Eye. *Current Biology*. 13(16):1451–57

Strutt H, Strutt D. 2008. Differential Stability of Flamingo Protein Complexes Underlies the Establishment of Planar Polarity. *Current Biology*. 18(20):1555–64

Strutt H, Thomas-MacArthur V, Strutt D. 2013b. Strabismus Promotes Recruitment and

Degradation of Farnesylated Prickle in Drosophila melanogaster Planar Polarity Specification. *PLoS Genet*. 9(7):e1003654

Strutt H, Warrington SJ, Strutt D. 2011. Dynamics of Core Planar Polarity Protein Turnover and Stable Assembly into Discrete Membrane Subdomains. *Developmental Cell*. 20(4):511–25

Strutt H, Price MA, Strutt D. 2006. Planar Polarity Is Positively Regulated by Casein Kinase Iε in Drosophila. *Current Biology*. 16(13):1329–36

Sweede, M., Ankem, G., Chutvirasakul, B., Azurmendi, H. F., Chbeir, S., Watkins, J., Helm, R. F., Finkielstein, C. V. and Capelluto, D. G. S. 2008. Structural and Membrane Binding Properties of the Prickle PET Domain †. *Biochemistry* 47, 13524–13536

Tada M, Heisenberg CP. 2012. Convergent extension: using collective cell migration and cell intercalation to shape embryos. *Development*. 139(21):3897–3904

Tada M, Smith JC. 2000. Xwnt11 is a target of Xenopus Brachyury: regulation of gastrulation movements via Dishevelled, but not through the canonical Wnt pathway. *Development*. 127(10):2227–38

Takeuchi, M., Nakabayashi, J., Sakaguchi, T., Yamamoto, T. S., Takahashi, H., Takeda, H. and Ueno, N. 2003. The prickle-Related Gene in Vertebrates Is Essential for Gastrulation Cell Movements. *Current Biology* 13, 674–679

Tao, H., Manak, J. R., Sowers, L., Mei, X., Kiyonari, H., Abe, T., Dahdaleh, N. S., Yang, T., Wu, S., Chen, S., et al. 2011. Mutations in prickle orthologs cause seizures in flies, mice, and humans. *The American Journal of Human Genetics* 88, 138–149

Tao H, Suzuki M, Kiyonari H, Abe T, Sasaoka T, Ueno N. 2009. Mouse prickle1, the homolog of a PCP gene, is essential for epiblast apical-basal polarity. *Proc Natl Acad Sci U S A*. 106(34):14426–31

Tao H, Inoue K-I, Kiyonari H, Bassuk AG, Axelrod JD, et al. 2012. Nuclear localization of Prickle2 is required to establish cell polarity during early mouse embryogenesis. *Developmental Biology*. 364(2):138–48

Taylor J, Abramova N, Charlton J, Adler PN. 1998. Van Gogh: a new Drosophila tissue polarity gene. *Genetics*. 150(1):199–210

Teves ME, Sears PR, Li W, Zhang Z, Tang W, et al. 2014. Sperm-Associated Antigen 6 (SPAG6) Deficiency and Defects in Ciliogenesis and Cilia Function: Polarity, Density, and Beat. *PLoS ONE*. 9(10):e107271

Thomas C, Strutt D. 2011. The roles of the cadherins Fat and Dachsous in planar polarity specification in Drosophila. *Dev. Dyn*. 241(1):27–39

Tissir F, Qu Y, Montcouquiol M, Zhou L, Komatsu K, et al. 2010. Lack of cadherins Celsr2 and Celsr3 impairs ependymal ciliogenesis, leading to fatal hydrocephalus. *Nat Neurosci*. 13(6):700–707

Torban, E., Patenaude, A.-M., Leclerc, S., Rakowiecki, S., Gauthier, S., Andelfinger, G., Epstein, D. J. and Gros, P. 2008. Genetic interaction between members of the Vangl family causes neural tube defects in mice. *Proc Natl Acad Sci U S A* 105, 3449–3454

Toriyama M, Lee C, Taylor SP, Duran I, Cohn DH, et al. 2016. The ciliopathy-associated CPLANE proteins direct basal body recruitment of intraflagellar transport machinery. *Nature Genetics*. 1–11

Tree DRP, Shulman JM, Rousset R, Scott MP, Gubb D, Axelrod JD. 2002. Prickle mediates feedback amplification to generate asymmetric planar cell polarity signaling. *Cell*. 109(3):371–81

Turk E, Wills AA, Kwon T, Sedzinski J, Wallingford JB, Stearns T. 2015. Zeta-Tubulin Is a Member of a Conserved Tubulin Module and Is a Component of the Centriolar Basal Foot in Multiciliated Cells. *Curr Biol*. 25(16):2177–83

Turner CM, Adler PN. 1998. Distinct roles for the actin and microtubule cytoskeletons in the morphogenesis of epidermal hairs during wing development in Drosophila. *Mech Dev*. 70(1-2):181–92

Twitty, V. C. 1928. Experimental studies on the ciliary action of amphibian embryos. *J. Exp. Zool*. 50, 319–344

Usui T, Shima Y, Shimada Y, Hirano S, Burgess RW, et al. 1999. Flamingo, a seven-pass transmembrane cadherin, regulates planar cell polarity under the control of Frizzled. *Cell*. 98(5):585–95

van Bokhoven H, Celli J, Kayserili H, van Beusekom E, Balci S, et al. 2000. Mutation of the gene encoding the ROR2 tyrosine kinase causes autosomal recessive Robinow syndrome. *Nature Genetics*. 25(4):423–26

Vinson CR, Adler PN. 1987. Directional non-cell autonomy and the transmission of polarity information by the frizzled gene of Drosophila

Vladar EK, Bayly RD, Sangoram AM, Scott MP, Axelrod JD. 2012. Microtubules enable the planar cell polarity of airway cilia. *Curr Biol*. 22(23):2203–12

Walentek, P., Bogusch, S., Thumberger, T., Vick, P., Dubaissi, E., Beyer, T., Blum, M. and Schweickert, A. 2014. A novel serotonin-secreting cell type regulates ciliary motility in the mucociliary epidermis of Xenopus tadpoles. *Development* 141, 1526–1533

Wallingford JB. 2012. Planar Cell Polarity and the Developmental Control of Cell Behavior in Vertebrate Embryos. *Annu. Rev. Cell Dev. Biol*. 28(1):627–53

Wallingford JB, Harland RM. 2001. Xenopus Dishevelled signaling regulates both neural and mesodermal convergent extension: parallel forces elongating the body axis. *Development*. 128(13):2581–92

Wallingford JB, Niswander LA, Shaw GM, Finnell RH. 2013. The Continuing Challenge of Understanding, Preventing, and Treating Neural Tube Defects. *Science*. 339(6123):1222002–2

Wallingford JB, Rowning BA, Vogeli KM, Rothbächer U, Fraser SE, Harland RM. 2000. Dishevelled controls cell polarity during Xenopus gastrulation. *Nature*. 405(6782):81–85

Wang J, Hamblet NS, Mark S, Dickinson ME, Brinkman BC, et al. 2006a. Dishevelled genes mediate a conserved mammalian PCP pathway to regulate convergent extension during neurulation. *Development*. 133(9):1767–78

Wang, Y., Yan, J., Lee, H., Lu, Q. and Adler, P. N. 2014. The proteins encoded by the Drosophila Planar Polarity Effector genes inturned, fuzzy and fritz interact physically and can re-pattern the accumulation of "upstream" Planar Cell Polarity proteins. *Developmental Biology* 394, 156–169

Wang Y, Guo N, Nathans J. 2006b. The role of Frizzled3 and Frizzled6 in neural tube closure

and in the planar polarity of inner-ear sensory hair cells. *J Neurosci*. 26(8):2147–56

Wang Y, Thekdi N, Smallwood PM, Macke JP, Nathans J. 2002. Frizzled-3 is required for the development of major fiber tracts in the rostral CNS. *J Neurosci*. 22(19):8563–73

Werner ME, Hwang P, Huisman F, Taborek P, Yu CC, Mitchell BJ. 2007. Actin and microtubules drive differential aspects of planar cell polarity in multiciliated cells. *Annu Rev Physiol*. 195(1):423–50

White J, Mazzeu JF, Hoischen A, Jhangiani SN, Gambin T, et al. 2015. DVL1 frameshift mutations clustering in the penultimate exon cause autosomal-dominant Robinow syndrome. *The American Journal of Human Genetics*. 96(4):612–22

White JJ, Mazzeu JF, Hoischen A, Bayram Y, Withers M, et al. 2016. DVL3 alleles resulting in a − 1 frameshift of the last exon mediate autosomal-dominant Robinow syndrome. *The American Journal of Human Genetics*. 98(3):553–61

Williams M, Yen W, Lu X, Sutherland A. 2014. Distinct Apical and Basolateral Mechanisms Drive Planar Cell Polarity-Dependent Convergent Extension of the Mouse Neural Plate. *Developmental Cell*. 1–13

Winter CG, Wang B, Ballew A, Royou A, Karess R, et al. 2001. Drosophila Rho-associated kinase (Drok) links Frizzled-mediated planar cell polarity signaling to the actin cytoskeleton. *Cell*. 105(1):81–91

Wong LL, Adler PN. 1993. Tissue polarity genes of Drosophila regulate the subcellular location for prehair initiation in pupal wing cells. *The Journal of Cell Biology*. 123(1):209–21

Wong H-C, Bourdelas A, Krauss A, Lee H-J, Shao Y, et al. 2003. Direct binding of the PDZ domain of Dishevelled to a conserved internal sequence in the C-terminal region of Frizzled. *Molecular Cell*. 12(5):1251–60

Wu J, Mlodzik M. 2008. The Frizzled Extracellular Domain Is a Ligand for Van Gogh/Stbm during Nonautonomous Planar Cell Polarity Signaling. *Developmental Cell*. 15(3):462–69

Wu J, Roman A-C, Carvajal-Gonzalez JM, Mlodzik M. 2013. Wg and Wnt4 provide long-range directional input to planar cell polarity orientation in Drosophila. *Nature Cell Biology*. 15(8):1–13

Yang C-H, Axelrod JD, Simon MA. 2002. Regulation of Frizzled by fat-like cadherins during planar polarity signaling in the Drosophila compound eye. *Cell*. 108(5):675–88

Yang Y, Mlodzik M. 2015. Wnt-Frizzled/Planar Cell Polarity Signaling: Cellular Orientation by Facing the Wind (Wnt). *Annu. Rev. Cell Dev. Biol*. 31(1):623–46

Ybot-Gonzalez P, Savery D, Gerrelli D, Signore M, Mitchell CE, et al. 2007. Convergent extension, planar-cell-polarity signaling and initiation of mouse neural tube closure. *Development*. 134(4):789–99

Yen WW, Williams M, Periasamy A, Conaway M, Burdsal C, et al. 2009. PTK7 is essential for polarized cell motility and convergent extension during mouse gastrulation. *Development*. 136(12):2039–48

Yin C, Kiskowski M, Pouille P-A, Farge E, Solnica-Krezel L. 2008. Cooperation of polarized cell intercalations drives convergence and extension of presomitic mesoderm during zebrafish gastrulation. *The Journal of Cell Biology*. 180(1):221–32

Yin, H., Copley, C. O., Goodrich, L. V. and Deans, M. R. 2012. Comparison of Phenotypes

between Different vangl2 Mutants Demonstrates Dominant Effects of the Looptail Mutation during Hair Cell Development. *PLoS ONE* 7, e31988

Ying G, Avasthi P, Irwin M, Gerstner CD, Frederick JM, et al. 2014. Centrin 2 Is Required for Mouse Olfactory Ciliary Trafficking and Development of Ependymal Cilia Planar Polarity. *Journal of Neuroscience*. 34(18):6377–88

Yu A, Rual J-F, Tamai K, Harada Y, Vidal M, et al. 2007. Association of Dishevelled with the Clathrin AP-2 Adaptor Is Required for Frizzled Endocytosis and Planar Cell Polarity Signaling. *Developmental Cell*. 12(1):129–41

Zakaria S, Mao Y, Kuta A, de Sousa CF, Gaufo GO, et al. 2014. Regulation of Neuronal Migration by Dchs1-Fat4 Planar Cell Polarity. *Curr Biol*. 24(14):1620–27

Zallen JA, Wieschaus E. 2004. Patterned gene expression directs bipolar planar polarity in Drosophila. *Developmental Cell*. 6(3):343–55

Zeng, H., Hoover, A. N. and Liu, A. 2010. PCP effector gene Inturned is an important regulator of cilia formation and embryonic development in mammals. *Developmental Biology* 339, 418–428

Vita

Mitchell Tyler Butler is the son of Thomas and Terri Butler. He graduated from Lakeside High School in Hot Springs, AR in 2003 and earned his B.S. in Biology from Georgetown University. His undergraduate thesis mentor was Dr. Elena Silva, and his research in the Silva lab was focused on the role of Sox21 in neural patterning. In 2008, he joined the lab of Dr. Rasika Harshey at the University of Texas at Austin as a research technician and studied mechanisms of *Salmonella* motility and virulence. He joined the graduate program at the University of Texas at Austin in 2011 and began his doctoral research in the lab of Dr. John Wallingford in 2012.

Permanent address: 102 Ravenwood Pl., Hot Springs, AR 71901

Referred Articles:

Butler, M.T., Wang, Q., Harshey, R.M. (2010). Cell density and mobility protect swarming bacteria against antibiotics. *Proceedings of the National Academy of Sciences of the USA*, 107(8), 3776-3781.

Lazova, M.D., Butler, M.T., Shimizu, T.S., Harshey, R.M. (2012). *Salmonella* chemoreceptors McpB and McpC mediate a repellent response to *L*-cystine: a potential mechanism to avoid oxidative conditions. *Molecular Microbiology* 84(4), 697-711.

Butler, M.T. and Wallingford, J.B. (2015). Control of vertebrate core planar cell polarity localization and dynamics by Prickle 2. *Development* 142: 3429-3439.

Butler, M.T. and Wallingford, J.B. (2017). Planar Cell Polarity in Development and Disease. *Nature Reviews Molecular Cell Biology*.

Butler, M.T., Shindo, A. and Wallingford, J.B. (In preparation). Asymmetric PCP protein dynamics coordinate polarized actomyosin contractility and convergent extension.

This manuscript was typed by the author.